PARTICIPATION OF *DE NOVO* SPHINGOLIPID BIOSYNTHESIS IN THE REGULATION OF AUTOPHAGY IN RESPONSE TO DIVERSE AGENTS

A dissertation
Presented to
The Academic Faculty

by

Kacee Hall Sims

In Partial Fulfillment
of the Requirements for the Degree
Doctor of Philosophy in the
School of Chemistry & Biochemistry

Georgia Institute of Technology
December 2011

PARTICIPATION OF *DE NOVO* SPHINGOLIPID BIOSYNTHESIS IN THE REGULATION OF AUTOPHAGY IN RESPONSE TO DIVERSE AGENTS

Approved by:

Dr. Alfred H. Merrill, Jr., Advisor
Schools of Biology and Chemistry & Biochemistry
Georgia Institute of Technology

Dr. Adegboyega K. Oyelere
School of Chemistry & Biochemistry
Georgia Institute of Technology

Dr. Donald Doyle
School of Chemistry & Biochemistry
Georgia Institute of Technology

Dr. M. Cameron Sullards
School of Chemisry & Biochemistry
Georgia Institute of Technology

Dr. Christine Payne
School of Chemistry & Biochemistry
Georgia Institute of Technology

Date Approved: October 24, 2011

See now the power of truth; the same experiment which at first glance seemed to show one thing, when more carefully examined, assures us of the contrary.

-- Galileo Galilei (1565-1642)

To my wonderful mother and husband. For believing in me and teaching me that even the largest task can be accomplished if it is done one step at a time.

Every time I think of you, I give thanks to my God

– Philippians 1:3

ACKNOWLEDGEMENTS

First and foremost, I offer my sincerest gratitude to my adviser, Dr. Al Merrill, who has supported me throughout my research with his patience and knowledge whilst giving me the room to work in my own way. His continual and convincing spirit of adventure with regard to research has made my graduate school experience both productive and stimulating. During the tough times, his joy and enthusiasm for our science was both contagious and motivational. I will always be grateful for the lessons that I have learned throughout this journey, both at and away from bench.

I would also like to express my thanks to my committee members: Dr. Cameron Sullards, Dr. Donald Doyle, Dr. Christine Payne, and Dr. Yomi Oyelere. Their time, interest, helpful comments, and insightful questions have been invaluable in the completion of this work.

In my daily work, I have been blessed with a group of wonderful individuals in the Merrill lab who have been a source of friendship, as well as good advice and collaboration. I am especially grateful to Elaine Wang for being an unmatched fount of knowledge and for always sharing her expertise in order to make me not only a better scientist but also a better experimentalist. I would also like to thank other members of the Merrill Lab, both past and present, who have contributed to this work in some way: Samuel Kelly, Dr. Sibali Bandyopadhyay, Dr. Holly Symolon, Dr. Jeremy Allegood, Dr. Christopher Haynes, Dr. Amin Momin, Katie Shaw, and Wenjing Zheng. It has truly been a pleasure to work with each of you.

To my wonderful family and friends, thank you for all of your endless love and support. I could not have done this without you. To my mother, thank you for being my

rock, sounding board, and number one fan. You have always been a constant source of encouragement and unconditional love to me on the good days and the bad days. For this, I will be forever indebted and grateful. And to my loving, supportive, encouraging, and patient husband, Jeremy, whose faithful support during the stages of this journey is more appreciated than words can adequately express. I am so fortunate to have both of you in my life to appreciate my laughter, to dry my tears, and most of all, to help me understand and accept life's ups and downs. To my father-in-law, Jerry, thank you for being a constant example that although there is no substitute for hard work and humility the rewards are worth it every time. I am beyond blessed to have you in my life. To my aunt, Susan, thank you for all of your prayers and continual interest in my studies. It is so nice to know that wherever life takes me, I will always have you a prayer warrior and cheerleader in you. To my amazing friends, you have each inspired me in some way, and I can't imagine this journey without you. Finally, it would be remiss if I did not mention my sweet, loving, faithful companion, Stanley James Sims, my miniature dachshund, who brings more joy to my life than can be imagined. Thank you for allowing me to slow down and enjoy life throughout this process.

Last but certainly not least, I thank my omnipresent God, for answering my prayers for the strength to plod on despite sometimes wanting to give up. Thank you so much, Dear Lord. For without You, none of this would be possible.

TABLE OF CONTENTS

LIST OF FIGURES

LIST OF SYMBOLS AND ABBREVIATIONS

ATG	Autophagy-Related
BSA	Bovine Serum Albumin
Cer	Ceramide
Cer1P	Ceramide 1-Phosphate
CERK	Ceramide Kinase
CERT	Ceramide Transfer Protein
CerS	Ceramide Synthase
DHCer	Dihydroceramide
DHGlcCer	Dihydroglucosylceramide
DHSL	Dihydrosphingolipid(s)
DHSM	Dihydrosphingomyelin
DES	Dihydroceramide Desaturase
DMEM	Dulbecco's Modified Eagle Medium
ER	Endoplasmic Reticulum
GalCer	Galactosylceramide
GFP	Green Fluorescent Protein
GlcCer	Glucosylceramide
GC	Golgi Complex
GSL	Glycosphingolipid(s)
4-HPA	4-Hydroxypalmitanilide
4-HPR	Fenretinide; 4-Hydroxyphenylretinamide
ISP1	Inhibitor of Serine Palmitoyltransferase
KLA	Kdo_2-Lipid A

3KSa	3-Ketosphinganine
3KSR	3-Ketosphinganine Reductase
LC ESI–MS/MS	Liquid Chromatography, Electrospray Ionization Tandem Mass Spectrometry
LC3	Microtubule Associated Protein 1 Light Chain 3
LPS	Lipopolysaccharide
MH-Cer	Monohexosylceramide
MH-DHCer	Monohexosyldihydroceramide
MRM	Multiple Reaction Monitoring
mTOR	Mammalian Target of Rapamycin
OA	Oleate
Pal	Palmitate
PBS	Phosphate Buffered Saline
ROS	Reactive Oxygen Species
Sa	Sphinganine
Sa1P	Sphinganine 1-Phosphate
SL	Sphingolipid(s)
SM	Sphingomyelin
SMPD1	Acidic Sphingomyelinase
SMS	Sphingomyelin Synthase
So	Sphingosine
S1P	Sphingosine 1-Phosphate
SphK	Sphingosine Kinase(s)
SPT	Serine Palmitoyltransferase
TLR4	Toll-like Receptor 4

SUMMARY

Sphingolipids are a complex family of molecules that participate in many aspects of cell structure and function, including an essential cellular process known as autophagy. Autophagy is a degradation and recycling pathway whereby intracellular components are sequestered into double-membrane vesicles, known as autophagosomes, for subsequent fusion with lysosomes and degradation. Autophagy takes part in cell survival, host immune defense against pathogens, and other biological processes, but is also sometimes lethal. Ceramide, sphingosine 1-phosphate, and more recently dihydroceramide have been shown to induce autophagy, which opens an interesting new field of cell regulation by sphingolipids. This dissertation describes two new cases in which sphingolipids participate in the induction of autophagy: a) RAW264.7 cells treated with Kdo_2-Lipid A, a lipopolysaccharide sub-structure with endotoxin activity equal to LPS; and b) MCF7 cells treated with fenretinde, a chemotherapeutic agent which has shown success in clinical trials. It also analyzes the structural properties of fenretinide that contribute to its ability to modulate sphingolipid metabolism through inhibition of dihydroceramide desaturase, thereby elevating dihydroceramide and induction of autophagy**.** Autophagy was monitored by following the redistribution of GFP-LC3 into discrete punctate vesicles in response to the agents and by Western blotting; in parallel, the sphingolipid composition of the cells was monitored by liquid chromatography, electrospray ionization tandem mass spectrometry. These analyses revealed that Kdo_2-Lipid A and fenretinide induce profound changes in sphingolipid metabolism in RAW264.7 and MCF7 cells, respectively, and that one of the purposes for increased *de novo* biosynthesis

is to enable the production of autophagosomes, as the autophagic response was inhibited by myriocin.

These studies have uncovered a direct link between sphingolipid metabolism and autophagy, which could pave the way for new therapeutic interventions for the treatment of pathogenic infection and be clinically useful in enhancing the efficacy of current cancer treatment strategies.

CHAPTER 1

SPHINGOLIPIDS: STRUCTURE, SYNTHESIS, AND SIGNALING

1.1 Structural Diversity of Sphingolipid Species

Sphingolipids (SL) are a complex family of phospho- and glycolipids found in essentially all eukaryotic and some prokaryotic organisms and viruses, as components of membranes and other biological structures where they influence cell structure, signaling, and interactions with the extracellular environment [1, 2]. SL are comprised of novel amine-containing sphingoid base backbones (2-aminoalka[ane or ene] 1,3 diols) that are distinguishable by chain length, the number of double bonds, and the presence of additional hydroxyls using the nomenclature depicted in Fig. 1.1 [1]. The diversity of sphingoid base backbones varies across different organisms with humans having primarily sphinganine (Sa), sphingosine (So), and 4-hydroxysphinganine (phytosphingosine) (Fig. 1.1) [1]. The sphingoid base backbone may be unmodified, phosphorylated, glycosylated, or otherwise modified through the addition of various headgroups at the primary hydroxyl and (or) an amide-linked fatty acid typically ranging from 14-30 carbons in length that is usually saturated, or with a single double bond (Fig. 1.1) [1, 2]. Due to the combinatorial nature of SL biosynthesis, these backbone, headgroup, and acyl chain variations give rise to tens of thousands of mammalian SL species (www.sphingomap.org), and knowledge about the types and amounts of these subspecies can be imperative to understanding both the intracellular and extracellular signaling consequences of various stimuli, including immune effectors and chemotherapeutic agents as discussed herein [2].

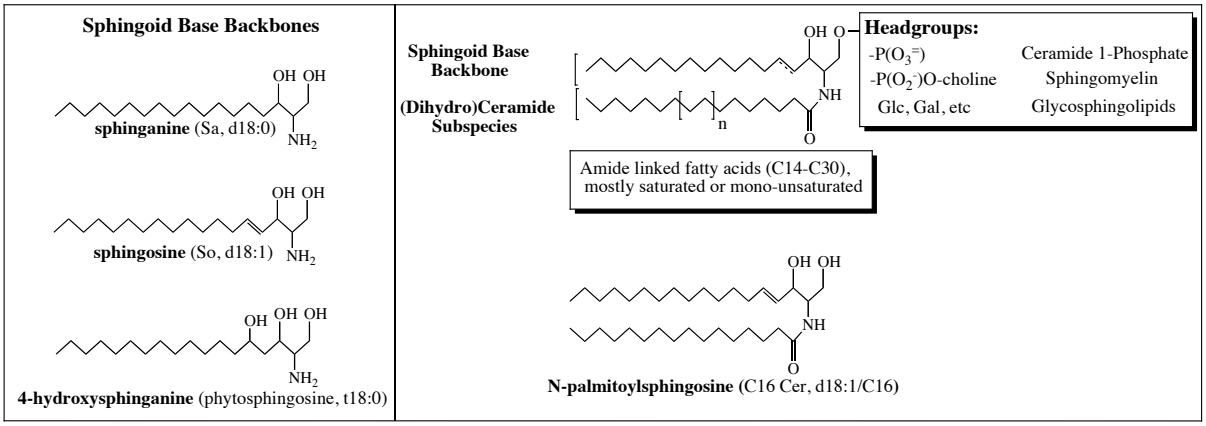

Figure 1.1 Representative Structures of Sphingoid Base Backbones and Modifications
Abbreviations: d18:0, dihydroxysphingoid base with two hydroxyl groups, 18 carbons, and no double bonds; d18:1, dihydroxysphingoid base with two hydroxyl groups, 18 carbons, and one double bond; t18:0 trihydroxysphingoid base with three hydroxyl groups, 18 carbons and no double bonds; Glc, glucose; Gal, galactose. After the addition of an amide linked fatty acid to form a (dihydro)ceramide species, the sphingoid base notation is followed by a semicolon or slash and identification of the carbon chain length and number of double bonds contained in the attached fatty acid, as shown for C16 Cer. This figure was adapted from [1].

1.2 Synthesis of Sphingolipid Species

1.2.1 *De novo* Biosynthetic Pathway

A significant portion of SL is derived from *de novo* biosynthesis in most organisms [3]. As a result, the first enzyme of the pathway serine palmitoyltransferase (SPT) is essential for the survival of cells in culture [3-5] and elimination of this enzyme has been found to be embryonic lethal for mice [3, 6] and fruit flies [3, 7]. As shown in Figure 1.2, SL biosynthesis *de novo* begins with the condensation of L-serine and palmitoyl-CoA to form 3-ketosphinganine (3KSa) catalyzed by SPT [1, 8]. This is followed by the rapid reduction of 3KSa to Sa by 3-ketosphinganine reductase (3KSR) [1, 9]. Sa is then phosphorylated by sphingosine kinase (SphK) to form sphinganine 1-phosphate (Sa1P) [3, 10] or N-acylated by a family of (dihydro)ceramide synthases (CerS) [3, 11]. To date, six CerS have been identified [1, 3, 12]. Each of these enzymes utilizes fatty acyl-CoA substrates of relatively defined chain lengths, as depicted in Fig. 1.2, resulting in the formation of distinct dihydroceramide (DHCer) subspecies [1, 13] which are, in most cases, desaturated by dihydroceramide desaturase (DES), resulting in the formation of ceramides (Cer) with acyl chains of various lengths [1, 14, 15]. Cer serves as the major branchpoint for the formation of more complex SL species [3], such as, sphingomyelin (SM) (through the addition of a phosphoryl choline headgroup by sphingomyelin synthase (SMS) [16-18]), Cer 1-phosphate (Cer1P), (via phosphorylation by ceramide kinase (CERK) [19, 20]), and monohexosylceramides (MH-Cer), (specifically glucosylceramide (GlcCer) and galactosylceramide (GalCer), through the addition of glucose or galactose from a sugar nucleotide by UDP-Glc:Cer glucosyltransferase (GlcCer synthase) or UDP-Gal:Cer galactosyltransferase (GalCer

synthase), respectively [3, 21, 22], which serve as precursors for the formation of hundreds of complex glycosphingolipids (GSL) [3]). Although, the majority of DHCer is desaturated to form Cer, it is worth noting that SMS [18], CERK [20], GlcCer synthase [23], and GalCer synthase [24] can accept DHCer subspecies as substrates in order to form the corresponding dihydrosphingolipids (DHSL), as depicted in Fig. 1.2.

1.2.2 Turnover Pathway

Cellular metabolic homeostasis of the sphingolipidome is often achieved through the coordinate biosynthesis and removal of SL species requiring a delicate balance between *de novo* biosynthesis, turnover, and recycling [3]. Therefore, in addition to *de novo* biosynthesis, (DH)Cer may also be produced from the breakdown or turnover of complex SL via the action of specific hydrolases, including sphingomyelinases, glycohydrolases, and lipid phosphatases (Fig. 1.2) [1]. (DH)Cer can also be further metabolized by the action of ceramidases, which catalyze the hydrolysis of (DH)Cer into the free fatty acid and the sphingoid base, Sa or So (Fig. 1.2) [1, 25-29]. The produced Sa and/or So is then subject to one of two fates: 1) it can be recycled via reacylation for entry back into the SL pathway [1, 30] or 2) it can be phosphorylated by SphK producing sphinganine 1-phosphate (Sa1P) or sphingosine 1-phosphate (S1P) [1, 31]. In turn, the sphingoid base phosphate can be de-phosphorylated through the action of specific phosphatases [1, 32] or irreversibly degraded through the action of sphingosine 1-phosphate lyase (lyase) to form ethanolamine phosphate and hexadec(an/en)al [1, 3, 33], which may be reduced to palmitate for re-incorporation into SL biosynthesis [1, 3, 34].

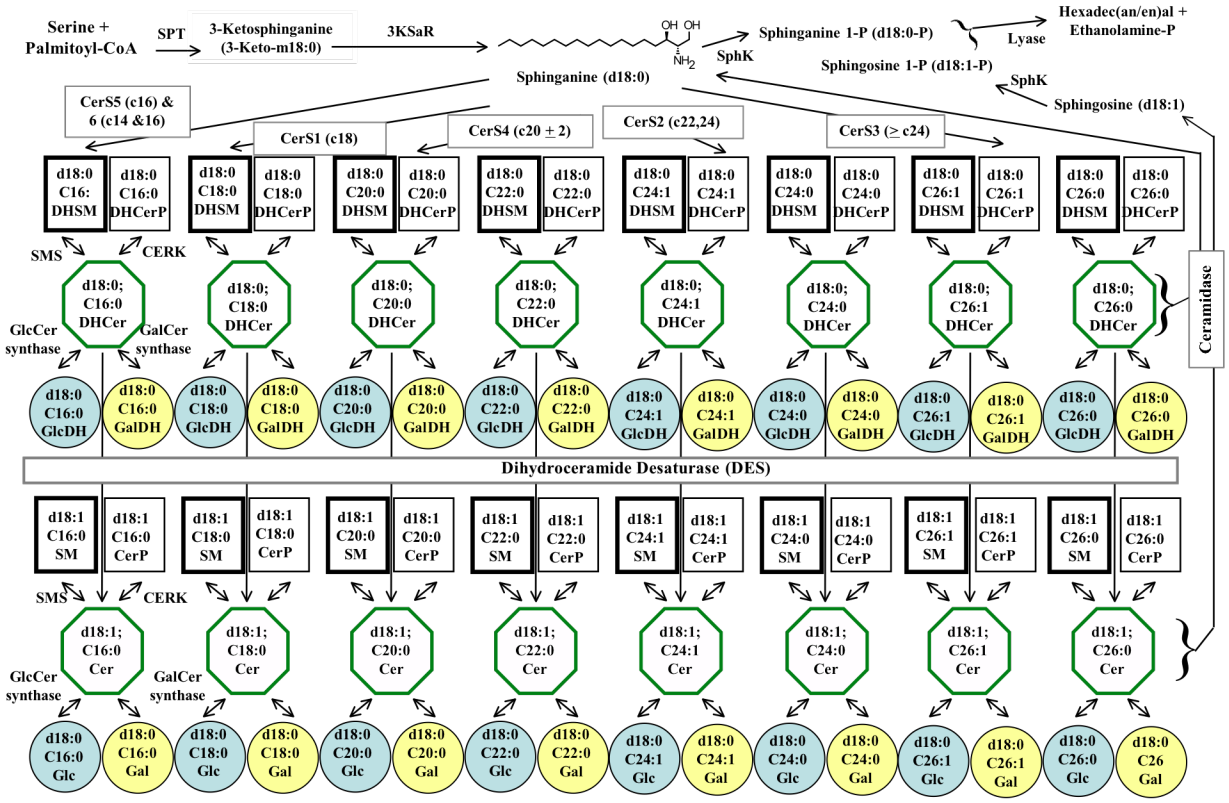

Figure 1.2 Sphingolipid Metabolism Pathways for *de novo* biosynthesis and turnover are shown as described in the text. Key: Sphingoid bases are depicted as (dx:y). Fatty acyl chains are depicted as (cx:y). Abbreviations: SPT, serine palmitoyltransferase; 3KSaR, 3-ketosphinganine reductase; SphK, sphingosine kinase; CerS, ceramide synthase; DHSM, dihydrosphingomylin; DHCerP, dihydroceramide phosphate; DHCer, dihydroceramide; GlcDH, glucosyldihydroceramide; GalDH, galactosyldihyroceramide; SM, sphingomyelin; CerP, ceramide phosphate; Cer, ceramide; Glc, glucosylceramide; Gal, galactosylceramide. Different sphingolipid species are identified as follows: green octagon, (DH)Cer; heavy black boxes, (DH)SM; thin gray boxes, (DH)CerP; blue circles, glucosyl(DH)Cer; and yellow circles, galactosyl(DH)Cer. This figure was adapted from [3].

1.2.3 Subcellular Localization of Sphingolipid Biosynthesis and Turnover

As shown in Figure 1.3, the enzymatic reactions of SL biosynthesis and turnover are distributed throughout various cellular compartments. SL biosynthesis *de novo* begins on the cytoplasmic surface of the endoplasmic reticulum (ER) [1, 9, 35]. Once formed in this compartment, Cer is trafficked to the Golgi complex (GC), where it can be converted into SM, Cer1P, and GlcCer, which serves as a precursor for more complex GSL [1]. Two distinct trafficking pathways have emerged for the transport of Cer from the ER to the GC [1, 35, 36]. Ceramide transfer protein (CERT) mediates the ER-to-GC trafficking of Cer via a suggested non-vesicular transport mechanism to the *cis* and medial GC for the synthesis of SM [1, 35-37] and to the *trans*-GC for the synthesis of Cer1P [3, 38]. A second vesicular transport pathway exists for the delivery of Cer to the GC for the synthesis of GlcCer [35, 36, 39]. In turn, GlcCer is transported by the recently identified golgi-associated four-phosphate adaptor protein 2 (FAPP2) to the distal golgi compartments for the synthesis of complex GSL [3, 35, 36, 40]. SM, CerP, and GSL are then trafficked from the GC to the plasma membrane through a vesicular transport mechanism where they become important components of plasma membrane structure and participate in numerous signaling events [3, 35, 41, 42]. In contrast to SM, Cer1P, and GlcCer, GalCer is synthesized from Cer in the lumen of the ER where it can be further diversified by sulfation into sulfatides [3, 43], which are trafficked to the plasma membrane where they participate in cell adhesion [3, 44].

The plasma membrane serves as one site for the turnover of SM, Cer1P, and GSL to Cer, as well as the downstream metabolites So and S1P [35]. SM and GSL can also be trafficked from the plasma membrane to other intracellular compartments such as the

lysosome, via the endocytic pathway, where they can be degraded by the action of sphingomyelinases and glucosidases to form Cer, which is further metabolized to So [1, 27]. The newly formed So is able to exit the lysosome and shows adequate cytosolic solubility to move between membranes including the ER, where it can be recycled for continued SL biosynthesis [35]. Additionally, Cer (and possibly other SLs) have recently been found to be components of intracellular membraneous vacuoles known as autophagosomes [3, 45], which acquire of lysosomal hydrolases in order to become autophagolysosomes as part of their degradation mechanism [3]. Therefore, it is likely that this compartment serves as another site of Cer hydrolysis [3].

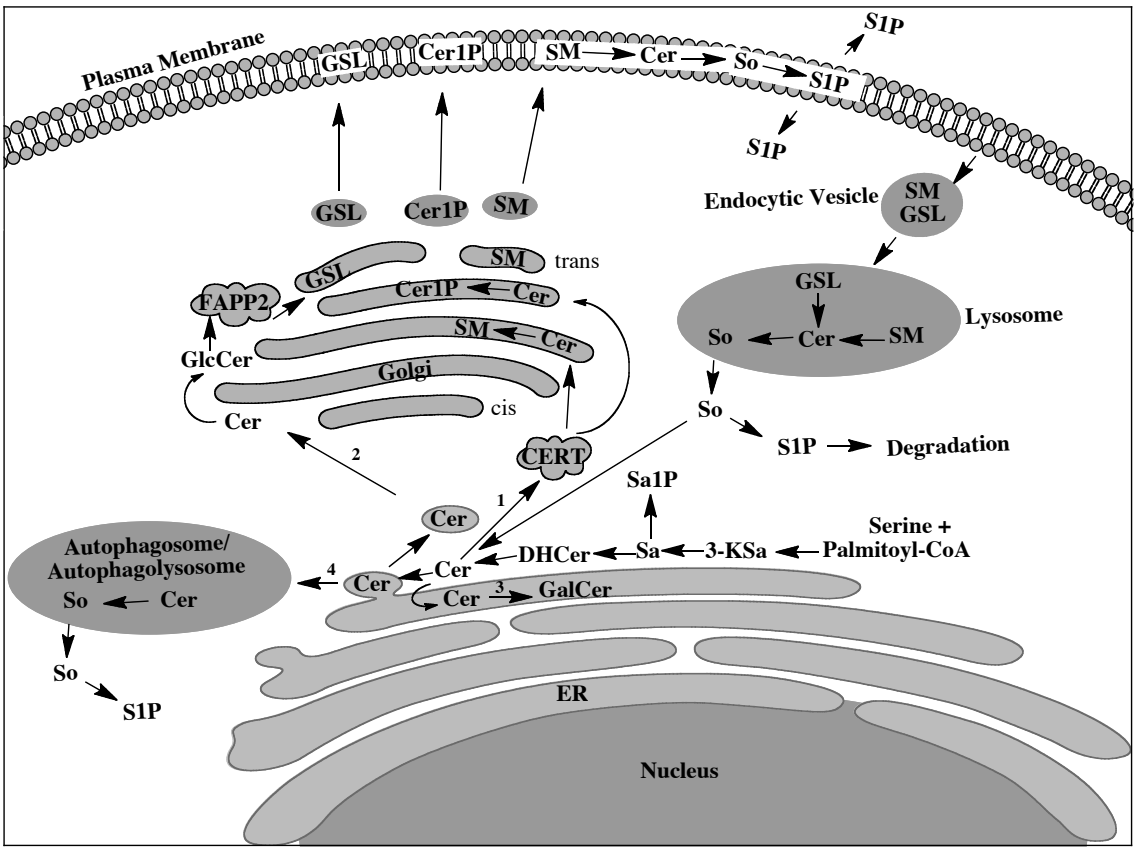

Figure 1.3 Schematic Representation of the Trafficking and Compartmentalization of Sphingolipid Metabolism This diagram shows the *de novo* biosynthetic pathway beginning in the ER with the condensation of serine and palmitoyl-CoA and leading to the formation of Cer. Cer may then be subject to several different fates: (1) It may be transported to the golgi via CERT-mediated trafficking for the synthesis of SM or Cer1P. (2) It may be delivered to the golgi via vesicular transport for the synthesis of GlcCer followed by the transfer of GlcCer to the lumen of the distal golgi via the action of FAPP2 for complex GSL biosynthesis. (3) It may be transported to the lumen of the ER for synthesis of GalCer. or (4) It may be incorporated into other intracellular compartments such as autophagosomes. Synthesized SM, Cer1P, and GSL are then delivered to the plasma membrane. Also shown is the turnover of SM via sphingomyelinases at the plasma membrane to Cer and downstream metabolites, So and S1P. Additionally, SM and GSL can be internalized through the endocytic pathway and trafficked to the lysosome where turnover takes place via the action of sphingomyelinase and ceramidase. Sphingosine (So) may then exit the lysosome and be recycled back into biosynthesis or phosphorylated and degraded. Also shown is the hypothesized hydrolysis of Cer to So within the autophagolysosome. This figure was adapted from [1, 35].

1.3 Signaling: Focus on Autophagic Pathway

SL such as So, Cer, S1P, and Cer1P are well documented to serve as important bioactive molecules involved in numerous cellular processes including, among others, growth, differentiation, inflammation, and apoptosis [1, 36]. These SL molecules directly regulate several downstream targets, which mediate their affects on cellular functions [1, 36]. For example, So has been found to induce apoptosis [46] and prevent the phorbol-ester dependent differentiation of promyelocytic leukemia cells (HL-60) [47], as well as inhibit cellular growth through cell cycle arrest in lymphoblastic leukaemic cells (Molt-4) [48]. These effects are, at least in part, modulated by the So-induced inhibition of protein kinase C (PKC) [49]. Additionally, Cer is known to be involved in the regulation of numerous apoptotic signaling pathways through the activation of its direct targets including, phosphoprotein phosphatases 1 and 2A [1, 50-54], many members of the PKC family [1, 55-57], and cathepsin D [1, 58, 59]. In contrast to the effects of So and Cer on cell growth and survival, S1P promotes proliferation and inhibits apoptosis with the delicate balance between these opposing molecules (So and Cer vs S1P) thought to be an important determinant of cell fate [60]. Furthermore, the phosphorylation of Cer to produce Cer1P has been associated with DNA synthesis [61], inhibition of apoptosis [62], and activation of cytosolic phospholipase A(2) (cPLA2) and the production of eicosanoids in response to inflammatory agonists [63]. In addition to the effects of these SL on the cellular functions discussed above, several of the aforementioned SL, including Cer and S1P, as well as a previously unrecognized bioactive SL, DHCer, have also been found to mediate an essential cellular process known as autophagy, which contributes to both normal cell functioning as well as disease [1, 35, 60].

1.3.1 Autophagic Process

Translated from Greek meaning “to eat oneself”, autophagy is an intracellular degradation and recycling pathway mechanism that is, in various forms, ubiquitous in eukaryotic cells, from yeast to mammals [64-66]. Indeed, genetic studies in yeast have identified many autophagy-related (ATG) genes essential for autophagy that are highly conserved across eukaryotes [67]. Conceptually, autophagy can be thought of as a seven-step process that involves (1) induction, (2) nucleation, (3) expansion, (4) completion, (5) fusion, (6) degradation, and (7) export (Fig. 1.4) [64-67].

Under normal conditions, a basal level of autophagy occurs as a housekeeping function in order to eliminate damaged or aged organelle and proteins [67]. However, cellular stresses such as nutrient starvation, pathogen infection, various drug treatments, and other environmental factors can induce a more dramatic autophagic response [67]. The induction of autophagy, in many cellular settings, is regulated by a serine/threonine kinase, mammalian target of rapamycin (mTOR) (Fig. 1.4), whose activity is inversely correlated with autophagy induction [68-71]. The mechanism by which mTOR interferes with autophagy induction in mammalian cells is currently unknown [68-71]. However, in yeast, mTOR affects autophagy by modulating the phosphorylation status of ATG protein 13 (Atg13) (Fig. 1.4) [68-71]. Activated mTOR phosphorylates Atg13 at multiple sites reducing its affinity for ATG protein 1 (Atg1), an evolutionarily conserved serine/threonine kinase required for autophagosome formation [68-71]. Atg1 associates with several autophagy proteins in addition to Atg13, including Atg17, Atg29, and Atg31 [68-71]. However, the interaction with Atg13 is required for Atg1 kinase activity [68-71]. Thus, activation of mTOR results in the suppression of autophagy [68-71]. In contrast,

the inhibition of mTOR represses Atg13 phosphorylation and the hypo-phosphorylated Atg13 associates with Atg1 promoting kinase activity and autophagy induction [68-71]. Recently, a mammalian ortholog of Atg1, which is required for autophagosome formation in both Hek293 and HeLa cell lines, has been identified, ULK (UNC-51-like kinase); however, the mammalian ortholog of yeast Atg13, Atg17, Atg29, and Atg31 have yet to be identified limiting the complete understanding of autophagy induction in mammalian systems and how the regulation of these processes couple with activation of vesicle nucleation and expansion (discussed below) [68-71].

During autophagic vesicle nucleation and expansion, proteins and/or organelles to be degraded are sequestered into double membrane intermediate vesicles known as autophagosomes [67]. Although the exact origin of the membrane of the mammalian autophagosome is controversial, studies have found that it is likely derived from a lipid bilayer formed from the ER and/or the trans Golgi network; however, *de novo* membrane formation from cytosolic lipids can not be excluded [72, 73]. The mechanisms of nucleation and expansion, which are still in the infancy of understanding, depend on the step-wise recruitment of specific ATG proteins, including two ubiquitin-like conjugation systems (Fig. 1.4) [67]. The initial step of vesicle nucleation involves the activation of Vps34, a mammalian phosphatidlyinositol 3-kinase, to generate phosphatidlyinositol-3-phosphate, which is essential for elongation and recruitment of Atg proteins to the membrane [72, 74]. Activation of Vps34 catalytic activity occurs via its association with Atg6/Beclin1 in a multiprotein complex [72, 74]. The mechanism by which this complex promotes autophagy has yet to be determined; however, the interaction between Beclin1 and Vps34 is essential for Vps34 kinase activity and thus vesicle nucleation [69, 70, 74].

Beclin1 binding partners associated with the complex have been found to influence the activation of Vps34 [69, 70, 74]. For example, the association of UV irradiation resistance-associated tumor suppressor gene (UVRAG) with the complex has been found to promote Vps34 kinase activity and positively regulate autophagy; whereas association of the anti-apoptotic Bcl-2 protein has been found to inhibit Vps34 kinase activity and negatively regulate autophagy [69, 70, 74-76]. As described by Liang and co-workers, these two binding proteins represent the so-called "Yin-Yang" regulatory mechanism, which keeps autophagy within a normal range at the basal level [75]. However, following the addition of cellular stressors, such as those described above, Bcl-2 dissociates from the complex, whereas UVRAG remains disrupting the homeostatic balance and promoting increased autophagy [75, 76].

Elongation of the nascent autophagosomal membrane requires two ubiquitin-like conjugation systems (Fig. 1.4) [72, 74]. In the first, Atg12 is complexed to Atg5 in an ATP-dependent manner with Atg7 acting as an E1 activating enzyme and Atg10 acting as an E2 carrier protein [72, 74]. The Atg12-Atg5 complex then pairs with Atg16 dimers to form a multimeric complex, which is thought to induce curvature in the growing membrane through asymmetric recruitment of LC3-II (discussed below) [72, 74]. Once autophagosome formation is complete, the Atg12-Atg5-Atg16 multimer dissociates from the membrane [72, 74]. The second ubiquitin-like system facilitates the conjugation of phosphatidylethanolamine with Atg8 mammalian homologue, microtubule-associated protein 1 light chain 3 (LC3) [72, 74]. Following synthesis, nascent LC3 is cleaved by a protease, Atg4, exposing a glycine residue at its C-terminus and forming a species known as LC3-I [72, 74]. The carboxyterminal glycine is then activated in an ATP-dependent

manner by E1-like Atg7, transferred to E2-like Atg3 and conjugated to phosphatidylethanolamine becoming the LC3-II species [72, 74]. While LC3-I displays a cytosolic localization, LC3-II associates with both the outer and inner portions of the autophagosomal membrane, where it is thought to play a role in the hemifusion of membranes [72, 74].

The autophagosome is completed following the fusion of the two membrane extremities [67]. The completed autophagosome then fuses with the lysosome to form the autophagolysosome, where the sequestered proteins and/or organelle are degraded by lysosomal hydrolases in a process requiring cathepsins B and D [72]. Finally, the resulting amino acids are exported to allow for ongoing cellular maintenance [67].

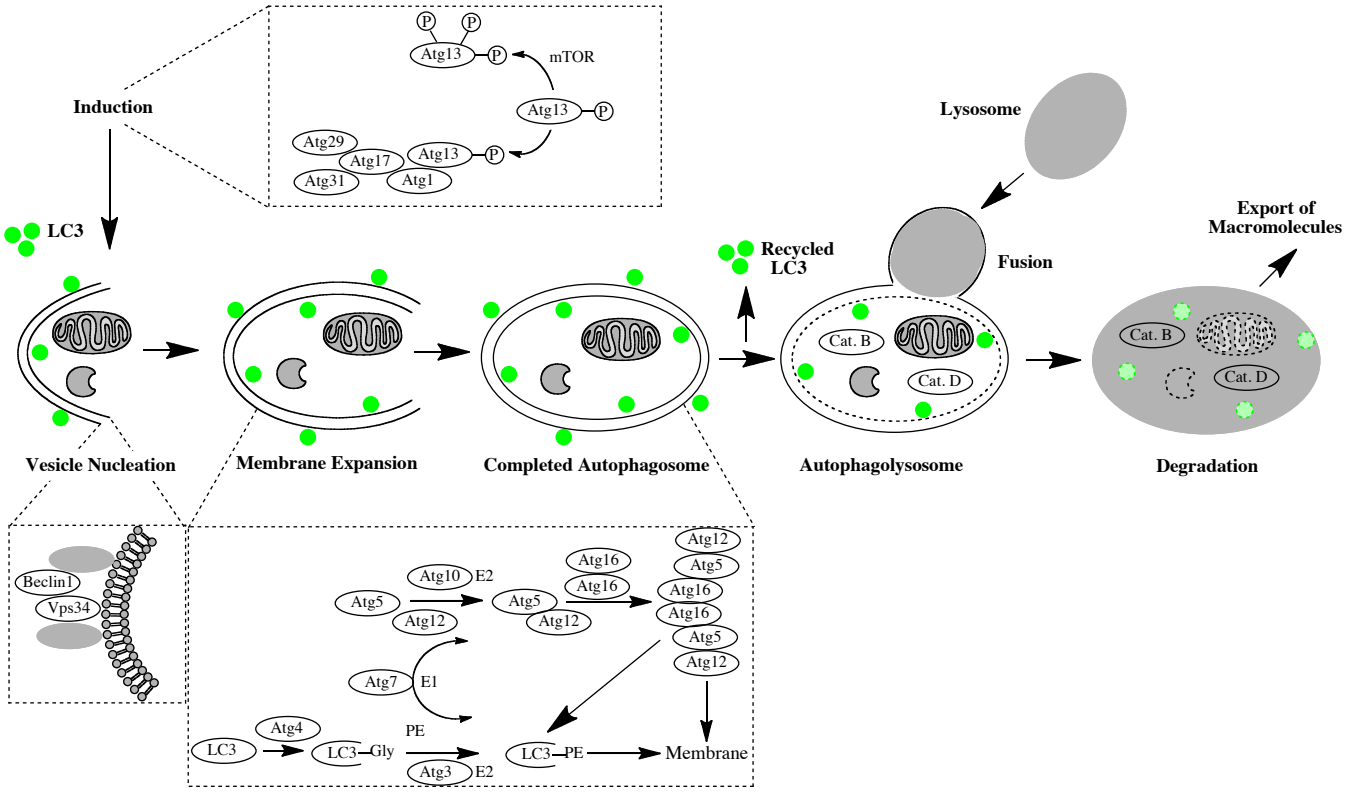

Figure 1.4 The Autophagic Process Following induction, autophagy begins with the nucleation of the isolation membrane, which engulfs cytosolic proteins and/or organelle to be degraded. LC3 is recruited to the isolation membrane, where it facilitates membrane elongation and closure to form the autophagosome. Upon completion, the autophagosome fuses with the lysosome and the LC3 on the outer portion of the autophagosomal membrane is recycled. Finally, the LC3 on the inner portion of the autophagolysosomal membrane and the engulfed proteins/organelle are degraded by lysosomal proteases and the resulting macromolecules are exported for continued cell maintenance. Also shown is the control of induction by mTor, as well as vesicle nucleation and membrane expansion/completion by the Vps34/Beclin-1 protein complex and Atg12-Atg5 and LC3 conjugation systems, respectively, as described in the text. This figure was adapted from [67, 68, 71].

1.3.2 Methods for Monitoring Autophagy

Studies of autophagy frequently use cells that stably or transiently express a green-fluorescent-protein (GFP)-tagged LC3 protein (GFP-LC3) [77-80], as depicted in Figure 1.4. Because LC3-I displays a cytosolic localization and LC3-II associates with both the outer and inner portions of the autophagosome, the activation of autophagy within cells stably or transiently expressing GFP-LC3 results in the appearance of LC3-II puncta [80]. Following fusion with the lysosome, the LC3-II on the outer portion of the membrane is recycled, and the LC3-II on the inner portion of the membrane is degraded with the sequestered proteins and/or organelle [80]. Therefore, GFP-LC3 is either visualized by fluorescence microscopy as diffuse throughout the cytosol or as discreet punctate vesicles representing autophagosomes and/or autophagolysosomes [79, 80].

It is worth noting that the use of transiently transfected cells is not recommended for assays of autophagy due to the aggregate prone nature of the GFP-LC3 protein when transiently overexpressed [79-81]. This pitfall may be avoided through the use of stable transfectants with a selection of clones that express appropriate levels of GFP-LC3 without non-specific aggregation [79-81]. Additionally, transfection reagent itself has been found to be a potent inducer of autophagy resulting in the possibility of a potentially false interpretation of autophagy induction when transfection reagent is used during experimental conditions and further emphasizing the importance of using GFP-LC3 stable transformants for autophagy analysis [82].

Quantitative analysis of GFP-LC3 puncta, and thus autophagic induction, is reported as the number of GFP-LC3 puncta/cell or as the percentage of cells with GFP-LC3 associated autophagosomes [79, 80]. In order to remove subjectivity and provide

consistency between independent experiments, a uniform method must be defined for determining 'puncta' regardless of the reporting method [79, 80]. This can be achieved through the use of software such as ImageJ, which allows the user to define both the fluorescence threshold, as well as the size threshold of the desired 'puncta'. Additionally, if the results are reported as the percentage of cells with GFP-LC3 autophagosomes, a third threshold should be established in order to distinguish 'autophagy active' cells since low numbers of puncta may be observed even under basal conditions due to the housekeeping functions of autophagy [79, 80].

In addition to fluorescence microscopy, biochemical assays can also be used to monitor autophagy. The conversion of LC3-I to LC3-II can be followed via SDS-PAGE and Western blotting [79, 80, 83]. Interestingly, although the molecular weight of LC3-II is greater than that of LC3-I, LC3-II experiences an increased mobility and migrates faster than LC3-I in SDS-PAGE [79, 80, 83]. This is thought to be due to the extreme hydrophobicity of LC3-II following its conjugation with phosphatidylethanolamine [79, 80, 83]. It is important to note that the conversion of LC3-I to LC3-II is a measure of phosphatidylethanolamine conjugation and not processing, as would be predicted by the apparent size reduction when monitoring SDS-PAGE [79, 80, 83]. LC3-I has a molecular mass around 16 kDa, and LC3-II is usually detected around a molecular mass of 14 kDa [79, 80, 83]. The amount of LC3-II correlates with autophagosome formation, and thus, it can be used as an indicator of autophagy induction [79, 80, 83].

Finally, in some cases, the induction of autophagy is accompanied by an increase in the mRNA expression of some of the aforementioned ATG genes, such as *Atg8/LC3* and *Atg12* [79, 84, 85]. Although, it is not currently clear whether increases in mRNA are

sufficient to induce autophagy, mRNA measurements may provide correlative data to support the other assay methods described above [79].

1.3.3 Autophagy: Relevance to Disease

Although the primary function of autophagy is to aid in the adaptation of cellular stress by enabling cells under adverse conditions to degrade cytosolic proteins and organelles in order to generate a supply of essential nutrients, autophagy has also been implicated in the pathogenesis of many diseases, including cancer [67, 86]. And more recently, autophagy has been identified as a component of innate immunity where it is involved in host defense and elimination of intracellular bacterial pathogens [67, 87-89].

Although the immune system is usually successful in eliminating pathogenic organisms, which target macrophages or epithelial cells and enter these cells via phagocytosis or by facilitating their own uptake [67]. Some pathogenic organisms effectively combat cellular defenses once inside the cell, and escape into the cytosol or modify the phagosome in order to establish a replicative niche within this vesicle [67, 89]. In these cases, a second line of defense may be activated -- autophagy -- in order to effectively eliminate these organisms. For example, *L. monocyogenes*, a virulent foodborne pathogen, readily escapes the phagosome following cellular entry, thrives on cytosolic nutrients, and begins to replicate within the host cell [89, 90]. Treatment of *L. monocyogenes* infected macrophages with the antibiotic chloramphenicol, which induces the expression of autophagy gene *Atg12* (discussed above) [91], sequesters the bacterium into double-membraned autophagosomes allowing for their removal from the cytosol and subsequent degradation within the autophagolysosome [90]. In addition to sequestering cytosolic bacterial pathogens, the induction of autophagy has also been shown to promote

the maturation of arrested phagosomes that have been transformed by certain pathogenic organisms into protective environments within the cell where they may survive and reproduce [67, 89]. *M. tuberculosis*, the causative agent of tuberculosis, readily persists and reproduces inside the phagosome ultimately forcing the lysis of the macrophage host cell and the release of mycobacteria into neighboring cells [67, 92]. Alternatively, the induction of autophagy in infected macrophages results in the fusion of the mycobacteria containing phagosomes with autophagosomes, degradation of the bacteria, and ultimately survival of the host cell [92]. Interestingly, the emergence of multi-drug resistant *M. tuberculosis* and other infectious strains are becoming a major health concern throughout the world [93]. With this in mind, the development of new therapeutic intervention strategies to supplement existing therapies is a high priority [93]. The research described herein [Chapter 2 and [45]] looks at the ability of an agent, which induces changes in SL metabolism, to be an effective inducer of autophagy in macrophage cells. Thus, paving the way for new therapeutic interventions that outsmart pathogens by modulation of autophagy through manipulation of the SL pathway.

Paradoxically, in addition to its role in cell survival, activation of autophagy can also be induced as part of a cell death response, and the accumulation of autophagosomes is characteristic of "type II" or "autophagic" cell death [1, 67]. One example of the dual role of autophagy is evident in cancer therapy [70, 94]. In tumor cells, autophagy is often observed in response to chemotherapy and radiation where it sometimes functions as a survival pathway in order to generate a supply of essential nutrients and re-establish cellular homeostasis during times of metabolic stress, as a means to prevent apoptotic cell death [70]. In these cases, the inhibition of autophagy provides a means to sensitize tumor

cells to chemotherapeutic agents [70]. For example, treatment of the chronic myelogeous leukemia cell line, K562, with imatinib, a currently used chemotherapeutic that inhibits tyrosine kinase activity, activates autophagy as a survival mechanism in order to avoid or delay apoptotic cell death [70, 95]. However, the inhibition of autophagy, through the use of pharmacological agents or the downregulation of autophagy genes with siRNA, accelerated the cell death response suggesting that the combination of autophagy inhibitors with conventional chemotherapeutic drugs could be valuable in the treatment of chromic myelogenous leukemia [95].

Conversely, malignant cells often acquire genetic deletions or mutations that render them resistant to the classical apoptotic cell death induced by many anti-cancer therapies, which ultimately results in poor prognosis [69, 96]. In these cases, the use of autophagy inducing drugs offers an alternative way to induce cell death in apoptosis-resistant tumors [69, 96]. One example of this principle involves treatment of MCF7 breast cancer cells, which do not express caspase-3 [97-99], a cysteine protease that plays a central role in executing apoptosis [97], with 4-hydroxyphenylretinamide (fenretinide; 4-HPR), a chemotherapeutic agent which has shown success *in vitro*, in animal experiments, and in select clinical trails [100]. The cytotoxic effects of 4-HPR, in many cancer lines, have been attributed to the induction of apoptosis and caspase activation [100]. However, treatment of apoptotic defective-MCF7 cells with 4-HPR, was found to result in cytotoxicity through the induction of autophagic cell death, as well [99]. This study supports the role of autophagy induction in the activation of an alternative cell death pathway in apoptotic defective cells as a means to increase cancer therapeutic efficacy [99]. This idea could prove to be particularly important in breast cancer, as a

recent study of malignant breast tissue samples revealed that 75% of the analyzed tissues were apoptotic defective lacking both transcription and expression of caspase-3 [96, 101].

Chapters 3 and 4 of this work explore the ability of the promising chemotherapeutic agent, 4-HPR, to alter SL metabolism and the role of SL biosynthesis in 4-HPR-induced autophagy and autophagic cell death. Additionally, Chapter 4 examines the ability of known modulators of SL biosynthesis to enhance 4-HPR-induced autophagic cell death, as a promising approach to improve cancer chemotherapy, particularly in apoptotic-defective breast cancer cells.

1.3.4 Sphingolipids and Autophagy

Because of their involvement in membrane organization and structure, as well as their participation in cell survival and cell death signaling pathways (as briefly discussed above) it is easy to imagine that SL might be unique mediators of autophagy. Indeed, bioactive SL species, including Cer, S1P, and most recently DHCer have been shown mediate two autophagic pathways, described as protective autophagy and autophagic cell death, which display opposing functions on cell fate [1, 102-110].

Several studies have elegantly established the ability of exogenous Cer to mediate autophagy [1, 102, 104, 105]. In colon (HT-29), breast (MCF7), and cervical (HeLa) cancer cells, C2-Cer and/or C6-Cer treatment has been found to stimulate autophagy by inhibiting the mTOR signaling pathway [102], which plays a central role in autophagy induction (discussed above), as well as by upregulating the transcription and expression of Beclin1[102] and promoting the dissociation of the Beclin1/Bcl-2 complex [104], which is important for vesicle nucleation and expansion (discussed above). C2-Cer treatment has also been associated with the induction of autophagic cell death in

malignant glioma (U373-MG and T98G) through activation of BNIP3, a mitochondria-associated protein that induces nonapoptotic cell death [105]. In addition to the induction of autophagy by short-chain Cer, current and potential anti-cancer agents, such as tamoxifen and Δ^9-tetrahydrocannabinol (THC), respectively, have been shown to induce autophagic cell death by increasing endogenous Cer [102, 104, 106, 111]. For example, treatment of MCF7 and HeLa cells with tamoxifen mimicked the effects exogenous of Cer, promoting autophagosome formation through inhibition of the mTOR signaling pathway [102], up-regulation of Beclin1/Atg6 [102], and promotion of the dissociation of the Beclin1/Bcl-2 complex [104]. Interestingly, inhibition of *de novo* Cer biosynthesis with the SPT inhibitior, myriocin/ISP1, prevented the tamoxifen-induced accumulation of autophagic vesicles [102, 104] suggesting that Cer made via the *de novo* biosynthetic pathway is an important mediator of autophagic cell death following treatment with this chemotherapeutic agent. Additionally, increases in *de novo* Cer production upstream of mTOR inhibition implicate this bioactive SL species in the THC-induced autophagic cell death of glioblastoma (U87MG) cells [106].

Whereas Cer-induced autophagy has been associated with autophagic cell death, increases in endogenous S1P have been found to induce survival-mediated or protective autophagy in MCF7 breast cancer cells during times of nutrient starvation [103, 112]. Inhibition of SphK with siRNA suppressed autophagy and increased cell death following starvation [103, 112]. Distinct from Cer-induced autophagy, S1P-induced autophagy acts independently of an increase in Beclin1 expression; however, inhibition of the mTOR-signaling pathway was observed [103, 112]. Interestingly, S1P-mediated autophagy was not inhibited by fumonisin B1 (FB1), an inhibitor of CerS, indicating that its mechanism

is not dependent on Cer formation [103]. Consistent with the Cer-independent effect, inhibition of sphingosine-1-phosphate phosphohydrolase-1 (SPP1), the enzyme that dephosphorylates S1P and Sa1P in the ER, was found to induce autophagy in the absence of alterations to Cer or DHCer species; whereas, S1P and Sa1P were significantly increased [107]. Furthermore, pharmacological inhibition of SphK with 3-(4-chlorophenyl)-adamantane-1-carboxylic acid (pyridin-4-ylmethyl)amide (ABC294640) induces autophagic cell death in various carcinoma cell lines [108], which is likely due to the inhibition of S1P induced protective autophagy and/or an accumulation of Cer.

In addition to the above investigations, DHCer has been most recently identified as a third SL-mediator of autophagy [1, 109, 110]. The ability of exogenously added DHCer to activate autophagy, as well as the ability of the anti-cancer agent 4-HPR to induce autophagy through increases in endogenous DHCer was first documented in the DU145 prostate cancer cell line [1], and these findings are extended to the Hek293 and MCF7 cell lines in Chapter 3 and Chapter 4 of this work, respectively. These studies were quite surprising, as DHCer has long been regarded as an innocuous molecule due to its inability to activate *in vitro* targets of Cer or affect Cer-mediated signaling pathways [1]. Recent studies have provided additional support for this finding and demonstrated the ability of exogenous increases in DHCer, via inhibition of DES, to induce both protective autophagy and autophagic cell death [109, 110]. For example, treatment of gastic cancer cells (HGC-27) with resveratrol is accompanied by a robust accumulation of autophagic vesicles in the absence of cellular toxicity [109]; while, treatment of prostate cancer cells (PC-3 and LNCaP) with gamma-tocotrienol resulted in autophagic cell death, which could be inhibited by ISP1 [110]. The idea that DHCer (and possibly other DHSL)

accumulation influences both protective autophagy and autophagic cell death is also apparent in Chapter 3 of this work, through a comparison of the cellular effects of 4-HPR and a novel DES inhibitor, 4-hydroxypalmitanilide (4-HPA). Intriguingly, none of the reported Cer-mediated autophagic pathways (discussed above) can be induced by both Cer and DHCer [102]; therefore, it is likely that novel signaling pathways and targets are responsible for this previously uncharacterized signaling function of DHCer and determine its effect on cell fate.

The studies described above provide evidence that bioactive SL have emerged as important effectors in regulating the autophagic pathway, as well as determining the associated cellular consequence, suggesting that SL might play a role in many, if not all forms, of autophagy. Thus the studies described herein provide further insight into the ability of bioactive molecules to influence SL metabolism and the ability of SL to regulate/induce autophagy in diverse cellular situations which could lead to novel strategies for manipulating autophagy in infection, cancer, and other disease.

1.4 Objective(s)

The over-arching objective of this study is to understand how two agents associated with infection and cancer treatment, Kdo_2-Lipid A (KLA) and 4-HPR, respectively, affect SL metabolism and the regulation of the autophagic pathway, through the use of lipidomic technologies, genomic analysis, and cellular biology techniques. Chapter 2 focuses on the ability of a TLR4 specific lipopolysaccharide (LPS), KLA, to induce changes in SL metabolism and to activate the autophagic pathway in RAW264.7 macrophage cells. In Chapter 3, the focus shifts to an analysis of the structural features 4-HPR that modulate SL metabolism, induction of autophagy, and sometimes cell death.

Chapter 4 examines the role of SL in 4-HPR-induced autophagic cell death in MCF7 breast cancer cells, as well as determines if autophagic cell death/cytoxicity can be enhanced through concurrent treatment with 4-HPR and other known modulators of SL biosynthesis. It is hoped that a better understanding of the inter-relationship between SL metabolism and autophagy will lead to new strategies for manipulating this process in infection, cancer, and other diseases.

CHAPTER 2

KDO_2-LIPID A, A TLR4 SPECIFIC AGONIST, INDUCES *DE NOVO* SPHINGOLIPID BIOSYNTHESIS, WHICH IS ESSENTIAL FOR THE INDUCTION OF AUTOPHAGY

2.1 Introduction

SL are a complex family of molecules [2] that participate in many facets of cell structure and function [35, 60]. For some categories of cells, such as macrophages, normal and abnormal functions have been associated with seemingly every SL subcategory, including So [113], S1P [114], Cer [115], Cer1P [116], SM [117], and both simple (e.g., GlcCer) [118] and more complex GSL [119-121]. Likewise, macrophage behavior can be modified by inhibition of *de novo* SL biosynthesis by L-cycloserine [122] and myriocin [123], and by SL analogs such as FTY720 [124], PCERA-1 (a Cer1P analog) [125], and α-galactosylceramide (α-GalCer) [126], *inter alia*.

As part of the characterization of the mouse macrophage lipidome by the LIPID MAPS Consortium (www.lipidmaps.org), the major SL subspecies of the mouse macrophage-like cell line, RAW264.7, have been quantified from the first detectable biosynthetic intermediate (Sa) through the branchpoint where Cer is partitioned into SM, Cer1P, GlcCer, and GalCer using liquid chromatography, electrospray ionization-tandem mass spectrometry (LC ESI-MS/MS) [127]. The Consortium has also investigated the effects of activation of these cells with KLA, a chemically defined substructure of bacterial LPS that is specifically recognized by the TLR4 receptor [128]. LPS has been previously reported to stimulate SL biosynthesis in liver [129] and extrahepatic tissues [130], and to elevate Cer in RAW264.7 cells by induction of turnover of pre-existing SL

[131]. Our studies have found that KLA nearly doubles the SL content of RAW264.7 cells, with increases in many of the SL subspecies summarized in the pathway scheme shown in Fig. 2.1. This report notes that two of the reasons that stimulated RAW264.7 cells have more SL are that KLA increases *de novo* biosynthesis but inhibits cell division, therefore, the size of the cells increases and they contain large numbers of intracellular vacuoles (autophagosomes). Induction of autophagy has previously been noted upon TLR4-activation and is thought to be important in phagocytosis and regulation of the inflammatory response [87, 132, 133]. This study has additionally established that *de novo* SL biosynthesis is required for autophagy, and that Cer are associated with autophagosomes, implying that they play structural and/or signaling roles in this important biochemical process.

2.2 Experimental Procedures

2.2.1 Materials

The suppliers for the reagents were: Kdo_2-Lipid A and the internal standard cocktail for SL analysis by LC ESI-MS/MS (Ceramide/Sphingoid Internal Standard Mixture II, LM-6005) (Avanti Polar Lipids, Alabaster, AL); [U-^{13}C] palmitic acid (98%) (Cambridge Isotopes, Andover, MA); fatty acid-free BSA (Calbiochem, La Jolla, CA); Hoechst 33342 (Invitrogen, Carlsbad, CA); myriocin/ISP1 (Biomol, Plymouth Meeting, PA); the mouse monoclonal antibody to SPT1 (anti-LCB1), anti-BiP/GRP78 and anti-GM130 (BD Biosciences, San Jose, CA); rabbit monoclonal anti-HA-tag and rabbit polyclonal LC3B antibody (Cell Signaling Technology, Boston, MA); mouse monoclonal anti-Cer antibody clone 15B4 (Alexis Biochemicals, San Diego, CA) This antibody clone has been successfully used in immunocytochemistry applications with no indication of

nonspecific reactions with other lipids [134-139]. The secondary Alexa Fluor-conjugated $F(ab)_2$ fragment goat anti-mouse antibody and goat anti-rabbit antibody were from Molecular Probes, Inc. (Eugene, OR.). The sources for liquid chromatography columns, solvents, and other reagents used for mass spectrometry were the same as in the published method [127].

2.2.2 Cells and Cell Culture

RAW264.7 cells were obtained from the American Type Culture Collection (Manassas, VA) and grown in DMEM (MediaTech, Manassas VA) supplemented with 10% heat-inactivated fetal calf serum (HyClone Logan, UT) and penicillin (100 U/mL) plus streptomycin (0.1mg/mL). The cells were maintained in a 37°C, 90% relative humidity, 5% CO_2 environment. All cell culture conditions, unless otherwise noted, followed the standard protocol adopted by the LIPID MAPS Consortium (www.lipidmaps.org): Warm the growth medium for 15 – 20 minutes in a 37°C water bath. After warming, place a volume of the warmed fresh medium into new vessels. (See below for plate size, cell density, and medium volume recommendations). To begin subculturing, aspirate the old medium from the cells and rinse them once with DPBS. Add fresh medium (~10 ml to 100 mm dish) to the cells and gently scrape the cells until all are dislodged. Pipette the cell suspension, with a 10 ml pipette, up and down five times, without introducing bubbles. Count the cells using a hemacytometer and dispense the cells into the new vessels growing the cells to no more than 80% confluence, (~2-3 days) before passing or harvesting. Recommended cell seeding and media volume for specific plate formats to obtain approximately 80% confluence in 2-3 days: 150 mm plates: 5 x 10^6/20 ml medium, 100 mm plates: 2 x 10^6/10 ml medium, 60 mm plates: 5 x

10^5/5 ml medium, 6-well plates: 3 x 10^5/well/3 ml medium, 12-well plates: 7.5 x 10^4/well/2 ml medium, 24-well plates: 5 x 10^4/well/1 ml medium, 96-well plates: 2 x 10^4/well/100 μl medium

2.2.3 Lipid Extraction and Analysis by LC-ESI MS/MS

The extraction and analysis method has been thoroughly described [127, 140]. The mass spectrometry data were collected using a PE Sciex API 3000 triple quadrupole and a 4000 quadrupole linear-ion trap mass spectrometer. For quantification, the samples were spiked with the internal standard cocktail (Avanti Polar Lipids, Alabaster, AL). DNA was quantified using the Quant-iT DNA Assay Kit, Broad Range (Molecular Probes), and the relationship 3 μg of DNA = 1 x 10^6 RAW264.7 cells, was empirically determined by comparison of DNA amount and number of cells counted using a hemocytometer.

2.2.4 Stable Isotope Labeling of Sphingolipids

Uniformly labeled ^{13}C-palmitate was mixed with fatty acid-free bovine serum albumin (BSA) at a 1:1 molar ratio to make a 1 mM solution[1], which was diluted to 0.1 mM with complete cell culture medium, and filter sterilized just before use. The [U-^{13}C]-palmitate/BSA was added to cells at the same time as the KLA or vehicle, incubated for up to 24 h, then the cells were extracted for lipid analysis as described previously [127, 140]. To quantitate the three categories of SL labeled with [U-^{13}C]-palmitate (i.e., in the sphingoid base backbone alone—which we designate "Base-labeled"—in the fatty acid

---

[1] Solutions containing BSA were tested for endotoxin contamination because we noted that fatty acid-free BSA from some suppliers was contaminated or became so during incubation at 37°C for the preparation of the fatty acid-BSA complex.

only—"Fatty acid-labeled"—and both the sphingoid base and fatty acid—"Dual-labeled"), the additional multiple reaction monitoring (MRM) pairs were added: the [M + 16] precursor ions and [M + 16] product ions for Base-labeled; [M + 16] precursor ions and [M + 0] product ions for "Fatty acid-labeled"; and [M + 32] precursor ions and [M + 16] product ions for "Dual-labeled." The MRM extracted ion chromatogram peak areas of all four SL isotopomers were integrated (Analyst 1.4), converted to picomoles using the peak areas of the internal standards, and normalized to the micrograms of DNA in the sample, except where otherwise noted.

2.2.5 Confocal Immunofluorescence Microscopy

RAW264.7 cells stably expressing GFP-LC3 were cultured on glass coverslips (VWR, Inc. West Chester, PA) in 24-well plates. Following treatment, cells were fixed with 4% formaldehyde for 15 minutes. Fixed cells were rinsed in PBS, and the nucleic acids were stained by incubating fixed cells with 1 μg/mL Hoechst 3342 for 7 min at room temperature. Stained cells were rinsed in PBS and mounted in Fluoromount G (Southern Biotechnology Associates, Inc., Birmingham, AL) prior to observation under a Zeiss LSM 510 inverted laser scanning confocal microscope (Heidelberg, Germany). Images were collected with the resident Zeiss confocal microscope software and analyzed using ImageJ version 1.41a (National Institute of Health). The ImageJ plug-in Analyze Particles was used to identify "autophagosomes" as defined by a threshold value of 159-255 [141] and a particle size of 0.07 to 7 μm^2 [142]. Statistical analysis was performed using a two-tailed Student's t-test.

2.2.6 Generation of RAW264.7 Cells Stably Expressing GFP-LC3

LC3A cDNA was obtained from Origene. To generate N-terminal GFP-tagged LC3, the LC3A gene was amplified using the following gene-specific primers: 5'-ATGCCCTCAGACCGGCCTTT-3' and 5'-GAAGCCGAAGGTTTCCTGGGAGG-3'. The PCR fragment corresponding to the coding sequence of LC3A was then cloned into pEGFP-C2/*SmaI* (Clonetech, Mountain View, CA) resulting pEGFP-C2-LC3A. Sequencing was used to confirm the fidelity of the construct.

RAW264.7 cells stably expressing GFP-LC3 were generated by transfection with pEFGP-C2-LC3A. Transfection was performed in 100-mm dishes (3.0×10^6 cells/dish) with 6 μg plasmid DNA/plate with GeneJuice® (Novagen; EMD Biosciences, San Diego, CA) according to the manufacturer's protocol. Following 48 h of exposure, cells were washed with PBS and selected in media containing 300 μg/mL of G418 (Sigma-Aldrich) for 14 days. The media was changed every other day. After two weeks, selected G418-resistant colonies were cloned by two rounds of limiting dilution in a 96 well plate order to establish fluorescent colonies originating from a single cell. In order to confirm localization and expression of the LC3, GFP-LC3-transfected RAW264.7 cells were cultured on 12 mm cover slips (VWR; West Chester, PA). Following exposure to Kdo_2-Lipid A (Avanti Polar Lipids; Alabaster, AL) for 24 h, cells were fixed in 4% formaldehyde and analyzed by fluorescence confocal microscopy.

2.2.7 Immunohistochemical Analysis of the ER and Golgi

For visualization of the ER and Golgi, fixed cells were permeabilized with 0.2% Triton X-100 for 5 min, blocked in 3% BSA, 2% serum in PBS for 2 h, and subjected to indirect immunofluorescence staining. Cells were incubated overnight at 4 °C with anti-BiP (1:500) for visualization of the ER or anti-GM130 (1:500) for visualization of the

Golgi diluted in 0.1% BSA in PBS. The cells were washed three times with PBS and incubated with the Alexa Fluor-conjugated secondary antibody (1:200) diluted in 0.1% BSA in PBS for 3 h at room temperature prior to nucleic acid staining.

2.2.8 Immunohistochemical Analysis of Ceramide Localization

Cer staining was performed through the adaptation of [134]. Briefly, for surface Cer staining, the non-specific binding sites of fixed cells were saturated for 2 h at room temperature with 3% BSA, 2% serum in PBS followed by overnight incubation at 4°C with anti-Cer Ab (1:50) diluted in 0.1% BSA. In order to visualize intracellular Cer, the staining protocol was continued with a second fixation with 4% formaldehyde for 20 min at room temperature. The cells were then washed twice with PBS and permeabilized with 0.2% Triton X-100 for 5 min. Non-specific intracellular binding sites were blocked with 3% BSA, 2% serum in PBS for 45 min followed by overnight incubation at 4°C with anti-Cer Ab (1:50) diluted in 0.1% BSA. The cells were then washed three times and incubated with the Alexa Fluor-conjugated secondary antibody (1:200) diluted in 0.1% BSA for 3 h at room temperature prior to nucleic acid staining.

2.2.9 Measurement of Cell Diameter and Area

RAW264.7 cells were cultured on glass coverslips (VWR, Inc. West Chester, PA) in a 24-well plate. Following treatment, cells were fixed with 4% formaldehyde in PBS at room temperature for 15 min. Fixed cells were rinsed in PBS and mounted in Fluoromount G (Southern Biotechnology Associates, Inc., Birmingham, AL) prior to observation under a Zeiss LSM 510 inverted laser scanning confocal microscope (Heidelberg, Germany). Bright field images were collected with the resident Zeiss confocal microscope software and cellular diameter measured using ImageJ version 1.41a

(National Institute of Health). The surface area was calculated using the measured diameter.

2.2.10 Analysis of Autophagy in CHO-LYB and CHO-LYB-LCB1 Cells

Cells were obtained from Professor Kentaro Hanada at the National Institute of Infectious Diseases in Tokoyo, Japan and verified to have the phenotype of being defective in *de novo* SL biosynthesis due to mutation of SPT1 (CHO-LYB) [143]. This pathway is restored in the CHO-LYB-LCB1 cell line by stable transfection with wild-type SPT1 [143]. In order to monitor autophagy, CHO-LYB and CHO-LYB-LCB1 cells were transfected with GFP-LC3. Transient transfection was performed using GeneJuice® transfection reagent (Novagen; EMB Biosciences, San Diego, CA) according to manufacturer's protocol. 24 h after transfection, cells were treated with vehicle control (EtOH) or 4-HPR (10 μM). 4-HPR is an established inducer of autophagy in a variety of cell lines [1, 99, 144]. Following 24 h treatment, cells were fixed with 4% formaldehyde in PBS at room temperature for 15 minutes. Fixed cells were rinsed in PBS and mounted in Fluoromount G (Southern Biotechnology Associates, Inc., Birmingham, AL) prior to observation under a Zeiss LSM 510 inverted laser scanning confocal microscope (Heidelberg, Germany). Autophagic cells were identified as cells with five or more GFP-LC3 punctate autophagosomes for each condition.

2.3 Results

Figure 2.1 depicts the early steps of SL biosynthesis with the average number of molecules per cell for each subspecies that has been quantified in RAW264.7 cells with and without KLA-activation. These averages have been calculated using the 24 h data from the LIPID MAPS time course studies and information about the reproducibility of

replicates, other time points, etc. can be obtained from the web site www.lipidmaps.org. The sum of all of these SL in RAW264.7 cells without KLA stimulation is ~1.5 x 10^9 molecules/cell (in other units: 0.82 nmol/μg DNA, 2.4 nmol/10^6 cells), which is a slight underestimation of the total SL content because it does not include small amounts of more complex GSL. For comparison, the sum of all of the lipids in RAW264.7 cells is 6.2 x 10^9 molecules per cell (3.4 nmol/μg DNA, 10.3 nmol/10^6 cells) (calculated from the data on www.lipidmaps.org, exempting triacylglycerols, cholesterol esters and diacylglycerols because they are likely to be found mostly in lipid droplets). Therefore, SL constitute approximately one fourth of the membrane lipid of these cells.

It is noteworthy that SM (1,200 x 10^6 molecules) and dihydroSM (DHSM) (240 x 10^6 molecules) account for a large fraction of this total (Fig. 2.1, upper numbers). In contrast, 3-KSa, the first intermediate of *de novo* SL biosynthesis, is too low to detect, which is consistent with previous estimates that it is rapidly reduced to Sa [14, 145]. Other intermediates of SL biosynthesis and turnover are present in more substantial amounts; for example, each RAW264.7 cell has, on average, 0.9 x 10^6 molecules of Sa, 20 x 10^6 molecules of DHCer, 41 x 10^6 molecules of Cer, and 9.5 x 10^6 molecules of So. In contrast, the amounts of Sa1P and S1P are very low (0.02 and 0.07 x 10^6 molecules), and Cer1P is intermediate (0.4 x 10^6 molecules). GlcCer is relatively prevalent (52.5 x 10^6 molecules), but RAW264.7 cells have much lower amounts of GalCer (0.3 x 10^6 molecules).

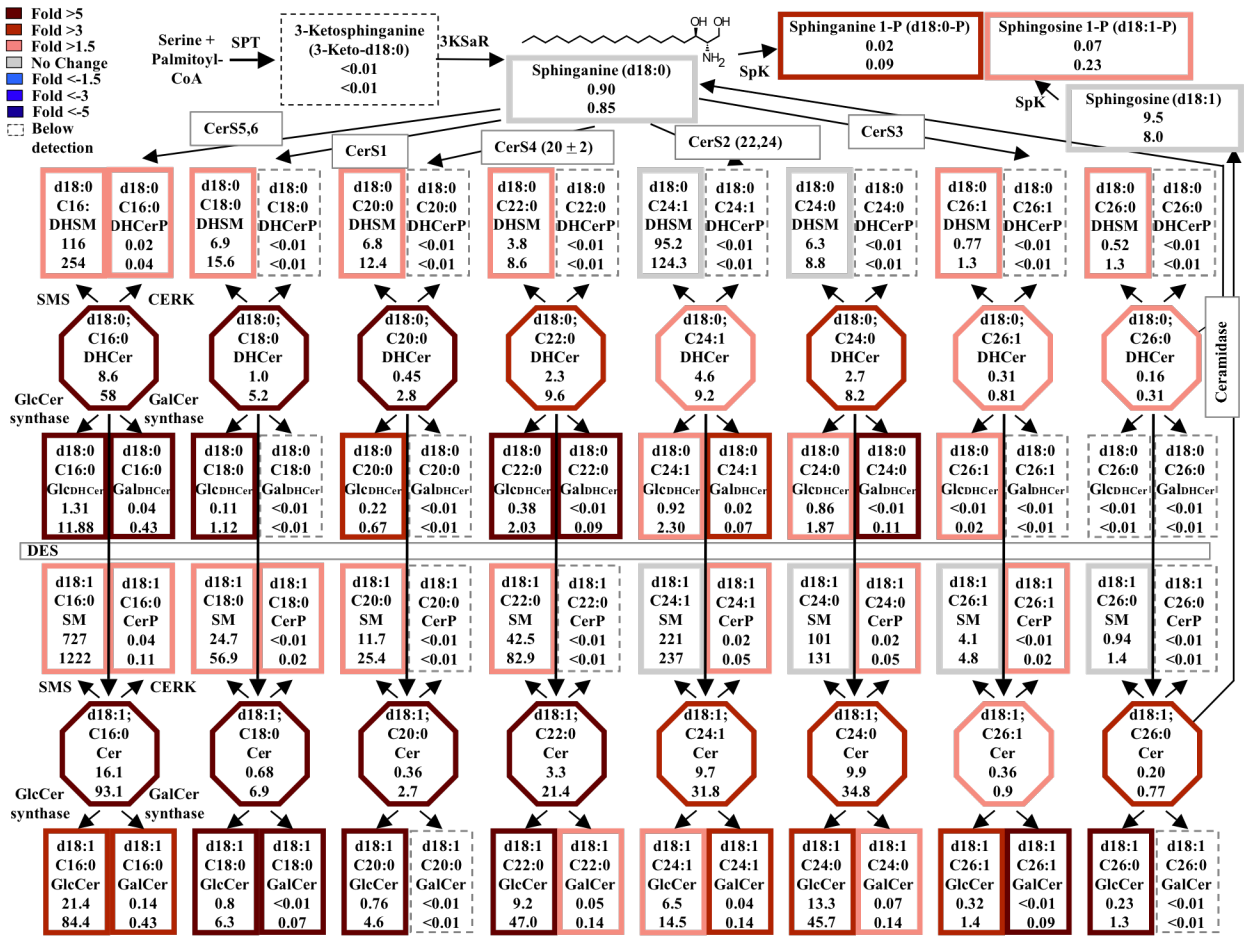

Figure 2.1 KLA Induces Substantial Increases in the Amounts of Multiple Cellular Sphingolipids RAW264.7 cells were incubated with vehicle control (PBS) or KLA (100 ng/mL). Following 24 h of treatment, cells were harvested for lipid extraction and analysis by LC ESI-MS/MS. The number of million molecules per cell for each sphingolipid species is shown for control (upper number) and KLA (lower number) treated cells with heat map coloration to illustrate the fold change of each subspecies. Data represent the mean (n=9).

2.3.1 KLA Induces Substantial Increases in the Amounts of Multiple Cellular Sphingolipids[2]

After 24 h of stimulation with KLA (Fig. 2.1, the lower numbers), almost every SL subspecies was higher than in the control, with about half increasing by ≥ 1.5-fold, as depicted by a heat map-style coloration of the borders (red reflecting increases). The SL sum increased to 2.7 x 10^9 molecules per cell (1.8-fold) at this time point. Interestingly, total lipids also increased 1.8 fold, from 6.2 to 10.9 x 10^9 molecules/cell (data not shown). This fold increase was calculated by the summation of all lipid species measured by the LIPID MAPS consortium (www.lipidmaps.org)[3].

The time course changes for each subspecies of DHCer and Cer are shown in Fig. 2.2, with sums for all the chain lengths in Fig. 2.2B and D. Significant differences in total DHCer and Cer for the KLA-treated and control cells were found 12 h after KLA addition, and both were ~5-fold higher for the KLA-treated cells at 24 h (Fig. 2.2B and D). It is interesting that control cells displayed a decrease in total DHCer and Cer over the time course. Although the reason for this decrease is unclear, it is expected to be the result of continued growth resulting in increases in cell density similar to decreases cholesterol metabolism as cells reach confluency [146]. This decrease in control cell lipids has also been found in other lipid categories, analyzed by the LIPID MAPS Consortium, such as certain species of fatty acids, glycerophospholipids, and sterol lipids.

---

[2] The KLA time course data (sphingolipid amounts as pmol/μg DNA and microarray data) described in this section are also shown on the LIPID MAPS website (www.lipidmaps.org) as required by the NIH as part of the data sharing requirement for this Consortium.

[3] This calculation does not include measured quantities of triglycerides or cholesteryl esters since a substantial portion is likely to be stored in cytoplasmic lipid droplets rather than cell membranes per se [122].

Elevations in the C16- subspecies of DHCer and Cer were evident at 8 h (Fig. 2.2A & C), and these subspecies were also the highest at 24 h (Fig. 2.2A & C and Fig. 2.3). A similar time course profile (i.e., with at least the C16-subspecies being elevated at 8 h) was seen for SM (Fig. 2.4A), MH-Cer (i.e., GlcCer and GalCer, which were analyzed together because the amounts of GalCer are very small, $\leq$5%) (Fig. 2.4B), and Cer1P (Fig. 2.4C), but the latter was not elevated versus time zero, but rather, against the time-matched control because the control cells displayed a curious decrease in Cer1P that occurred less in the KLA-treated cells. DHSM and monohexosyl-DHCer (MH-DHCer) also increased for the KLA treated cells versus the control, but the amounts were much smaller (Fig. 2.5).

The SL that responded most rapidly to KLA was sphinganine (Fig. 2.6A), which was significantly different from the control at the earliest time point (0.5 h) and elevated by >2-fold between 2 and 8 h, when it began to decline and equaled the control at 24 h. Sphingosine also increased, as did Sa1P and S1P, but the sphingoid base 1-phosphates increased later (i.e., at 4 h for S1P and 8 h for Sa1P) (Fig. 2.6B).

These changes are consistent with *de novo* SL biosynthesis being higher for KLA-stimulated RAW264.7 cells because Sa is the first detectable pathway intermediate, followed by DHCer then Cer (Fig. 2.1). Cer might be elevated due to turnover of more complex SL (as discussed below), however, the increase in DHCer is not likely to come from turnover because this is not equivalent to the decrease in DHSM (c.f. Fig. 2.2A and B with Fig. 2.5).

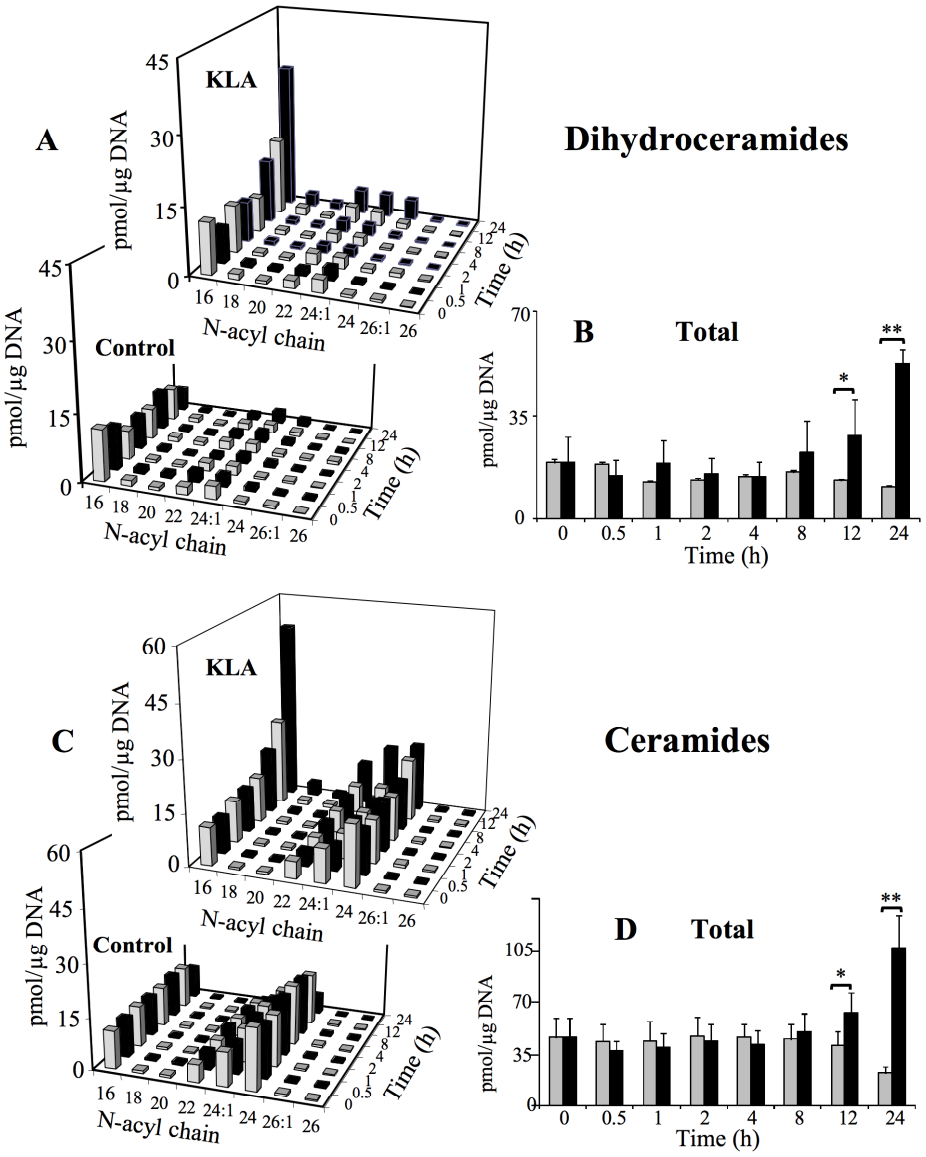

Figure 2.2 KLA Induces Time Dependent Increases in Ceramide and Dihydroceramide
RAW264.7 cells were incubated with vehicle control (PBS) or KLA (100 ng/mL). Following treatment, cells were harvested at the indicated time points for lipid extraction and analysis by LC ESI-MS/MS. *A*, Amounts of the major chain length subspecies of DHCer. Data represent the mean (n=9). *B,* Amounts of total DHCer (a summation of all chain lengths) in KLA versus control conditions. Data represent the mean $\pm$ SEM (n = 9); *p $\leq$ 0.05; **p $\leq$ 0.001. *C*, Amounts of the major chain length subspecies of Cer. Data represent the mean $\pm$ SEM (n = 9). *D,* Amounts of total Cer (a summation of all chain lengths) in KLA versus control conditions. Data represent the mean $\pm$ SEM (n = 9); *p $\leq$ 0.05; **p $\leq$ 0.001.

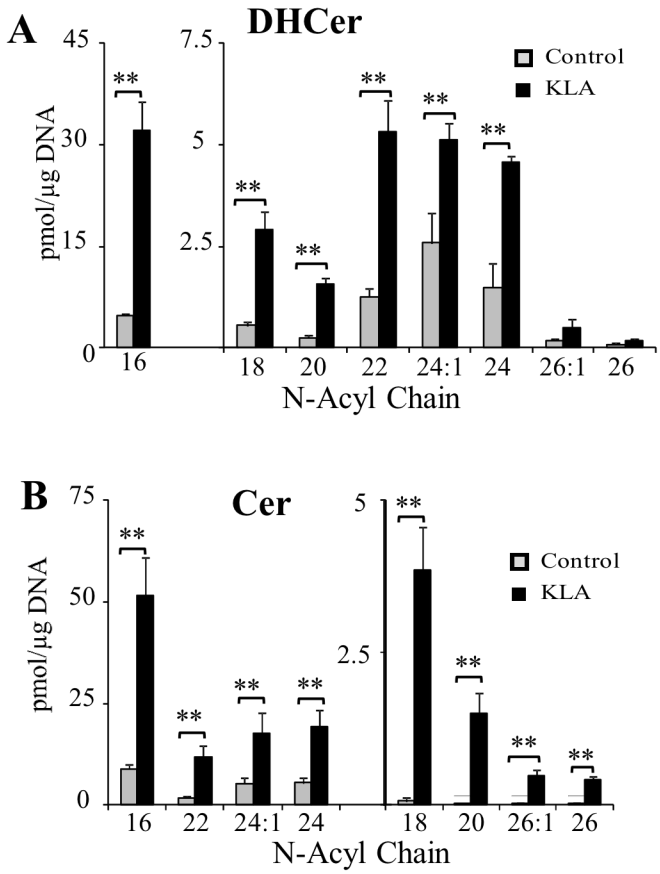

Figure 2.3 Dihydroceramides and Ceramides of RAW264.7 Cells Incubated PBS (Control) or KLA for 24 h RAW264.7 cells were incubated with vehicle control (PBS) or KLA (100 ng/mL) for 24 h then the sphingolipids were analyzed by LC ESI-MS/MS. The data represent the mean + SEM (n = 9); *$p < 0.05$; **$p < 0.001$.

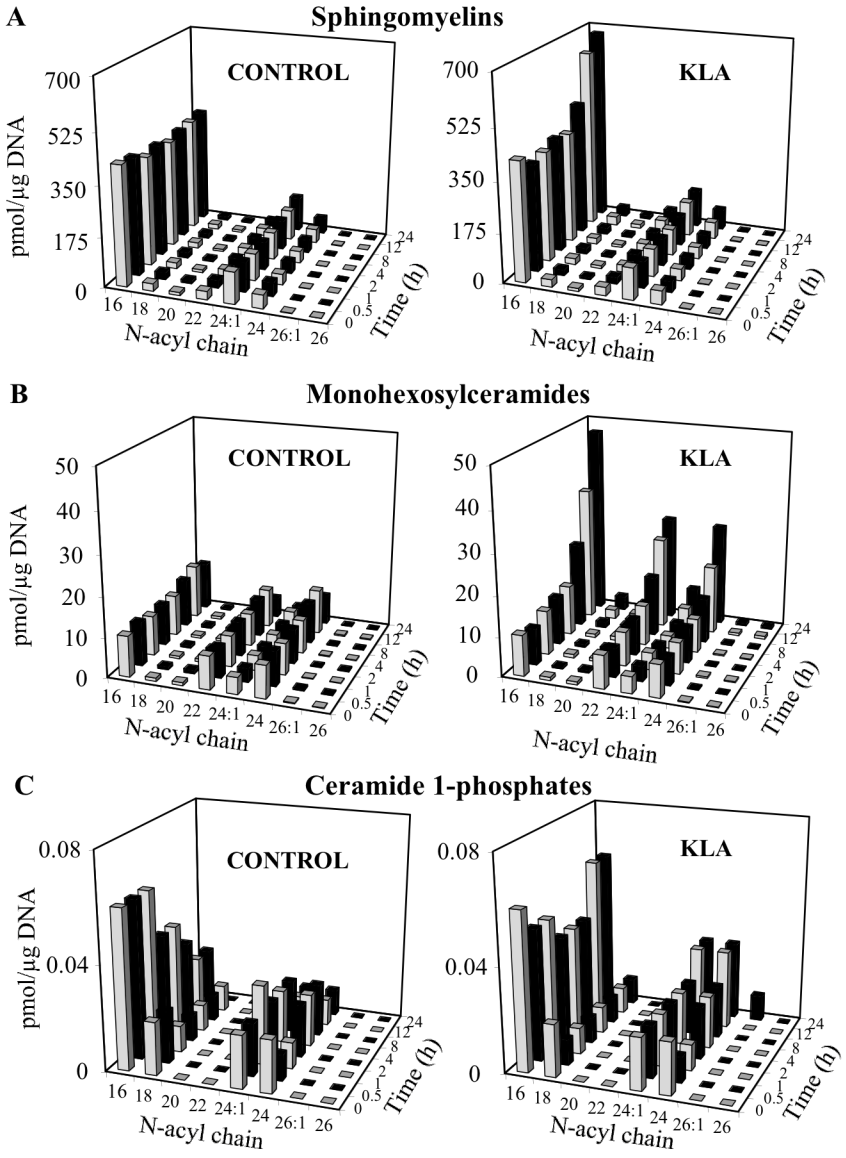

Figure 2.4 KLA Induces Time Dependent Increases in Ceramide Metabolites RAW264.7 cells were incubated with vehicle control (PBS) or KLA (100 ng/mL). Following treatment, cells were harvested at the indicated time points for lipid extraction and analysis by LC ESI-MS/MS. Amounts of the major chain length subspecies of Cer metabolites: sphingomyelins (*A)*, monohexosylceramides *(B)*, and ceramide 1-phosphates *(C)* are shown. Data represent the mean (n=9).

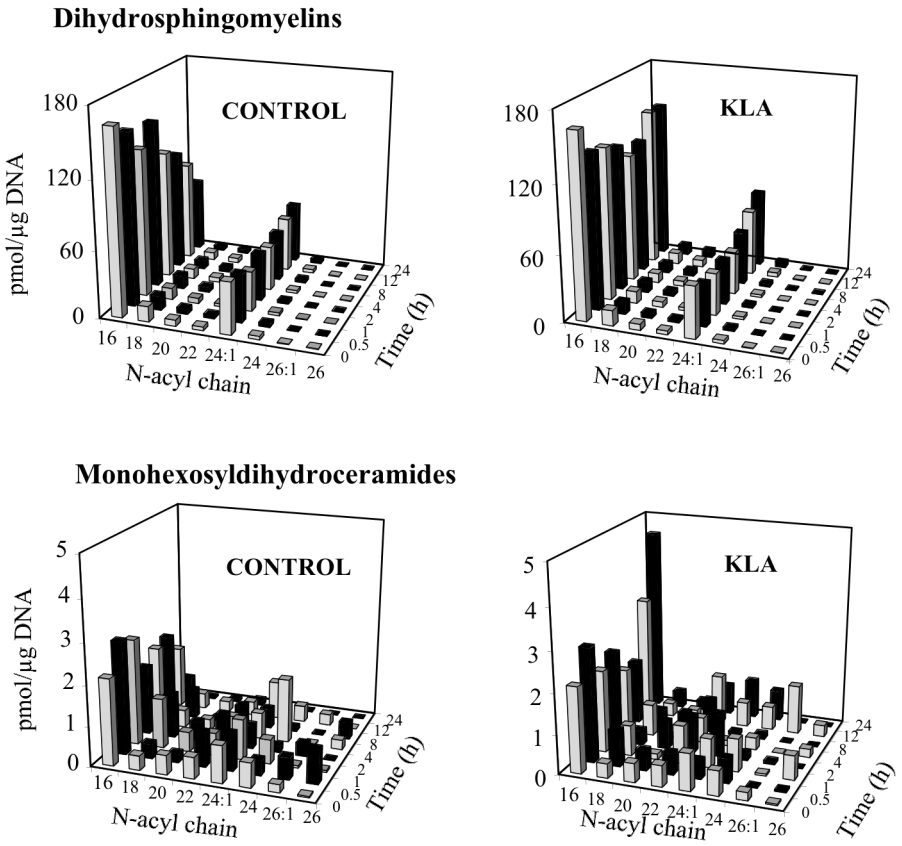

Figure 2.5 KLA Increases Dihydroceramide Metabolites RAW264.7 cells were incubated for various times with vehicle control (PBS) or KLA (100 ng/mL). Following treatment, cells were harvested at the indicated time points for lipid extraction and analysis by LC ESI-MS/MS. Data represent mean (n = 9).

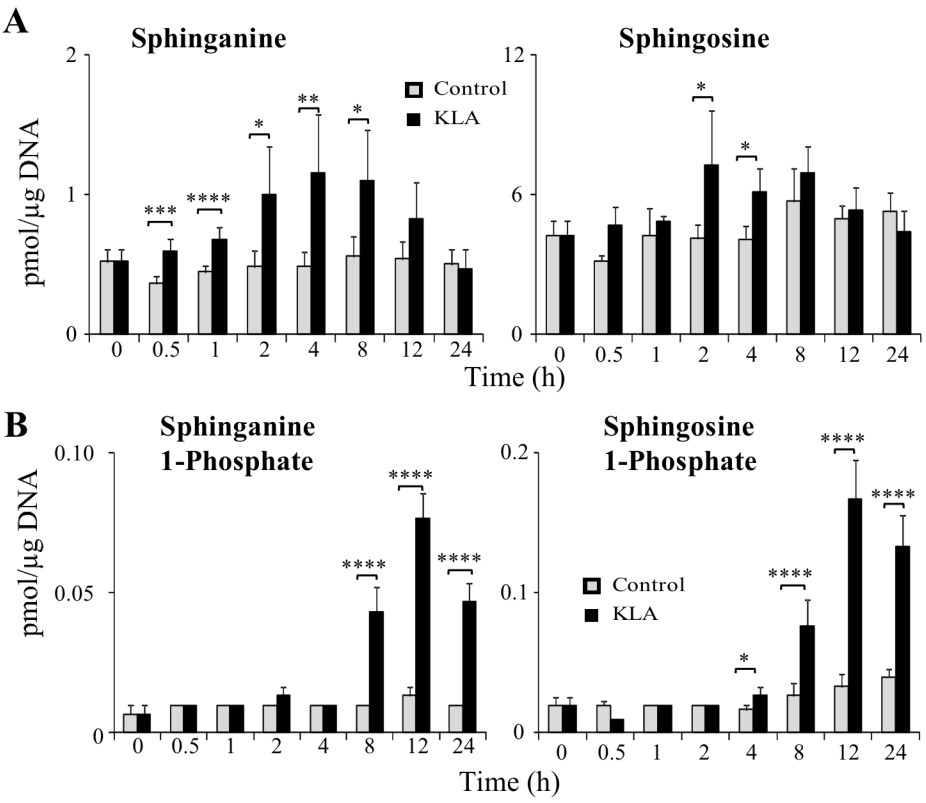

Figure 2.6 KLA Alters the Amount of Sphingoid Bases and Sphingoid Base Phosphates
RAW264.7 cells were incubated with vehicle control (PBS) or KLA (100 ng/mL). Following treatment, cells were harvested at the indicated time points for lipid extraction and analysis by LC ESI-MS/MS. *A*, Amounts of sphingoid bases, sphinganine and sphingosine. Data represent the mean (n=9). *B*, Amounts of sphingoid base phosphates, sphinganine 1-phosphate and sphingosine 1-phosphate. Data represent the mean $\pm$ SEM (n = 9); *p $\leq$ 0.05; **p $\leq$ 0.01; ***p $\leq$ 0.005; ****p $\leq$ 0.001.

2.3.2 Correlation of Gene Expression with Metabolite Changes in KLA-treated RAW264.7 Cells[2]

As part of the LIPID MAPS studies, the Consortium has also analyzed changes in the mRNAs for many of the enzymes of this pathway by microarray analysis (www.lipidmaps.org) (Fig. 2.7) and the results for the 24 h time point are displayed in Fig. 2.8 using a web-based display tool, GenMAPP v2.1, that was expanded to include most of the genes currently known for these steps of *de novo* SL biosynthesis [147]. According to this analysis, KLA caused relative increases in mRNAs for both of the major subunits of serine palmitoyltransferase (SPT1 and 2), at least one of the Cer synthases (CerS4), DHCer desaturase (DES1), and synthases for SM (SMS1) and GlcCer. The microarry data also suggest that KLA-stimulated RAW264.7 cells have elevated mRNAs for acid sphingomyelinase (SMPD1), sphingosine kinase (SphK1 and 2), and S1P lyase (Fig. 2.8), which are consistent with the previous report that LPS induces SM turnover [131, 148] and the elevation of sphingoid base phosphates (Fig. 2.6) (although elevation of S1P lyase might also indicate that there is elevated cleavage of the latter). Mindful of the caveats inherent in microarray analysis, these results suggest that KLA affects expression of mRNAs for multiple steps of the pathway, which is consistent with the changes in essentially all subcategories of SL (Fig. 2.1-2.6) and the previous literature on the effects of LPS on SL metabolism [129-131, 149].

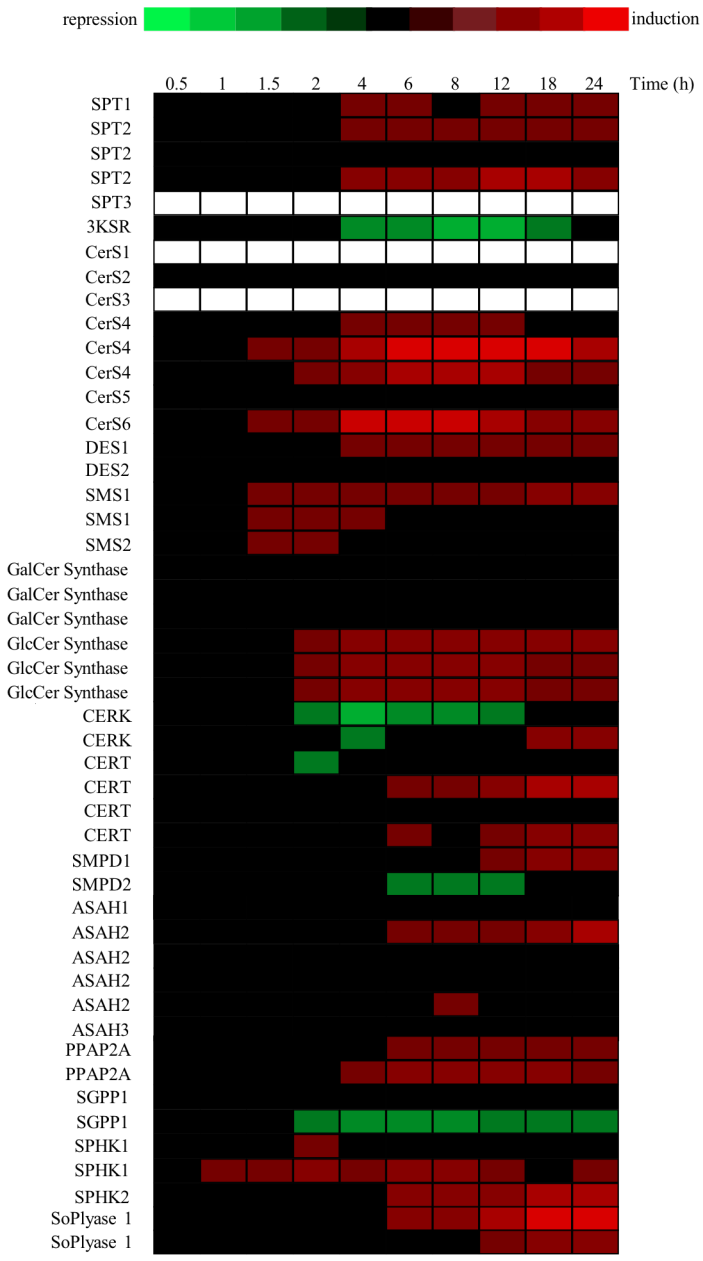

Figure 2.7 mRNA Expression of Genes Involved in Sphingolipid Biosythesis Following KLA Stimulation RAW 264.7 cells were harvested 0.5, 1.0, 1.5, 2.0, 4.0, 6.0, 8.0, 12.0, 18.0, and 24 h after treatment with 100ng/ml KLA. The gene symbols (*mus musculus)* used at www.lipidmaps.org for the enzymes of the sphingolipid pathway: SPT family (sptlc1 and sptlc2), 3KSR (FVT1), CerS (lass2, lass4, lass5, and lass6). DES family (Degs1 and Degs2), SMS 1 (Tmem23), SMS2 (4933405A16RIK), GalCer Synthase (ugt8a), GlcCer synthase (ugcg), CERK (CERK), CERT (Col4a3bp), SMPD1 (SMPD1), SMPD2 (SMPD2), ASAH1 (ASAH1), ASAH2 (ASAH2), ASAH3 (ASAH3), PPAP2A (PPA2A), SGPP1 (SGPP1), SPHK1 (SPHK1), SPHK2 (SPHK2), S1Plyase1 (sgp11)

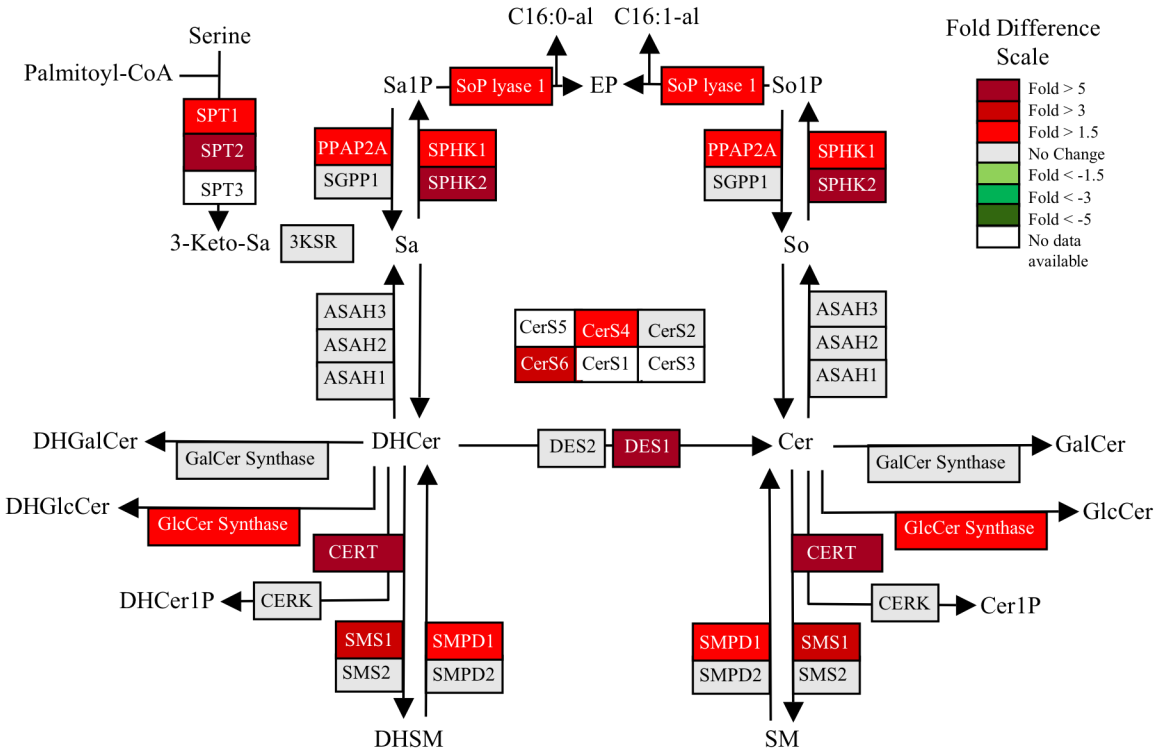

Figure 2.8 KLA Increases mRNA Expression of Genes Involved in Sphingolipid Biosynthesis
Gene expression data for the sphingolipid metabolic enzymes following 24 h of treatment with KLA (100 ng/mL) using the KEGG based microarray analysis tool (GenMAPP v2.1) that has been modified in order to display this pathway more completely (www.sphingomap.org). The coloration is $\log_2$-fold change in expression following treatment with KLA (100 ng/mL) for 24 h from microarray data generated by the LIPID MAPS Consortium (www.lipidmaps.org). The sphingolipid metabolites and genes (with the gene abbreviations shown in boxes, or enzyme names where gene names are ambiguous) are given for the condensation of serine and palmitoyl-CoA to form 3-ketosphinganine (3-ketoSa) by serine palmitoyltransferase (SPT), which is reduced to sphinganine (Sa), acylated to dihydroceramides (DHCer) by (DH)Cer synthases (CerS) and incorporated into more complex DH-sphingolipids (the 1-phosphate (DHCer1P) sphingomyelins (DHSM), glucosylceramides (DHGlcCer) galactosylceramides (DHGalCer) or desaturated to Cer followed by headgroup addition. Also included are a number of the catabolic genes, e.g., sphingomyelinases (SMPD), ceramidases (ASAH), sphingosine kinases (SphK) for the formation of sphinganine 1-phosphate (Sa1P) and sphingosine 1-phosphate (S1P), and phosphatases for the reverse reaction and the lyase that cleaves sphingoid base 1-phosphates to ethanolamine phosphate (EP), hexadecanal (C16:0al) and hexadecenal (C16:1al).

2.3.3 Analysis of *de novo* Sphingolipid Biosynthesis in KLA-Treated RAW264.7 Cells

For further insight into the effect of KLA on SL metabolism, the SPT inhibitor ISP1 [150] was used to block *de novo* SL biosynthesis. As shown in Fig. 2.9A, ISP1 reduced the KLA-induced elevation of Cer somewhat, completely eliminated the increase in MH-Cer, and actually decreased SM (reflecting SM turnover that was not evident in the original analysis of SM amount, Fig. 2.4A, because the rate of SM biosynthesis is greater than turnover). Fig. 2.9B shows the effect of ISP1 on KLA treated cells over time as well as the individual Cer chain lengths. ISP1 caused an initial decrease in all of the Cer subspecies, but only slightly blunted the increase in Cer between 12 and 24 h (c.f., Fig. 2.9B and 2.2C). One of the most interesting features of these Cer data is that they display different acyl-chain profiles for the Cer of the cells treated for 24 h with ISP1+ KLA versus those treated with KLA alone. The Cer of KLA-induced RAW264.7 cells is relatively similar to that of the controls (i.e., C24:0 > C24:1 > C22:0 (Fig. 2.2C) whereas the profile in cells treated with ISP1 + KLA has C24:1 as the predominant very-long-chain subspecies (Fig. 2.9B). The latter subspecies distribution is similar to that for SM (i.e., C24:1>C24:0) (c.f., Fig. 2.9B with Fig. 2.4A and 2.2C).

Thus, these results suggest that some of the increases in Cer are due to *de novo* biosynthesis (i.e., ISP1 inhibited). The portion that is not inhibited is likely to come from turnover of more complex SL. It is likely that this Cer is derived from SM since the SM amounts decrease and the N-acyl chain length distribution of the Cer in the cells treated with ISP1 + KLA for 24 h. A third factor that might affect the Cer subspecies distribution of these SL is our observation that KLA alters the fatty acyl-CoA

composition of the cells (Fig. 2.10). Therefore, stable isotope labeling was used to monitor the compounds that are made *de novo* versus via turnover.

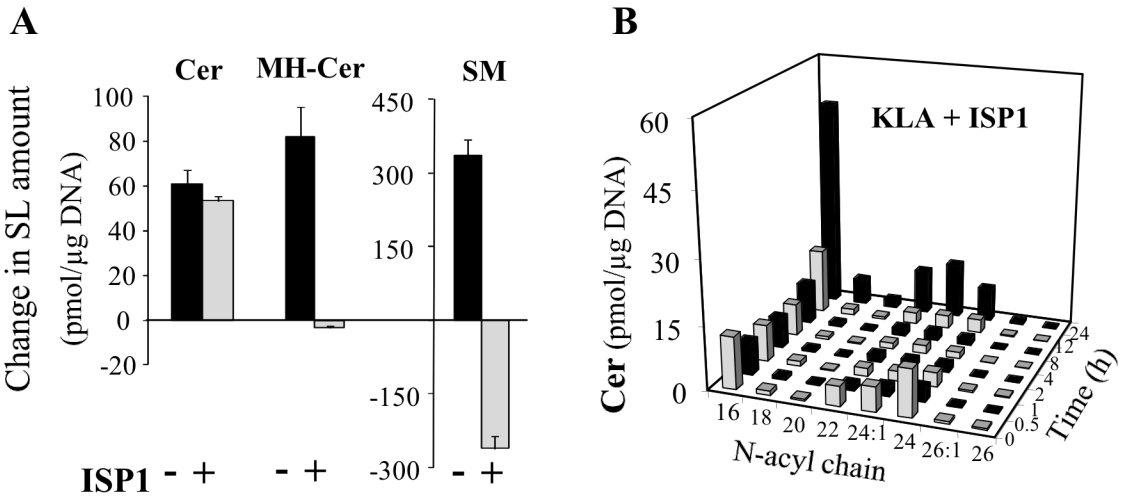

Figure 2.9 Effect of ISP1 on Sphingolipid Biosynthesis in KLA-Treated RAW264.7 Cells
RAW264.7 cells were incubated for 24 h with vehicle control (PBS), KLA (100 ng/mL), ISP1 (1 µM), or KLA+ ISP1. For cells treated with KLA + ISP1, ISP1 was added 1 h prior to the addition of KLA. Following treatment, cells were harvested for lipid extraction and analysis by LC ESI-MS/MS. *A*, Change in the amounts of Cer, MH-Cer, and SM for cells treated with KLA or KLA + ISP1. Data represent the mean $\pm$ SEM (n = 3) *B*, Amounts of the major chain length subspecies of ceramide in cells treated with KLA + ISP1. Data represent the mean (n = 3).

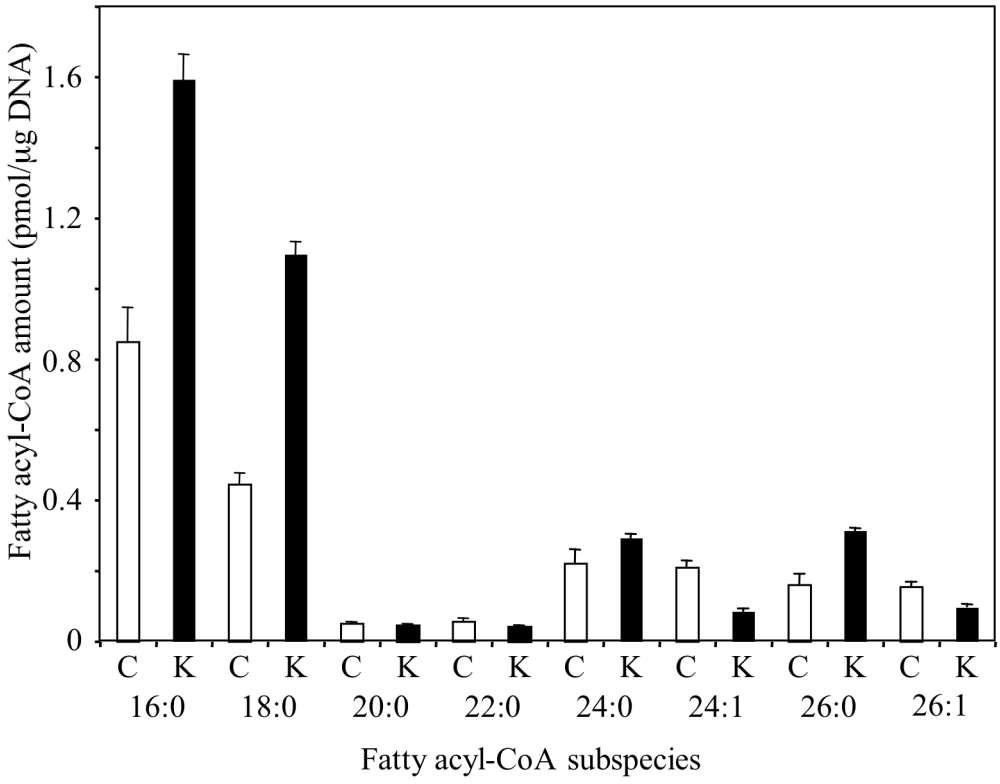

Figure 2.10 Amounts of Fatty Acyl-CoAs in RAW264.7 Cells with and without KLA Stimulation RAW264.7 cells were incubated for 24 with vehicle control (PBS) or KLA (100 ng/mL). Following treatment, cells were harvested at the indicated time points for lipid extraction and analysis by LC ESI-MS/MS for the amounts of various chain length fatty acyl-CoAs that are utilized by CerS to make SL. Data represent mean $\pm$ SEM (n = 3).

2.3.4 Analysis of *de novo* Sphingolipid Biosynthesis in RAW264.7 Cells by [^{13}C] Palmitate Labeling

The most direct way to monitor *de novo* SL biosynthesis is to follow the incorporation of [U-^{13}C]palmitate because this precursor is converted into [U-^{13}C]palmitoyl CoA and utilized in the first step of sphingoid base biosynthesis as well as for the N-acylation of sphingoid bases (Fig. 2.1). Thus, cells will contain four isotopically distinct compounds, all of which can be analyzed by LC ESI-MS/MS: SL with only ^{12}C (plus natural abundance ^{13}C, which is corrected for), which reflect pre-existing SL and those made with endogenous unlabeled palmitate; SL labeled in only the sphingoid base backbone (which we term "base-labeled"); SL with a labeled sphingoid base plus an amide-linked ^{13}C-fatty acid (which we term "dual-labeled"); and SL labeled in only the amide-linked fatty acid, which are likely to be comprised of at least some ^{12}C-sphingoid bases that have been released by turnover then reacylated using [^{13}C]-fatty acyl-CoA. The base- and dual-labeled SL are unambiguously made by *de novo* biosynthesis, therefore, have been examined in control and KLA-treated cells.

The sum of base and dual-labeled [^{13}C]Cer increases over time for both control and KLA-treated RAW264.7 cells (Fig. 2.11A), with a plateau between 4 and 12 h then decreasing for the control cells, whereas label incorporation continues approximately linearly for the entire 24 h for the KLA-treated cells. Label incorporation has a similar subspecies distribution pattern for the control and the KLA-treated cells for the first 12 h (Fig. 2.11B) (even though the amounts of labeled Cer is greater in the KLA-treated cells, as also displayed in Fig. 2.11A), but the patterns diverge at 24 h, where the C16-Cer subspecies predominates in the KLA-treated cells. As predicted, all of these backbone

and dual labeled SL arise from *de novo* biosynthesis because ISP1 completely eliminated the incorporation (Fig. 2.11A and 2.11C, left graph). In contrast, the right graph of Fig. 2.11C shows the unlabeled (^{12}C-) Cer in the same cells, which is almost identical to Fig. 2.9B—i.e., the Cer amounts decrease over the first ~8 h but afterwards increase despite the presence of ISP1. Therefore, this later increase in [^{12}C]Cer must reflect the appearance of unlabeled Cer from another source.

Overall, these results confirm that *de novo* biosynthesis accounts for initial increases in Cer in KLA-treated RAW264.7 cells and a portion of the increase at 12 and 24 h, but at 12 and 24 h Cer also arises from an unlabeled pool(s)—i.e. from turnover of pre-existing SL (and most likely SM, since turnover of SM has been shown in Fig. 2.9A, and the N-acyl-chain distributions of SM and this Cer are similar (c.f., Fig. 2.4A versus 2.9B and 2.11C, as discussed above).

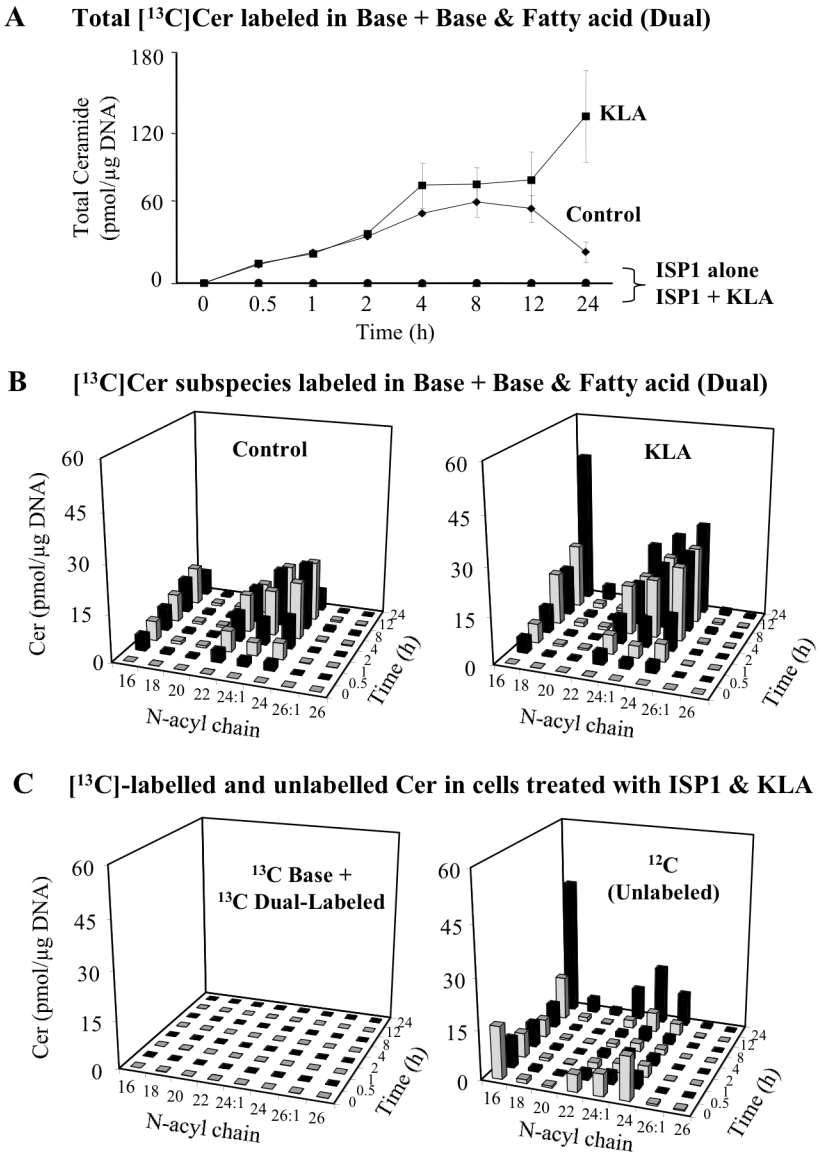

Figure 2.11 Analysis of *de novo* Sphingolipid Biosynthesis in RAW264.7 Cells by [^{13}C]Palmitate Labeling RAW264.7 cells were incubated with 0.1 mM [U-^{13}C]-palmitic acid (as the BSA complex) with vehicle control (PBS), KLA (100 ng/mL), ISP1 (1 µM), or KLA+ ISP1. For cells treated with KLA + ISP1, ISP1 was added 1 h prior to the addition of KLA for the times shown. The appearance of ^{13}C in newly synthesized sphingolipids was quantified by mass spectrometry as described under *Materials and Methods*. *A,* Summation of Base (Backbone) labeled and Dual (Backbone and Fatty Acid) labeled Cer subspecies. Data represent the mean ± SEM (n = 3). *B*, Summation of Base (Backbone) labeled and Dual (Backbone and Fatty Acid) labeled Cer species in cells treated with Control (left) or KLA (right) Data represent the mean (n = 3). *C*, Summation of Base (Backbone) labeled and Dual (Backbone and Fatty Acid) labeled Cer species (left) and ^{12}C (unlabeled) Cer species (right) in cells treated with KLA + ISP1. Data represent the mean (n = 3).

2.3.5 KLA Inhibits Cell Growth and Increases the Size of RAW264.7 Cells

In contemplating why the RAW264.7 cells acquire such substantial amounts of additional SL (and lipids overall) upon activation, as well as why the [^{13}C]-labeled SL of the control cells decrease on a per cell basis between 12 and 24 h (Fig. 2.11A), it occurred to us that this might be related to cell growth—i.e., that SL biosynthesized by growing cells will be distributed into multiple daughter cells upon division, whereas growth inhibited cells that continue to synthesize SL will accumulate them unless turnover is more rapid. Activation of RAW264.7 cells by LPS is known to inhibit cell growth [151], and Fig. 2.12A shows that this also occurs with KLA. Based on the measured μg DNA per dish, the KLA-treated cells cease to grow after 4 to 6 h (during which the μg DNA increases from 1 to 1.6 μg DNA, or 3.3 to 5.3 x 10^5 cells, and remains at this number at 24 h), whereas, the control cells triple (i.e.; from approximately 1 to 2.9 μg DNA corresponding to an increase in cell number from 3.3 to 9.6 x 10^5 cells) in 24 h. Therefore, the major contributor to the increase in SL in the KLA-treated cells is that the biosynthesized lipids remain with the original cells rather than being divided into daughter cells. The lower graph in Fig. 2.12A shows that ISP1 is also partially growth inhibitory.

The greater amount of lipid in KLA activated RAW264.7 cells would be predicted to increase cell size, and LPS has been reported to increase the diameter of this cell line [152]. The diameter of the RAW264.7 cells with and without KLA treatment for 24 h was estimated by measuring the cell size distribution using bright field microscopy. As shown in Fig. 2.12B, the KLA-treated cells appear somewhat larger, and a graph of the relative distribution of the measured diameters (Fig. 2.12C) shows that the

distribution curve is shifted to the right for KLA-treated cells, and shows a non-Gaussian distribution. From these data, the average cell diameters for the control and KLA-activated cells were calculated to be ~10.5 and ~13.0 microns, respectively. An increase in diameter of this magnitude (24%) would correspond to a ~53% increase in surface area (Fig. 2.12D), which is similar to that estimated following LPS treatment of RAW264.7 cells [153].

Thus, continued SL biosynthesis with an expansion of membrane area (and cell size) in RAW264.7 cells that are growth inhibited by KLA is a major contributor to the increase in SL content of these cells, and probably the increase in lipid amount overall. The difference between the change in cell surface area (1.5 x, although this is only a rough approximation) and the change in lipid amount (1.8 x) probably reflects an accompanying increase in intracellular membranes. Activation of the TLR4 receptor of RAW264.7 cells by LPS is known to induce the formation of the vacuolar structures referred to as autophagosomes [87, 133], therefore, these were examined next.

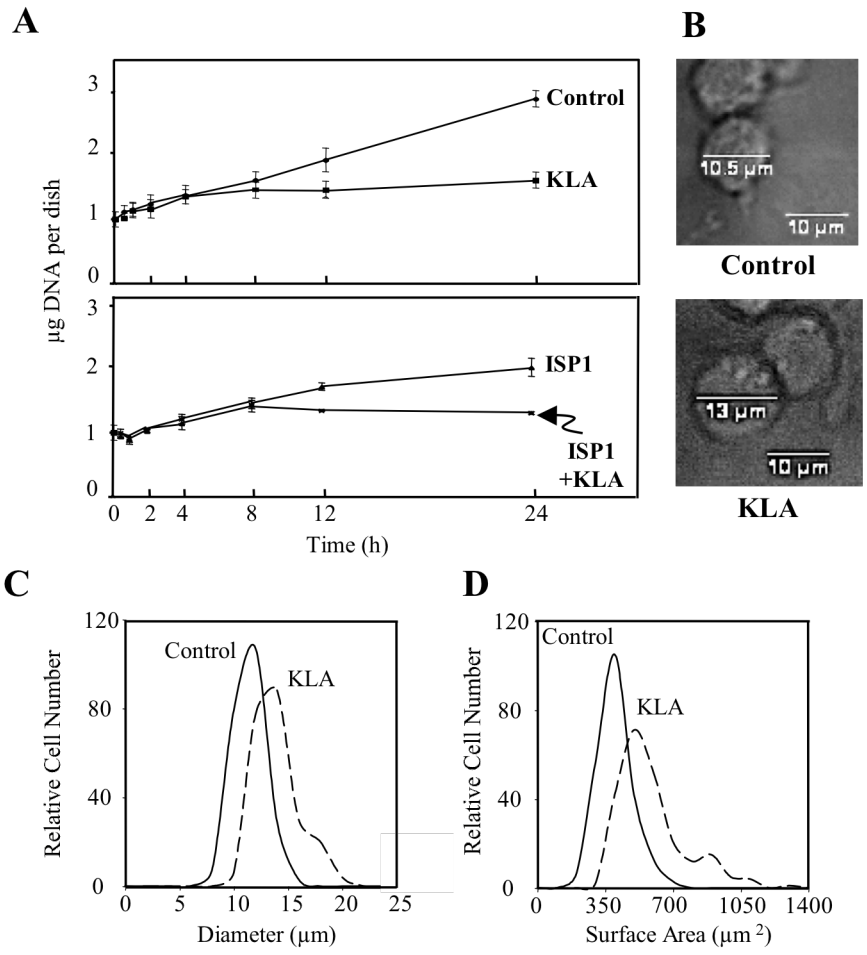

Figure 2.12 KLA Reduces Cell Number and Increases Cell Size in RAW264.7 Cells
A, µg DNA per dish following treatment with vehicle control (PBS), KLA (100 ng/mL), ISP1 (1 µM), or KLA+ ISP1 for various times. Data represent the mean ± SEM (n = 3). *B,* Representative bright field images with measured cellular diameter for control and KLA-treated cells. For each experimental condition, 225 cells were analyzed. Data represent the mean. *C,* Relative cellular diameter and *D,* relative cellular surface area distribution patterns are shown. For each experimental condition, 225 cells were analyzed.

2.3.6 KLA Induces Autophagy in RAW264.7 Cells, and KLA-Induced Autophagy is Dependent on *de novo* Sphingolipid Biosynthesis

Autophagosomes are particularly interesting from a SL perspective because exogenously added Cer, or cellular accumulation of Cer due to disruption of SL metabolism, has been shown to induce autophagy in other cell types [1, 102, 104]. Studies of autophagy frequently use cells that stably or transiently express a green-fluorescent-protein (GFP)-tagged LC3 protein (microtubule-associated protein 1 light chain 3) [77] that, like wild-type LC3, is recruited from the cytosol to become part of the autophagosome due to conjugation of the C-terminal glycine with phosphatidylethanolamine [77, 78]; therefore, the appearance and accumulation of GFP-LC3 puncta is widely used to assess autophagy [77].

As shown in Fig. 2.13, KLA treatment of RAW264.7 cells stably expressing GFP-LC3 induced the characteristic redistribution of GFP-LC3 from diffuse fluorescence throughout the cytosol (left panels of Fig. 2.13A) to numerous punctate fluorescent vesicles (right panels of Fig. 2.13A). A quantitative analysis of the confocal microscopic images revealed that a small but statistically significant increase in the number of cells expressing GFP-LC3 puncta and the number of GFP-LC3 puncta/cell following KLA treatment can be seen as early as 2 h, but the largest differences are seen later (Fig. 2.13B).

Consistent with these findings, the LIPID MAPS microarray data set for the RAW264.7 cells (www.lipidmaps.org) reveal that KLA elevates the mRNAs for *Atg8/LC3* and *Atg12*, which are positively correlated with autophagy (Fig. 2.14A) [84, 85], and an elevation in the lipidated form of LC3 (LC3-II) was detected by Western blot

analysis in both RAW264.7 cells stably transfected with GFP-LC3 and untransfected RAW264.7 cells (Fig. 2.14B) [65, 77]. Taken together the above data establish that KLA induces autophagy in RAW264.7 cells.

To determine if *de novo* SL biosynthesis is required for the induction of autophagy by KLA, RAW264.7 cells stably expressing GFP-LC3 were treated with ISP1 for 1 h then KLA was added and the numbers of autophagosomal puncta were analyzed (Fig. 2.15). By both visual inspection (Fig. 2.15A) and quantitative analysis of the confocal images (Fig. 2.15B), it is evident that inhibition of *de novo* SL biosynthesis by ISP1 blocked the appearance of GFP-LC3-associated autophagosomes. This is doubly interesting because it not only links *de novo* SL biosynthesis with KLA-induced autophagy but also establishes that the elevation of Cer due to SL turnover (which was minimally affected by ISP1) (Fig. 2.9B and 2.11C) is not sufficient to induce autophagy.

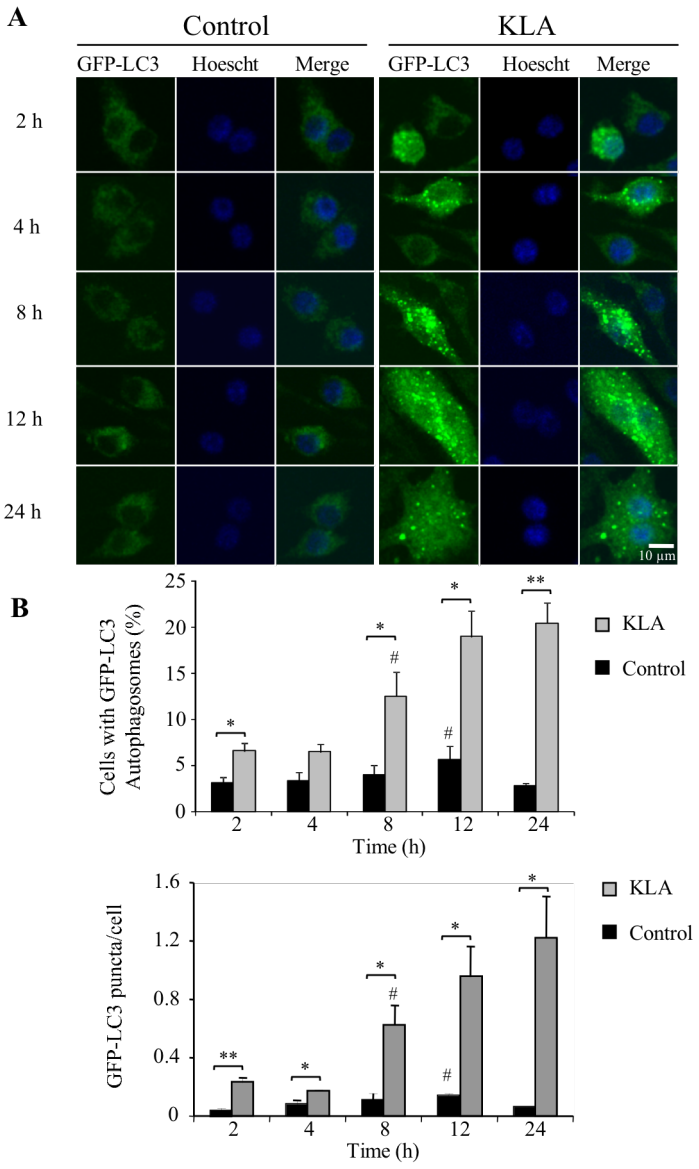

Figure 2.13 KLA Induces Autophagy in RAW264.7 Cells RAW264.7 cells stably expressing GFP-LC3 were incubated for various times with vehicle control (PBS) or KLA (100 ng/mL). *A*, Representative images. *B*, The number of cells displaying GFP-LC3 puncta (upper panel) and the number of GFP-LC3 puncta/cell (lower panel) were quantified using ImageJ. For each experimental condition, a minimum of 260 cells/experiment were counted. Data represent mean $\pm$ SEM (n = 3); # (n=2); *p $\leq$ 0.05; **p $\leq$ 0.01.

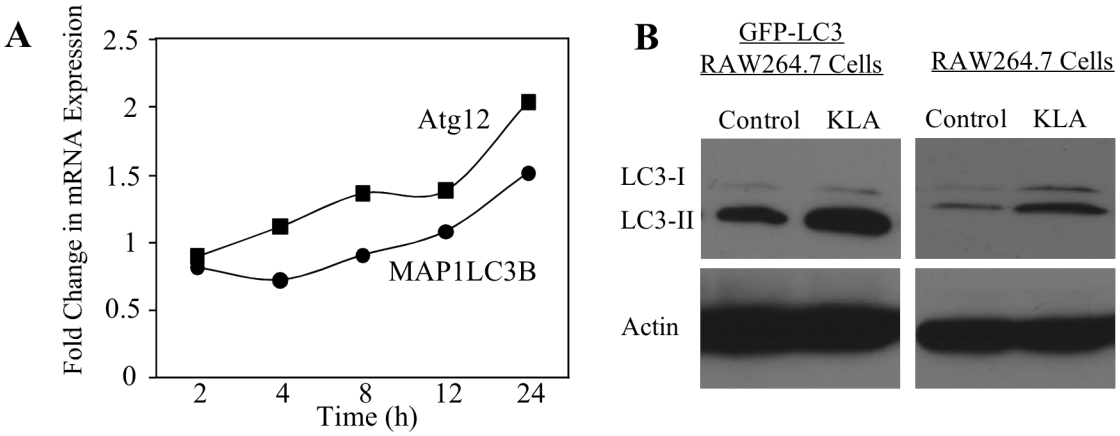

Figure 2.14 Additional Evidence that KLA Induces Autophagy in RAW264.7 Cells
A, RAW264.7 cells were incubated in the absence (control) or presence of KLA (100 ng/mL), harvested at 2, 4, 8, 12, and 24 h and for each time point an Agilent array was used to determine the mRNA expression level of various genes including LC3 (Map1LC3B) and Atg12. *B*, RAW264.7 cells were incubated for 24 h with vehicle control (PBS) or KLA (100 ng/mL) prior to immunoblot analysis using LC3 or β actin antibodies.

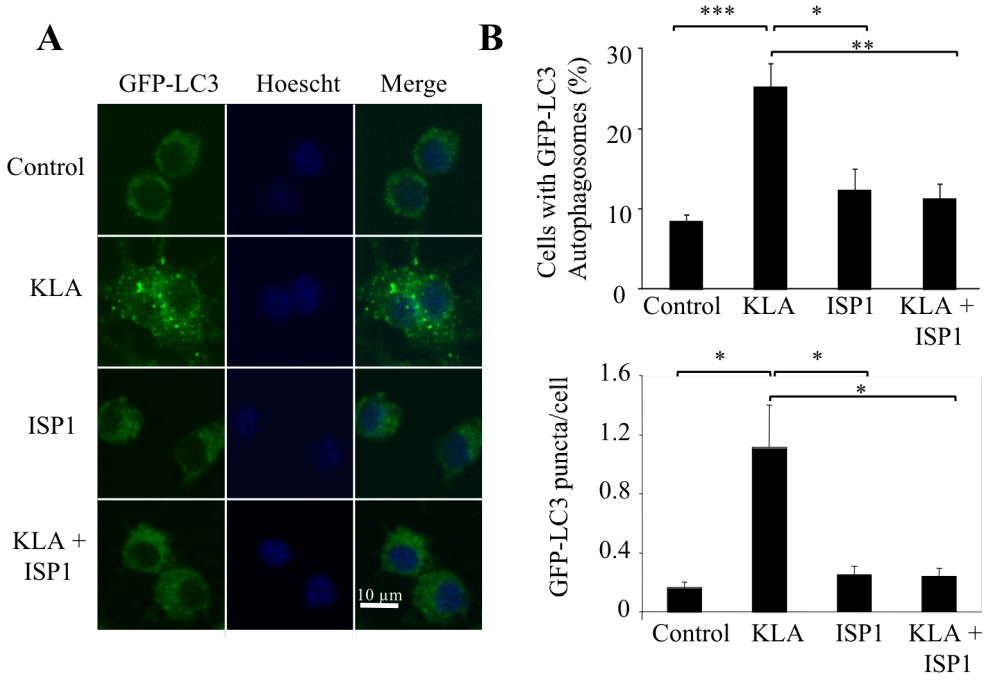

Figure 2.15 KLA-Induced Autophagy is Dependent on *de novo* Sphingolipid Biosynthesis
RAW264.7 cells stably expressing GFP-LC3 were incubated for 24 h with vehicle control (PBS), KLA (100 ng/mL), ISP1 (1 µM), or KLA+ ISP1. For cells treated with KLA + ISP1, ISP1 was added 1 h prior to the addition of KLA. *A*, Representative images. *B*, The number of cells displaying GFP-LC3 puncta (upper panel) and the number of GFP-LC3 puncta/cell were quantified using ImageJ. For each experimental condition, a minimum of 195 cells/experiment were counted. Data represent mean $\pm$ SEM (n = 4). *p $\leq$ 0.05; **p $\leq$ 0.01; ***p $\leq$ 0.001.

2.3.7 Confirmation that *de novo* Sphingolipid Biosynthesis is Required for Autophagy using CHO-LYB Cells

Since conditions for complete knock-down of *de novo* SL biosynthesis using siRNA have not been established yet for these RAW264.7 cells, the requirement for *de novo* SL biosynthesis for autophagy induction was confirmed using another cell model, the CHO-LYB cell line, which lacks SPT activity due to mutation of SPT1 [143]. When these cells were transfected with GFP-LC3 and treated with a reagent known to induce autophagy, 4-HPR [1, 99, 144], there was no increase in fluorescent puncta versus the control (Fig. 2.16). However, when this cell line has been stably transfected with SPT1 (CHO-LYB-LCB1 cells) to restore *de novo* SL biosynthesis [143], it responds to 4-HPR with robust accumulation of GFP-LC3 punctate autophagosomes (Fig. 2.16), as has been seen in other cell lines [1, 99, 144]. Therefore, these results confirm that *de novo* SL biosynthesis is required for induction of autophagy.

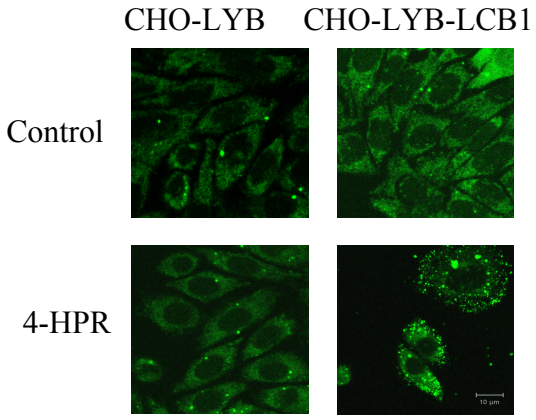

Figure 2.16 Confirmation that *de novo* Sphingolipid Biosynthesis is Required for Autophagy using CHO-LYB Cells CHO-LYB and CHO-LYB-LCB1 cells transfected with GFP-LC3 were incubated with vehicle control (EtOH) or 4-HPR (10 μM) for 24 h. Representative images for each condition are shown.

2.3.8 Evidence that KLA Promotes the Co-Localization of Ceramide with Autophagosomes

SL biosynthesis *de novo* originates in the ER [9] followed by trafficking of Cer (and other metabolites) to the GC by vesicular and CERT-mediated processes [154]. Since the ER and GC are thought to be membrane components for autophagosome formation [155-158], it is possible that *de novo* biosynthesized Cer and/or other SL are incorporated into autophagosomes for structural and/or signaling purposes. To determine if Cer is associated with autophagosomes, we examined RAW264.7 cells using an anti-Cer antibody that has been previously characterized for subcellular localization studies [134-139]. In unstimulated RAW264.7 cells, this antibody co-localized mainly in the perinuclear, GC, as has been previously observed for other cells using anti-Cer antibodies [134] and fluorescent Cer analogs [8] (Fig. 2.17A). However, following addition of KLA, the immunofluorescence clearly shifts to punctate vesicles that co-localize with the autophagosomal marker, GFP-LC3 (Fig. 2.17A). Furthermore, inhibition of *de novo* SL biosynthesis with ISP1 had no noticeable effect on the anti-Cer antibody immunofluorescence associated with the GC (in control or KLA-treated cells), but blocked the KLA induced co-localization of Cer with autophagosomes (Fig. 2.17A). The quantitative analysis of multiple confocal images shows that this suppression was highly significant (Fig. 2.17B) whether expressed as the total number of cells with GFP-LC3 puncta co-localized with Cer (Fig. 2.17B, *upper panel*) or as the number of autophagic cells (i.e. those cells with 5 or more GFP-LC3 puncta) with GFP-LC3 puncta co-localized with Cer (Fig. 11B, *lower panel*). The lack of effect of ISP1 on the GC localization is not surprising because Cer from SL turnover is known to reach the GC by retrograde

trafficking [159, 160]. Thus, these findings are strongly suggestive that the anti-Cer antibody immunofluorescence reflects Cer (and possibly related compounds such as DHCer) incorporation into autophagosomes in KLA-activated RAW264.7 cells.

Cer accumulation has been noted to cause disassembly of the GC [161], therefore, to determine if the punctate structures seen in these studies might be due to disorganization/fragmentation of the ER/GC network, we also used antibodies against GM130, a resident protein found in the *cis*-Golgi, and BiP/GRP78, a chaperone protein found in the ER, to examine the structure of the GC and ER. As shown in Fig. 11C, KLA did not significantly alter the localization of GM130 or BiP/GRP78 suggesting that Cer's assocation with the autophagosome is not due to its ability to disrupt the ER/GC (Fig. 2.17C).

All together, these findings are strongly suggestive that *de novo* biosynthesized Cer (and possibly related compounds such as DHCer) are incorporation into autophagosomes but not via a general recruitment of the ER or GC.

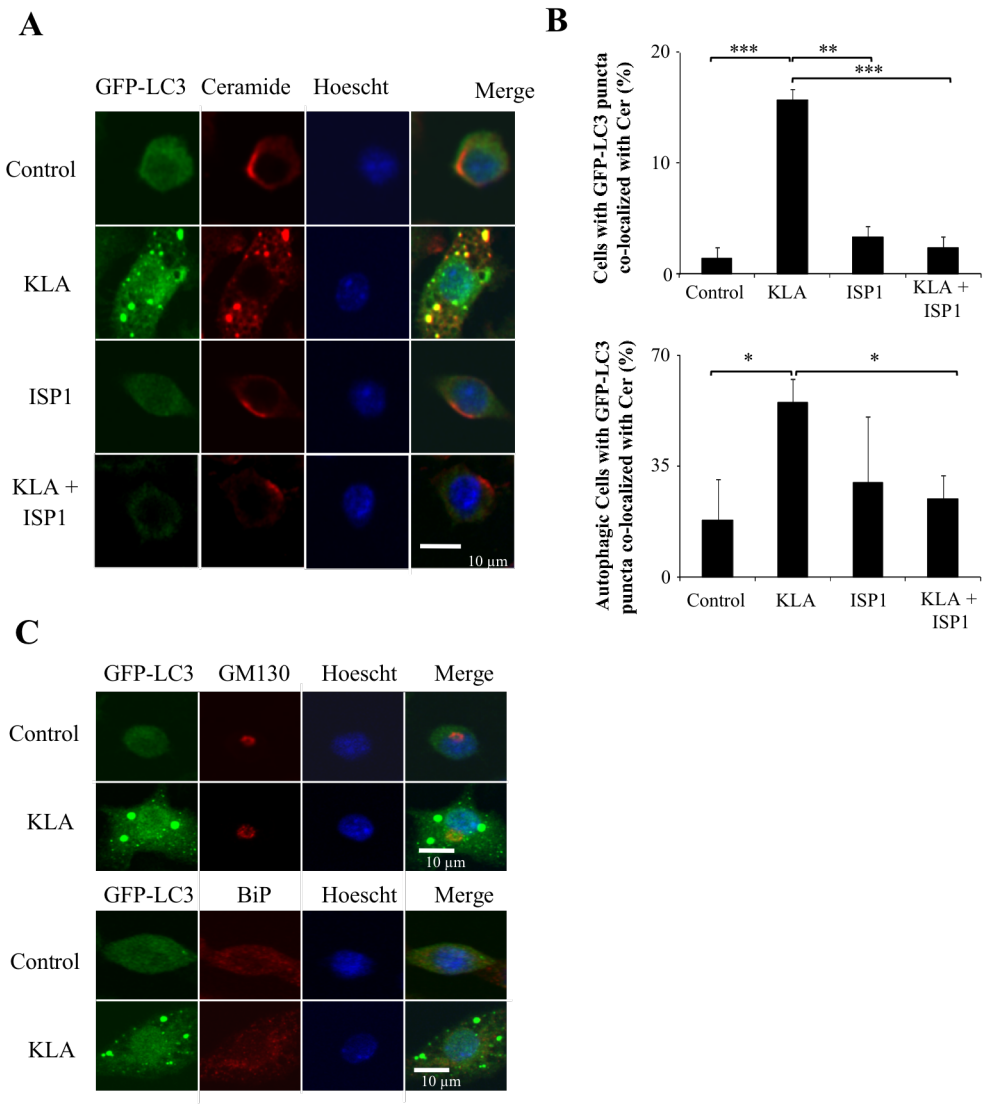

Figure 2.17 KLA Promotes the Co-localization of Ceramide with the Autophagosome RAW264.7 cells stably expressing GFP-LC3 were incubated for 24 h with vehicle control (PBS), KLA (100 ng/mL), ISP1 (1 µM), or KLA + ISP1. For cells treated with KLA + ISP1, ISP1 was added 1 h prior to the addition of KLA. *A,* Following treatment, the extra- and intracellular Cer was stained for all conditions. Representative images. *B,* The number of cells displaying GFP-LC3 puncta co-localized with ceramide (upper panel) was quantified using ImageJ. For each experimental condition, a minimum of 150 cells/experiment were analyzed for ceramide co-localization. Data represent mean $\pm$ SEM (n = 4). *Lower panel,* The number of autophagic cells displaying GFP-LC3 puncta co-localized with Cer was quantified using ImageJ. For each experimental condition, a minimum total of 40 autophagic cells were analyzed for Cer co-localization. Data represent mean $\pm$ SEM (n = 4). *p $\leq$ 0.05. **p $\leq$ 0.01; ***p $\leq$ 0.001. *C,* RAW264.7 cells stably expressing GFP-LC3 were incubated for 24 h with vehicle control (PBS) or KLA (100 ng/mL). Following treatment, the GC and ER were stained using antibodies against GM130 and BiP, respectively

2.4 Discussion

These studies have determined the cellular amounts of the SL of RAW264.7 cells from the first detectable intermediate (Sa) through Cer and its initial metabolites (SM, GlcCer, etc.), and established how KLA, a TLR4 receptor agonist, alters the amounts of many of these compounds. Through the use of an inhibitor of *de novo* SL biosynthesis and stable isotope labeling, we found that both control and KLA-stimulated RAW264.7 cells are actively engaged in *de novo* SL biosynthesis; however, soon after KLA treatment, the cells stop dividing, resulting in an increase in the cell size and SL content.

Most of the changes in SL were due to *de novo* biosynthesis and are reminiscent of the induction of SL biosynthesis in liver [129] and a number of extrahepatic tissues [130]. Increases in Cer are an interesting exception because it was also derived from another source, most likely the turnover of cellular SM, which is also in agreement with previously noted activation of sphingomyelinase and production of Cer in LPS treated cells [131]. It is intriguing that the amount of Cer that can be attributed to *de novo* biosynthesis when the cells are incubated with [^{13}C]palmitate is similar to the total Cer in experiments without stable isotope labeling, and when cells are treated with ISP1 in addition to KLA (Fig. 2.2, 2.9, and 2.11). This suggests that the cells have mechanism(s) to maintain some form of "Cer homeostatsis" by coordination of the formation and removal of this compound to/from multiple sources.

We think that one of the most important findings of these studies is that activation of RAW264.7 cells not only increased the cellular SL content but also cell size (~24%), surface area (~53%), and the production of the intracellular membrane vacuoles termed autophagosomes. Furthermore, *de novo* SL biosynthesis was shown to be necessary for

autophagosome formation, which—to the best of our knowledge—is the first demonstration of the requirement for SL for a "normal" biological process for induction of autophagy, although exogenous addition of SL, or their endogenous accumulation when SL metabolism has been disrupted, has been noted to induce autophagy in other cell types [1, 102-105]. Consistent with a requirement for *de novo* SL biosynthesis for autophagy, we found that CHO-LYB cells are refractory to induction of autophagy by 4-HPR until a functional SPT1 was reintroduced into the cells (Fig. 2.16). Therefore, SL may play an essential role in many, if not all, forms of autophagy.

It is not yet known with certainty if the *de novo* biosynthesized SL(s) required for autophagy is (are) (DH)Cer *per se*, although the anti-Cer antibody co-localization studies suggest that this might be the case. This raises the possibility that the production of (DH)Cer and possibly other SL [103] by *de novo* biosynthesis in the ER might be a driving force for formation of the autophagosomal vacuole, in what has been referred to as the "membrane extension" step [162] that occurs after many of the associated autophagosomal proteins have been recruited. If this process requires participation by the ER, this might explain why elevation of Cer by SL turnover did not appear to be adequate for induction of autophagy by KLA in RAW264.7 cells; which is also consistent with the previous observation that treatment of HT29 cells with bacterial sphingomyelinase to generate Cer had no effect on autophagy induction [102]. Furthermore, since the enzymes for *de novo* Cer biosynthesis reside in the ER [9], it is imaginable that they might be recruited into autophagosomes and, perhaps, continue to produce SL there. However, a preliminary experiment using antibodies against the first two enzymes in *de novo* SL biosynthesis, serine palmitoyltransferase subunit 1 (SPT1, also called "LCB1") and

3KSR, found no evidence that the enzymatic machinery for *de novo* SL biosynthesisis is recruited to the autophagosome. Therefore, the idea of how ceramide becomes associated with the autophagosome is an interesting area for continued study.

There are additional reasons to suspect that Cer might play a role in autophagy. First, Cer has been identified as a mediator in the ER-localized dissociation of the Beclin-Bcl-2 complex, which facilitates autophagosomal vesicle nucleation [68, 76, 104]. Second, activation of macrophages invokes ER stress [163], which is one of the up-regulators of autophagy [164] and might involve SL as intermediaries or modulators [165]. And third, Cer has been shown to inhibit the activation of the Akt/mTOR cascade resulting in the induction of autophagy [102], and the microarray analysis by the LIPID MAPS Consortium (www.lipidmaps.org) suggests that KLA decreases mTOR mRNA; therefore, KLA might induce autophagy through repression of the Akt/mTOR signaling pathway at multiple levels. All of the above might be interrelated, or mean that there are multiple roles for SL in autophagy, as has often proven to be the case in other biological processes.

There is a strong likelihood that additional SL [103] and other lipid categories (e.g., phosphatidylethanolamine) [77, 78] are involved in autophagy, and that the categories differ among organisms. In yeast, sterol glycoside appears to be critical for membrane extension [162], which suggests that future studies should explore if—by "lipid homology"— MH-Cer (GlcCer and/or GalCer) might play a role in induction of autophagy in mammalian cells. Balances among lipid categories might also be important, as illustrated by the induction of autophagy by cholesterol overloading [166]. Considering how many lipid categories are changed by KLA in RAW264.7 cells

(www.lipidmaps.org), there are many other possibilities to be explored. The studies described in this chapter have, at least, mapped the changes in SL metabolism in activated RAW264.7 cells and demonstrated a direct link between *de novo* SL biosynthesis and autophagy, one of the important cell behaviors of cells of the innate immune system.

CHAPTER 3

INHIBITION OF DIHYDROCERAMIDE DESATURASE AND PERTURBATION OF CELLULAR SPHINGOLIPID METABOLISM BY 4-HYDROXYPALMITANILIDE VERSUS 4-HYDROXYPHENYLRETINAMIDE (FENRETINIDE): IMPLICATIONS FOR MODULATION OF DIHYDROCERAMIDE METABOLISM AND CELL FUNCTION BY SYNTHETIC AND NATURAL COMPOUNDS

3.1 Introduction

4-HPR is a synthetic retinoid undergoing evaluation as an anti-cancer agent in human clinical trials for breast [167, 168], ovarian [169], neuroblastoma [170], lung [171] and other [172] cancers. Its mode of action appears to involve multiple mechanisms [173], ultimately resulting in apoptosis [174] and/or autophagic cell death [99]. One of its potent cellular effects, which has been proposed to participate in its cytotoxicity [175] and induction of autophagy [1], is the alteration of SL metabolism.

4-HPR was initially thought to induce SL biosynthesis *de novo* and elevate Cer [175] until analysis of cellular SL using LC ESI-MS/MS revealed that it actually increases DHCer and downstream complex DHSL, Sa, and Sa1P [1, 176-178] due to blockage of the desaturation of DHCer to Cer [1] in addition to its known increase in *de novo* biosynthesis. Inhibition of DES has been confirmed by *in vitro* enzymatic assays [178, 179], which also confirmed that the 4-HPR metabolite, 4-oxo-4-HPR, is more potent [178, 180], whereas, inhibition is substantially eliminated by methylation of the phenolic hydroxyl (i.e., in 4-methoxyphenylretinamide) [179]. The latter observation

indicates that the phenolic hydroxyl plays a major role in DES inhibition, but what is not yet known is if the retinoid moiety *per se* is required, or might be substituted by other functionalities. This information could be important because a number of bioactive compounds with phenolic substituents, such as resveratrol [109], also elevate DHCer but have been assumed to be unlikely to function as direct inhibitors of DES [179].

The current study has explored the factors that account for elevation of DHSL in cells treated with 4-HPR and structurally related compounds using Hek293 cells and LC ESI-MS/MS for analysis of their effects on cellular SL; and, where pertinent, their effects as DES inhibitors have also been examined using *in situ* and *in vitro* DES assays. This included the possibility that elevation of *de novo* biosynthesis *per se* might cause accumulation of DHSL; however, the major finding was that compounds as simple as 4-hydroxypalmitanilide (4-HPA, palmitic acid in amide linkage with aminophenol) inhibit DES, elevate cellular DHSL and induce autophagy, as has been previously noted for 4-HPR and other molecules which increase DHCer [1, 99, 109, 144, 181]. Moreoever, in contrast to 4-HPR, 4-HPA has little effect on cell viability and provides researchers with a useful tool for the studying the cellular effects of the accumulation of DHCer – particulary cell-fate decisions associated with the induction of autophagy.

3.2 Experimental Procedures

3.2.1 Materials

The suppliers for the reagents were: Succinimidyl 6-(N(7-nitrobenz-2-oxa-1,3-diazol-4-yl)amino)hexanoate (NBD-hexanoate succimidyl ester) (Molecular Probes, Carlsbad,Ca); C6-NBD-ceramide, C6-NBD-glucosylceramide and C6-NBD-sphingomyelin (Avanti Polar Lipids, Alabaster, AL); D-*erythro*-dihydrosphingosine, reduced nicotinamide adenine dinucleotide (NADH), N-(4-hydroxyphenyl)retinamide (4-

HPR)(IUPAC name: (2E,4E,6E,8E)-N-(4-hydroxyphenyl)-3,7-dimethyl-9-(2,6,6-trimethylcyclohexen-1-yl)nona-2,4,6,8-tetraenamide), 4-hydroxypalmitanilide (4-HPA), 4-Acetamidophenol (Sigma Aldrich, St. Louis, MO); Brefeldin A (Epicenter, Madison, WI); NADPH-regenerating system (BD Biosciences, Bedford, MA); palmitanilide (PA) (TCI America, Portland, OR); D-*threo*-1-ethylendioxyphenyl-2-palmitoylamino-3-pyrrolidino-propanol (D-*t*-oEtDO-P4), a glucosylceramide synthase inhibitor [182] was a gift from Dr. James A. Shayman (University of Michigan Medical Center, Ann Arbor, MI).

3.2.2 Cells and Cell Culture

Hek293 cells (from the American Type Culture Collection, Mannassas, VA) and the SPT1/2 overexpressing cells (previously described) [183] were grown in DMEM/F12 (MediaTech, Manassas,VA) supplemented with 10% heat-inactivated fetal calf serum (Hyclone, Logan, UT) and penicillin (100 U/mL) plus streptomycin (0.1 mg/mL). The cells were maintained in a 37°C, 90% relative humidity, and a 5% CO_2 environment.

3.2.3 Synthesis of C6-NBD-Dihydroceramide

A solution of 5.9 mg (15 µmol) of succinimidyl 6-(N(7-nitrobenz-2-oxa-1,3-diazol-4-yl)amino)hexanoate in 0.2 ml of 99.8% DMF was added to a solution of 3.9 mg (13µmol) of D-*erythro*-dihydrosphingosine and 20 µl N,N-di-isopropylethylamine in 0.3 ml of dry DMF, and the mixture was incubated at 40ºC for 20 h. Following evaporation of the solvent, a small portion of the residue was dissolved in $CHCl_3/CH_3OH$ (1:1, v/v) and the purity of the NBD-dihydroceramide was analyzed by TLC on silica gel plates using $CHCl_3/CH_3OH/H_2O$ (80:19:1, v/v/v) for the solvent system and detection of the C6-NBD-dihydroceramide by fluorescence under UV light. The purity of the reaction product was further confirmed by HPLC analysis (see below).

3.2.4 *In situ* Dihydrocermide Desaturase Assay and Lipid Extraction

Hek293 cells (1.4×10^5 cells/well) were seeded into 6-well plates 24 h prior to the assay. The synthesized C6-NBD-dihydroceramide (in ethanol) was injected into serum-free culture medium to achieve a final concentration of up to 5 μM (the final ethanol concentration did not exceed 0.5%, v/v), as previously described [184]. The dishes were returned to the tissue culture incubator for the indicated time, then the cells were washed twice with cold PBS prior to harvesting by scraping into a minimal volume of PBS and placed in 13 x 100 mm borosilicate test tubes. The cells were centrifuged for 2 min in a table top centrifuge, the supernatant was removed, and the pellet was re-suspended in 1.4 ml of $CHCl_3/CH_3OH$ (1:2, v/v) by brief sonication. To this was added 1 ml of $CHCl_3$ and 3 ml of H_2O followed by gentle mixing, then the tubes were centrifuged to separate the phases. The lower ($CHCl_3$) layer was collected and the solvent evaporated with an AES2000 automatic environmental speedvac (Thermo Savant, Waltham, MA). The fluorescent SL were analyzed by HPLC as described below.

3.2.5 *In vitro* Dihdyroceramide Desaturase Assay

Semi-intact cells were prepared as described by Funakoshi et al. [185], and resuspended in Hepes/KCl buffer (H/KCl buffer, 25 mM Hepes-KOH, pH 7.2, 115 mM KCl). Aliquots of the perforated cells were checked with Trypan blue to determine the extent of perforation (which was from 90 to 95%) and to determine the protein amount using a BCA assay. The components of the assay mixture were prepared on ice and contained 200 μg of protein from the semi-intact cell suspension, 3.33 mM NADH and 2.6 mM NADPH (as a component of the NADPH-regenerating system) to ensure adequate reductants were available for the desaturase activity [15, 186], and 4-HPR at

final concentrations of 0 to 10 μM. H/KCl buffer was added to bring the total volume to 99 μl, then 1 μl of 500 μM C6-NBD-dihydroceramide (in ethanol) was added, on ice, mixed, and the assay tubes were placed in a shaking water bath at 37 ºC for 1 h. The reaction was stopped by the addition of 700 μl of $CHCl_3/CH_3OH$ (1:2, v/v). The lipids of interest were extracted by the addition of 230 μl of $CHCl_3$ and 420 μl of 0.1 M KCl. The $CHCl_3$ phase was then removed and allowed to evaporate. Following evaporation of chloroform, the resulting products were analyzed by HPLC.

3.2.6 HPLC Analysis of NBD-Sphingolipids

HPLC analysis was conducted using a Shimadzu (Kyoto, Japan) Model LC-10AS liquid chromatograph with a Waters (Milford, MA) Radial Pak C18 column (4 μm, type 8NVC184) and 10 μm μBondapak C18 Guard insert, and an isocratic solvent system ($CH_3OH/H_2O/H_3PO_4$, 800:200:1.5, v/v/v) at a flow rate of 1 mL/min. The individual NBD-SL were detected using a Shimadzu RF-535 spectrofluorometer with an excitation wavelength of 460 nm and an emission wavelength of 537 nm, and identified by comparison with commercially available C6-NBD-SL (Avanti Polar Lipids, Alabaster, AL).

3.2.7 Lipid Extraction and Analysis by LC ESI-MS/MS

The extraction and analysis methods have been thoroughly described [127] and the LC ESI-MS/MS was conducted using a Perkin Elmer Series 200 MicroPump system coupled to a PE Sciex API 3000 triple quadrupole mass spectrometer (Applied Biosystems, Foster City, CA), and a Shimadzu LC-10 AD VP binary pump system coupled to a Perkin Elmer Series 200 autoinjector coupled to a 4000 QTrap (Applied Biosystems, Foster City, CA) operating in a triple quadrupole mode. The internal

standard cocktail for quantitation was obtained from Avanti Polar Lipids (Alabaster, AL). Protein concentration was determined using a BCA Assay Kit (Pierce, Rockford, IL). Statistical analysis was performed using a two-tailed Student's t-test.

3.2.8 Stable Isotope Labeling of Sphingolipids

Stable isotope labeling was conducted using [U-^{13}C]-palmitate as recently described [140]. In brief, the [U-^{13}C]-palmitate was prepared as the 1:1 (mol:mol) complex with fatty acid-free bovine serum albumin (BSA) as a 1 mM solution in PBS which was diluted to 0.1 mM with complete cell culture medium, filter sterilized, and added to the cells. After the indicated times of incubation, the unlabeled (^{12}C-) and the three categories of SL labeled with [U-^{13}C]-palmitate (i.e., in the sphingoid base backbone alone—which we designate "Base-labeled;" in the fatty acid only—"Fatty acid-labeled;" and in both the sphingoid base and fatty acid—"Dual-labeled") were quantified by LC ESI-MS/MS by comparison of the the peak areas of the analytes of interest with the spiked internal standards [140]. The sum of the "Base-labeled" and "Dual-labeled" data for a given SL subspecies has been used for the unambiguously "*de novo*" biosynthesized molecules since these both have [^{13}C] in the sphingoid base backbone from utilization of [U-^{13}C]palmitoyl-CoA by the first enzyme of the pathway, serine palmitoyltransferase (Fig. 3.1).

3.2.9 Viability Studies

Viability was monitored using WST-1 (Roche Applied Science, Indianapolis, IN). The cells were seeded in 96-well plates at 2 x 10^4 cells/well for 24 h, then treated with 4-HPR or 4-HPA for the indicated times. Next, viability was estimated by adding the WST-1 reagent to the wells and incubating for up to 60 min at 37°C. The absorbance of the

dye was measured at 450 nm. The data represent n=6 replicates given as mean ± SEM with evaluation of the statistical significance of differences between groups using a two-tailed Student's t-test.

3.2.10 Western Blotting

Hek293 cells were treated with 4-HPA (50 μM) or 4-HPR (5 μM) for 24 h then harvested in RIPA buffer (PBS, 1% Nonidet P-40, 0.5% sodium deoxcholate, and 0.1% SDS) and solubilized by sonication followed by 30 min of incubation on ice. After centrifugation at 12,000 x g for 10 min at 4°C, and the supernatant was collected and the protein amount determined using the BCA Assay Kit (Pierce, Rockford, IL). Aliquots of each sample (50 μg of protein) were separated on a 15% SDS-PAGE gel (Bio-Rad, Hercules, CA) and transferred to a PVDF membrane (Millipore, Billerica, MA). Membranes were blocked in 5% milk/Tris buffered saline containing 0.1% Tween 20 (TBS-T) for 1 h at room temperature and incubated overnight at 4°C with rabbit anti-LC3B (1:500) (Cell Signaling Technology, Boston, MA) and mouse anti-ß actin (1:1000) (Cell Signaling Technology, Boston, MA) primary antibodies. The blot was washed with TBS-T and incubated with horseradish peroxidase conjugated anti-rabbit (Jackson ImmunoResearch Laboratories, West Grove, PA) and anti-mouse (Pierce, Rockford IL) secondary antibodies for 2 h at room temperature, and analyzed using an enhanced chemiluminescent substrate (ECL) (Pierce, Rockford, IL).

3.3 Results

3.3.1 4-HPR Increases Dihydroceramide and other Metabolites with the Sphinganine Backbone in Hek293 Cells

As has been seen with several cell lines [1, 176-178], 4-HPR does not elevate Cer, but rather, causes substantial elevations in DHCer (more than 100-fold versus cells treated with only the vehicle) as determined by LC ESI-MS/MS (see middle panels in Fig. 3.1; results for specific chain-length subspecies of DHCer and Cer are shown later in this chapter (Fig. 3.13)). This was accompanied by: elevations in downstream DHSL, which include DHSM, MH-DHCer (shown on the second rows of Fig. 3.1) and Sa and Sa1P (top row, Fig. 3.1); decreases in Cer and MH-Cer but not SM (third row of Fig. 3.1) and a decrease in So (bottom row); and a small increase in S1P (lower right panel of Fig. 3.1). These results are consistent with the inhibition of DES by 4-HPR as shown by layout of these data in a pathway context in Fig. 3.1.

The total amount of (DH)SL in the 4-HPR treated cells (the sum of the DHSL + SL) was increased by ~2.6 fold when compared with the total (DH)SL of the control (i.e., 12278 pmol/mg for the 4-HPR-treated cells vs 4736 pmol/mg protein in control), which is also indicative that 4-HPR induces *de novo* SL biosynthesis, as has been noted previously [175, 178] (these previous findings are the basis for the "+" arrows at SPT and CerS in Fig. 3.1). This will be experimentally addressed later in this study.

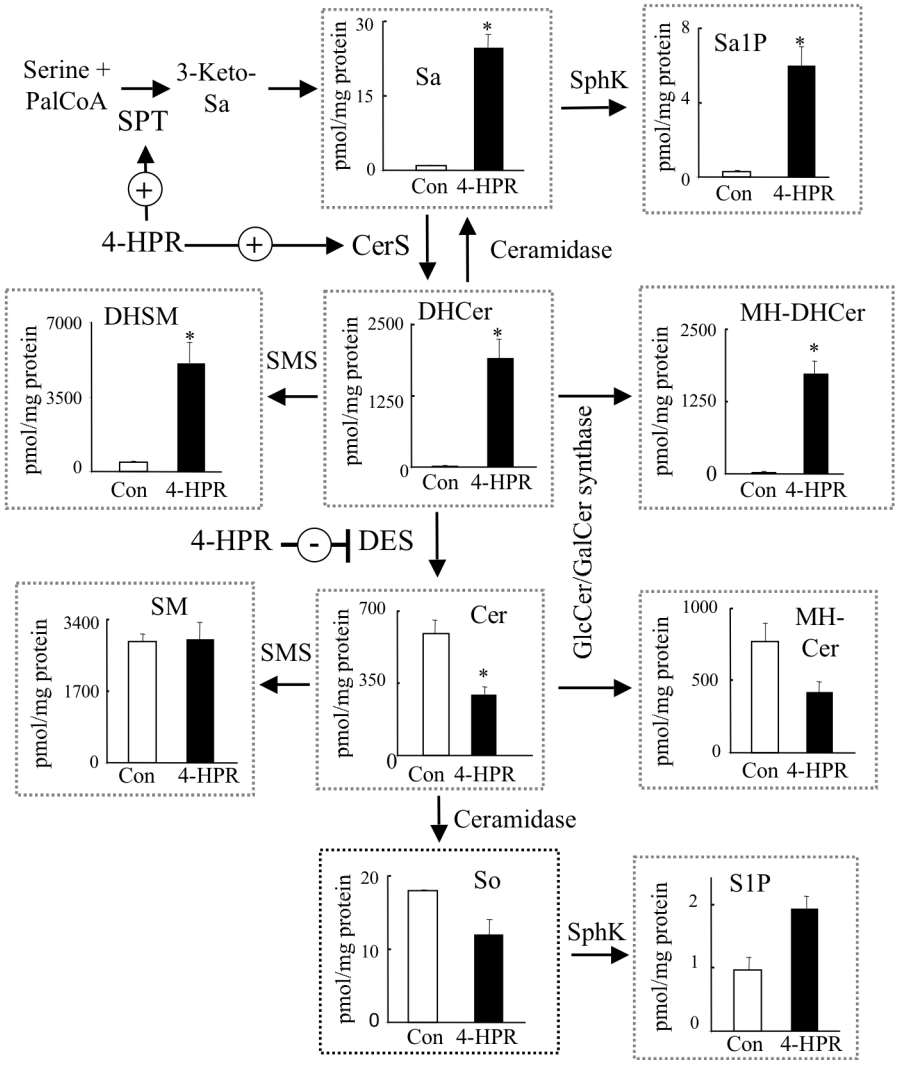

Figure 3.1 4-HPR Induces Significant Increases in Total Dihydrosphingolipids in Hek293 Cells
Hek293 cells were incubated with vehicle control (EtOH) or 4-HPR (5 μM). Following 24 h of treatment, cells were harvested for lipid extraction and analysis by LC ESI-MS/MS. Data represent the mean ± SEM (n = 3); *p < 0.05.

3.3.2 Direct Evidence for 4-HPR Inhibition of DES and C6-NBD-Dihydroceramide Desaturation in Hek293 Cells

Inhibition of DES by 4-HPR could be demonstrated by both *in situ* (Fig. 3.2A) and *in vitro* (Fig. 3.2B) assays using C6-NBD-DHCer as the substrate. The *in situ* assay capitalized on the known ability of NBD-Cer analogs, including NBD-DHCer [184], to be taken up by cells and quickly converted to downstream NBD-labeled SL [187, 188]. Thus, 1 h after C6-NBD-DHCer was added to intact Hek293, analysis of the metabolites by HPLC (Fig. 3.2A, left panel) shows that some of the original C6-NBD-DHCer remains and at least three metabolites have been produced in essentially equal amounts: C6-NBD-dihydroglucosylceramide (DHGlcCer; this was identified as having the Glc headgroup by inhibition by D-*t*-EtDO-P4, as shown in Fig. 3.3)[182], C6-NBD-Cer and C6-NBD-GlcCer. In contrast, when 4-HPR was also added (Fig. 3.2A, right panel), the C6-NBD-Cer and C6-NBD-GlcCer are nearly eliminated, as predicted for DES inhibition by 4-HPR.

4-HPR inhibited DES activity when assayed *in vitro* with semi-permeabilized cells (Fig. 3.2B). We found it difficult to assay DES activity in homogenized Hek293 cells, which is consistent with the reported lability of this enzyme [15]; however, the conversion of C6-NBD-DHCer to C6-NBD-Cer was readily detected when the cells were permeabilized using the protocol developed by Hanada and co-workers in studies of Cer trafficking by CERT [185], as shown in the left elution profile of Fig. 3.2B (the appearance of small amounts of C6-NBD-DHGlcCer might indicate the presence of a small fraction of resealed cells). The production of C6-NBD-Cer was reduced by ~65% by 1 μM 4-HPR, and nearly completely blocked by 10 μM (Fig. 3.2B, middle and right

elution profiles), which is consistent with the reported [179] IC_{50} of ~ 2 μM for 4-HPR when C8-DHCer was used as the substrate.

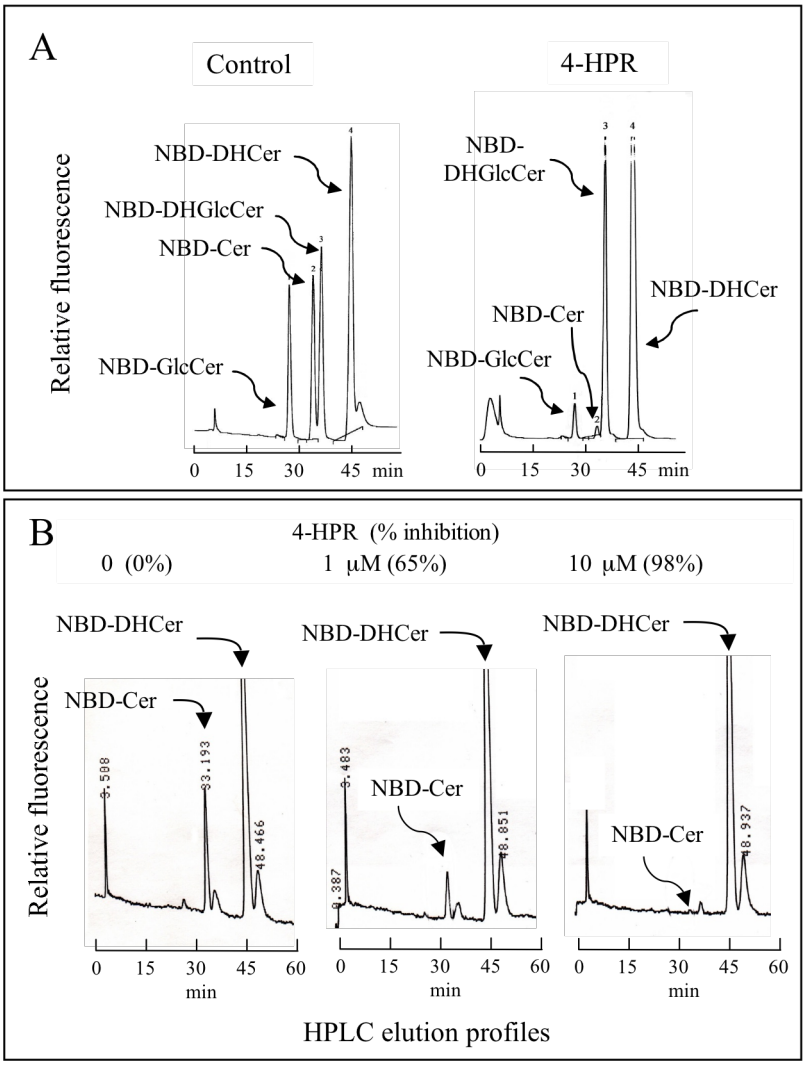

Figure 3.2 4-HPR Inhibits C_6-NBD-Dihydroceramide Desaturation *in situ* and *in vitro* in Hek293 Cells. *A,* Hek293 cells were incubated with or without 10 μM 4-HPR for 1 h prior to the addition of 5 μM C_6-NBD-DHCer. Incubation was continued for an additional hour. The lipids were then extracted and analyzed by reverse phase HPLC with detection of the NBD-fluoresence, as described under *Materials and Methods*. The fluorescent products were identified by comparison with standards. Abbreviations: NBD-GlcCer, NBD-glucosylceramide; NBD-Cer, NBD-ceramide; NBD-DHGlcCer, NBD-dihydroglucosylceramide; NBD-DHCer, NBD-dihydroceramide; and NBD-SM, NBD-sphingomyelin. Data collection was terminated prior to the elution of NBD-dihydrosphingomyelin (NBD-DHSM) from the column. *B*, Semi-intact Hek293 cells were prepared as described in the text and incubated with an NADPH regenerating system, 5 μM C6-NBD-DHCer and the shown concentrations of 4-HPR. After 60 min at 37°C, the assay was terminated through the addition of lipid extraction solvents and analyzed by reverse phase HPLC as described under Materials and Methods. Inhibition was quantified by the reduction of peak area of NBD-Cer versus NBD-DHCer. The fluorescent products were identified by comparison with standards described above.

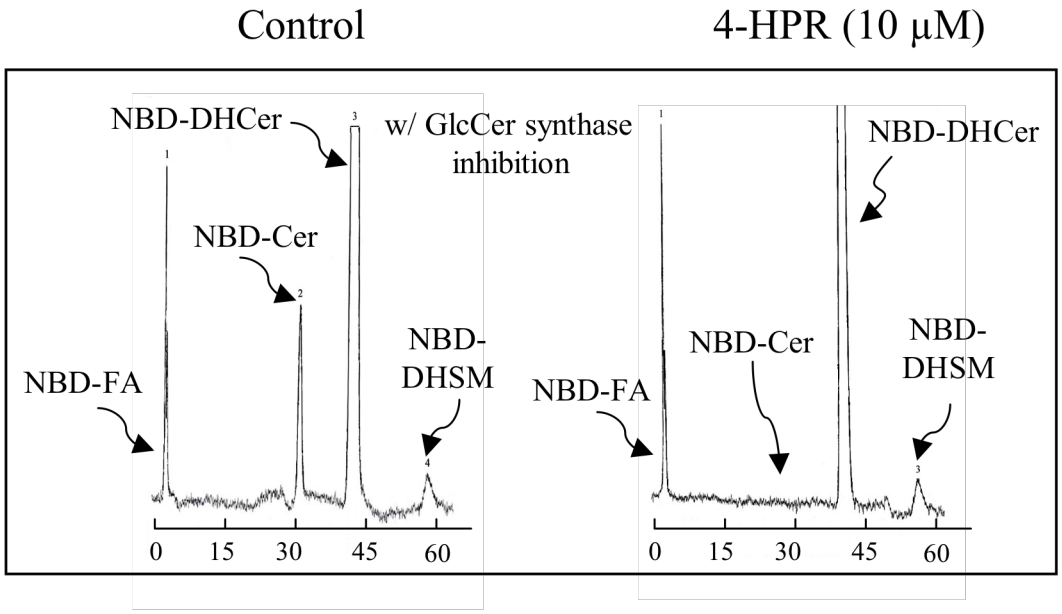

Fig. 3.3 *In situ* Assay of DES with C6-NBD-Dihydroceramide in the Presence of an Inhibitor of Glucosylceramide Synthase Because C6-NBD-Cer and C6-NBD-DHGlcCer elute very close to each other on HPLC, a GlcCer synthase inhibitor (D-threo-1-ethylendioxyphenyl1-2-palmitoylamino-3-pyrrolidino-propanol, D-t-EtDO-P4) was used to confirm our interpretation of the elution profile. As shown in this figure, pre-treatment of the Hek293 cells with D-t-EtDO-P4 completely eliminated the peaks that we had interpreted to be C6-NBD-GlcCer and C6-NBD-DHGlcCer (see Fig. 3.2 in main text), which confirmed our assignments for these compounds. It is also interesting that inhibition of glycosylation elevated the amount of free C6-NBD-fatty acid (at the column throughput) and C6-NBD-DHSM, as one would anticipate due to elimination of one of the branches of (DH)Cer metabolism (c.f., pathway shown in Fig. 3.1 of the main text).

3.3.3 Does Elevated *de novo* Sphingolipid Biosynthesis Contribute to Accumulation of Dihydrosphingolipids in 4-HPR-Treated Cells?

Although the accumulation of DHSL in Hek293 cells treated with 4-HPR correlated well with inhibition of DES activity *in situ* and *in vitro*, there might also be a substantial contribution from the elevation of *de novo* SL biosynthesis by 4-HPR if this results in production of DHCer more rapidly than they can be utilized by DES, i.e., making the desaturation step rate-limiting. To test this hypothesis, we compared DHCer accumulation in wild-type Hek293 cells and Hek293 cells that overexpress both subunits of SPT (referred to as SPT1/2 cells), which have an approximately 6-fold higher SPT activity [183]. At both of the time points examined (3 and 6 h), *de novo* SL biosynthesis (as assessed by production of ^{13}C –labeled SL with the label from U-^{13}C-palmitate in the backbone sphingoid base) was 5 to 8-fold higher for the SPT1/2 cells (Fig. 3.4A) than the Hek293 cells (Fig. 3.4B). The SPT1/2 cells displayed much higher DHSL than the Hek293 cells (c.f. upper graphs in panels A and B); however, the DHCer/Cer ratio (Fig. 3.4C) was still much lower (~0.25) than that found in Hek293 cells treated with 4-HPR (>6) (Fig 3.5A).

The right panels of Fig. 3.4 display the effects of 4-HPR on the incorporation of [^{13}C]palmitate into the sphingoid base backbones of (DH)SL of SPT1/2 cells (Fig. 3.4D) and Hek293 cells (Fig. 3.4E). For the latter, note that the total incorporation of [^{13}C]palmitate (~3 nmol/mg protein at 6 h) was close to the sum for the SPT1/2 cells without 4-HPR (~5 nmol/mg protein at 6 h), therefore, the SPT1/2 cells appear to be a reasonable model to test the hypothesis that elevating the rate of production of DHCer from *de novo* (DH)SL biosynthesis (as occurs in Hek293 cells treated with 4-HPR) might

elevate DHSL by making the DES step rate-limiting. The conclusion from these studies is that elevation of the rate of (DH)SL biosynthesis by several fold does, indeed, elevate the amounts of DHCer and other DHSL somewhat, but this is likely to account for only a small fraction of the elevation of DHSL upon 4-HPR treatment.

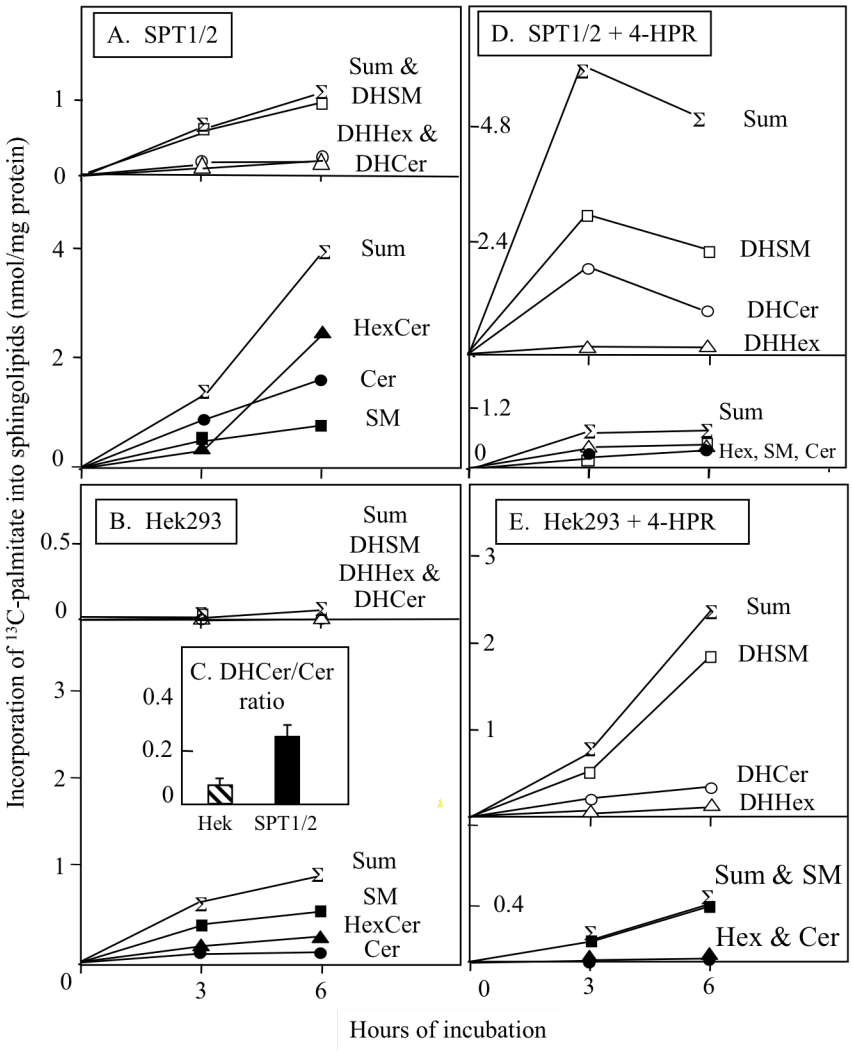

Figure 3.4 *De novo* Sphingolipid Biosynthesis from [U-^{13}C]Palmitate by Hek293 Cells and SPT1/2 Cells with and without 4-HPR.

3.3.4 The Presence of the Retinoid Group is not Essential for Inhibition of DES and Dihydrosphingolipid Elevation

Previous studies have shown that modification of 4-HPR by introduction of a ketone into the cyclopropene ring (4-oxo-4-HPR) of the all *trans*-retinoic acid (ATRA) portion, or by methylation of the phenolic hydroxyl of the aminophenol affect the potency of inhibition [179], but not whether these structural components are particularly active or essential. Figure 3.5 shows the effects of the individual components (ATRA in panel B and *p*-aminophenol in panel C) on the DHCer/Cer ratio of Hek293 cells, with the not-too-surprising lack of significant effects compared to 4-HPR (Fig. 3.5A) (with respect to the retinoid group, 9- and 13-*cis*-retinoic acids were also negative, data not shown). However, if the ATRA is replaced by a simple acetyl group (4-acetamidophenol), there was a small but noteworthy elevation in the DHCer/Cer ratio as shown both on the same scale as 4-HPR in the lower graph and in an expanded version in the upper right region of panel D). This raised the intriguing possibility that other simple alkyl amides—especially ones with longer acyl chains to provide greater hydrophobicity—might be able to substitute for the ATRA component of 4-HPR.

This was examined using an analog with an alkyl chain comparable to that of a typical DHCer (C16) in amide linkage with 4-aminophenol (4-hydroxypalmitanilide, 4-HPA, shown in Fig. 3.6A). Treatment of Hek293 cells with 1 μM 4-HPA significantly increased essentially all N-acyl chain length-DHCer, and the elevation of total DHCer with 10 μM 4-HPA begins to approach that of 4-HPR (c.f., Fig. 3.1 and 3.6B). Additionally, 10 μM 4-HPA significantly decreased the C16-, C22-, C24:1-, and C24-subspecies of Cer when compared with control treated cells (Fig. 3.6C). 4-HPA

significantly increased DHSM and MH-DHCer (Fig. 3.7A and B) as well as Sa and Sa1P (Fig. 3.7C) while decreasing SM and MH-Cer (Fig. 3.7A and B) and So (Fig.3.7C), and minimally affecting S1P (Fig. 3.7C).

The optimal alkyl chain length for DES inhibition by this type of analog has not been determined, but N-(4-hydroxyphenyl)decanamide was also found to inhibit activity *in vitro* (using the assay exemplified in Fig. 3.2B) with a potency similar to that of 4-HPR (Fig. 3.8).

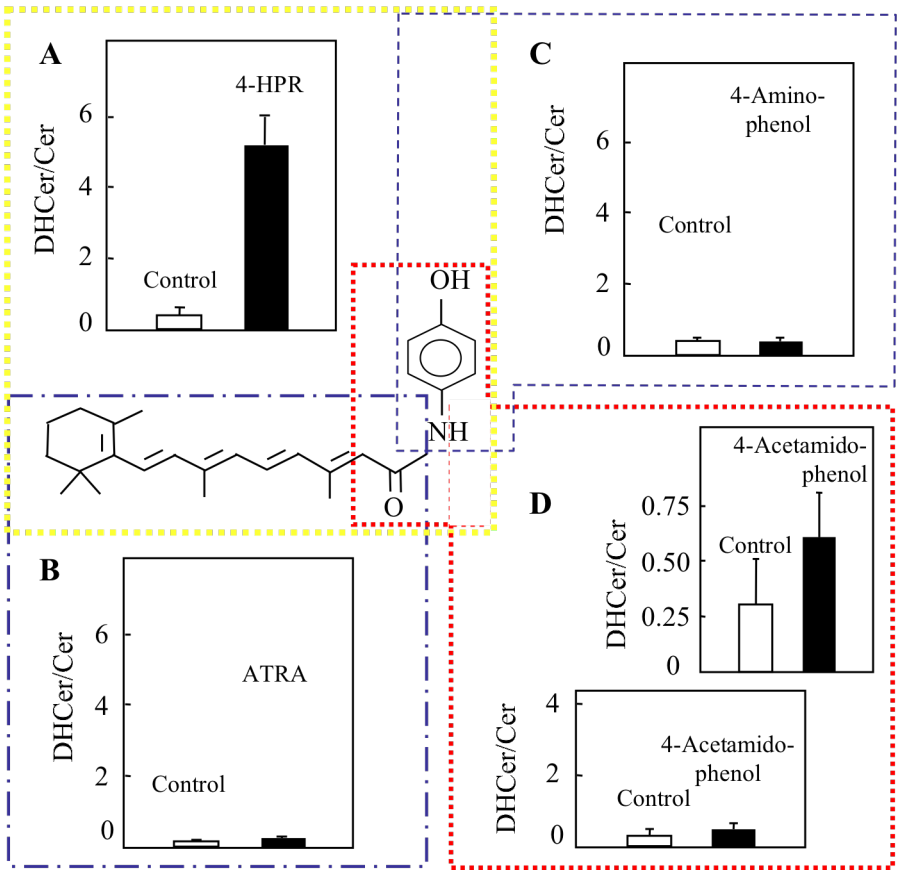

Figure 3.5 Effect of all-*trans*-Retinoic Acid, 4-Aminophenol, and 4-Acetamidophenol Compared to 4-HPR on Dihydroceramide Accumulation in Hek293 Cells Hek293 cells were incubated with vehicle control and *A*, 4-HPR (10 µM), *B*, ATRA (10 µM), *C*, 4-aminophenol (200 µM), or *D*, 4-acetamidophenol (100 µM). Following treatment, cells were harvested for lipid extraction and analysis by LC ESI-MS/MS. Data represent the mean ± (n=3). Ratio of C16DHCer to C16Cer in treatment versus control are shown.

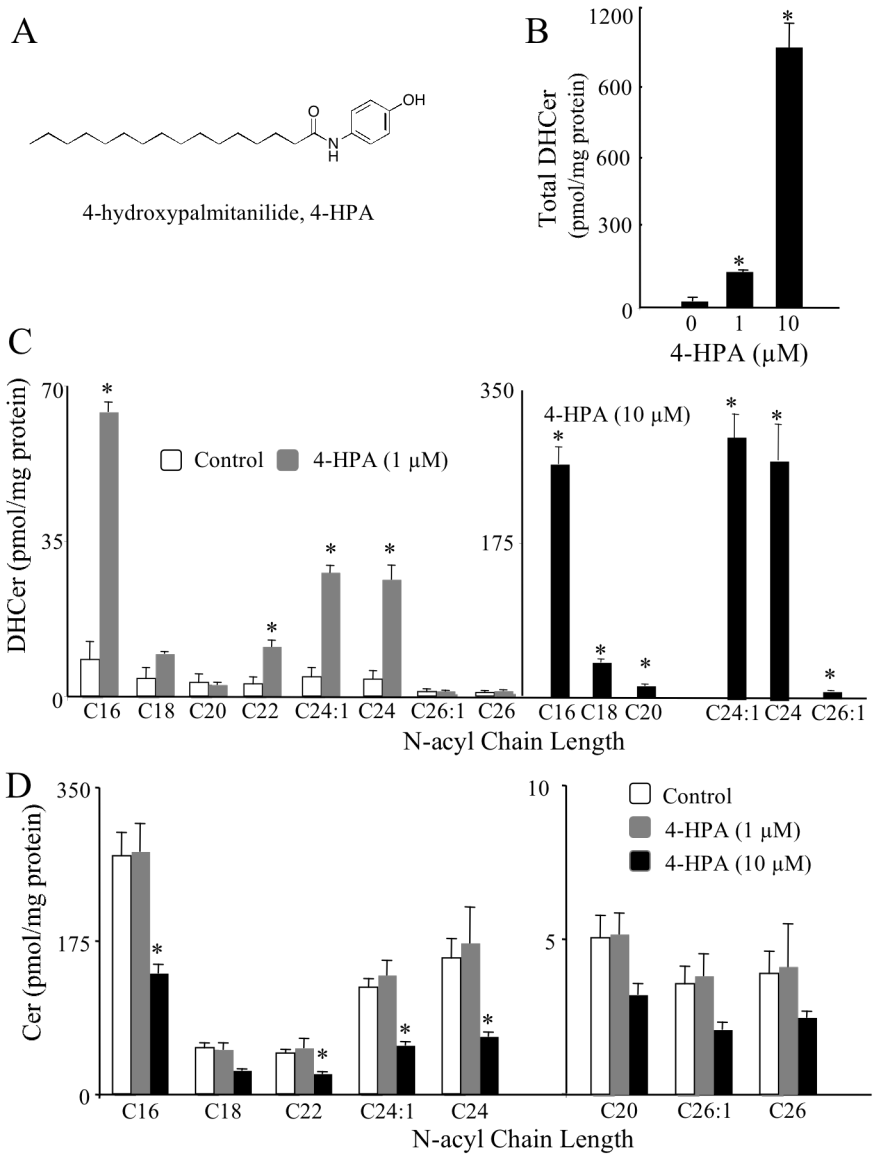

Figure 3.6. Dihydroceramide and Ceramide Species in 4-HPA-Treated Hek293 Cells Hek293 cells were incubated with vehicle control (EtOH) or 4-HPA (1 μM or 10 μM). Following treatment for 24 h, cells were harvested for lipid extraction and analysis by LC ESI-MS/MS. *A*, Structure of 4-HPA *B,* Amounts of total DHCer (a summation of all chain lengths) in 4-HPA versus control conditions. Data represent the mean + SEM (n = 3); *p < 0.05. *C,*Amounts of the major chain length subspecies of DHCer. Data represent the mean ± (n=3); *p < 0.05. *D,* Amounts of the major chain length subspecies of Cer. Data represent the mean + SEM (n = 3); *p < 0.05.

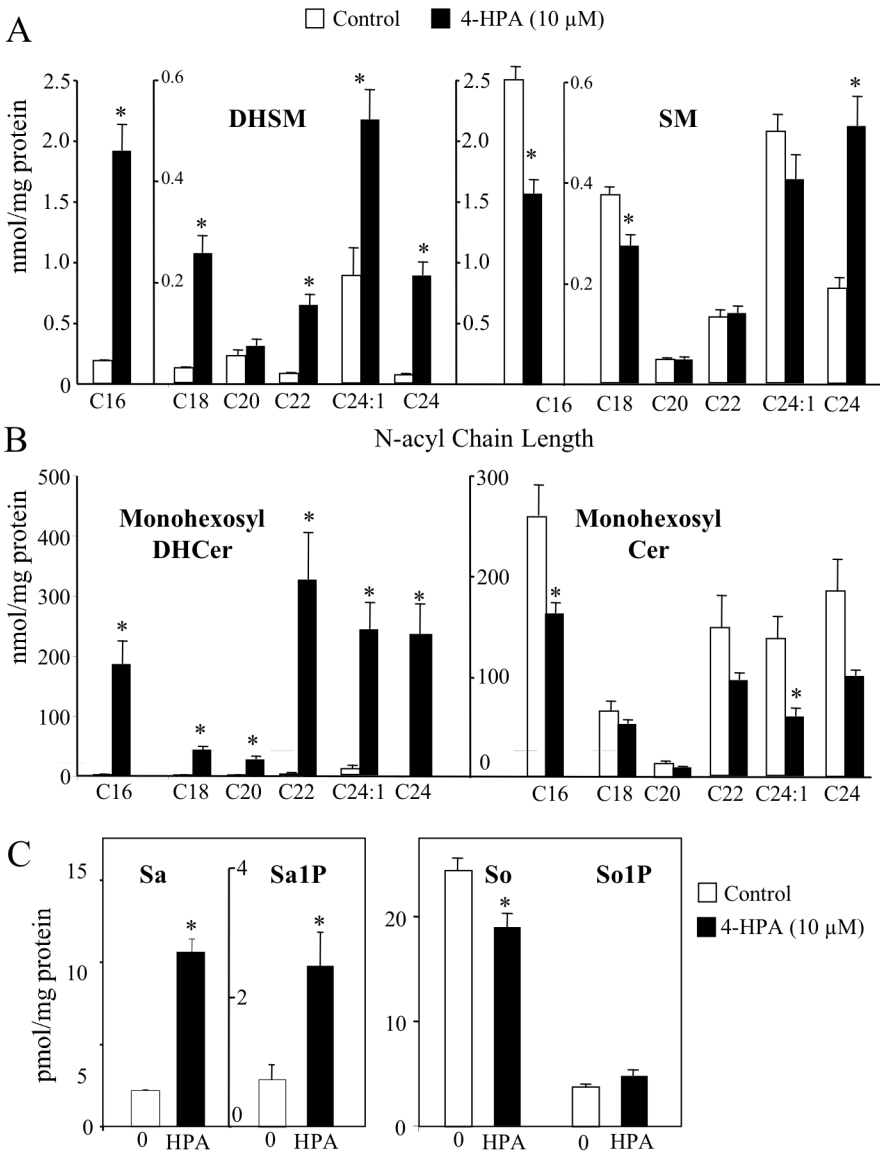

Figure 3.7 (Dihydro)sphingomyelin, Monohexosyl(dihydro)ceramide, Sphingoid Bases, and Sphingoid Base Phosphates in 4-HPA-Treated Hek293 Cells Hek293 cells were incubated with vehicle control (EtOH) or 4-HPA (10 μM). Following treatment for 24 h, cells were harvested for lipid extraction and analysis by LC ESI-MS/MS. *A*, Amounts of the major chain length subspecies of DHSM and SM. *B*, Amounts of the major chain length subspecies of MH-DHCer and MH-Cer. Data represent the mean ± (n=3); *p < 0.05. *C,* Amounts of Sa, Sa1P, So, and S1P. Data represent the mean + SEM (n = 3); *p < 0.05.

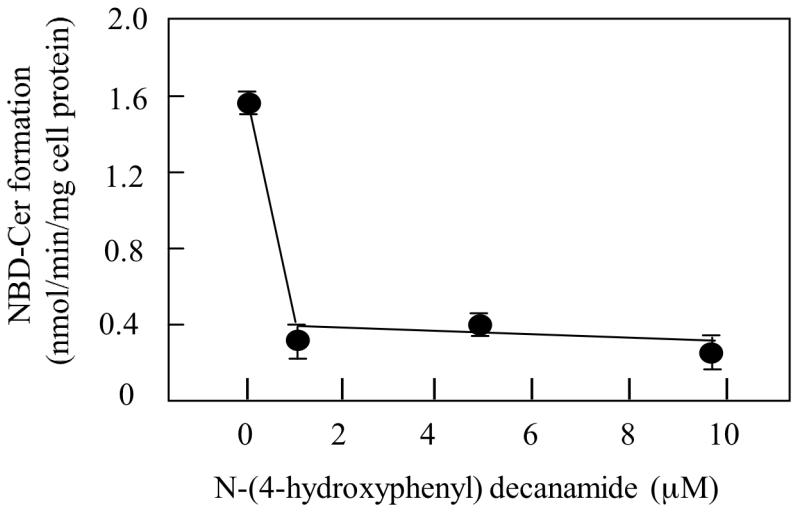

Figure 3.8 *In vitro* Assay of DES with C6-NBD-Dihydroceramide in the Presence of N-(4-hydroxyphenyl)decanamide Semi-intact Hek293 cells were prepared as described in the text and incubated with an NADPH regenerating system, 5 μM C6-NBD-DHCer and the shown concentrations of 4-hydroxyphenyldecanamide. After 60 min at 37°C, the assay was terminated through the addition of lipid extraction solvents and analyzed by reverse phase HPLC as described under Materials and Methods. Inhibition was quantified by the reduction of peak area of NBD-Cer versus NBD-DHCer

3.3.5 The Presence of the Phenol Group is Essential for Inhibition of DES and Dihydrosphingolipid Elevation

While treatment of Hek293 cells with 4-HPA largely recapitulates the changes in (DH)SL seen with 4-HPR, the same concentrations of palmitanilide (PA), which lacks the phenol group, had no effect on total DHCer (Fig. 3.9A) or total Cer (Fig. 3.9B) versus the control. These findings establish that the phenol group of 4-HPA is imperative for the effective inhibition of DES, in agreement with the recent report that methylation of the phenolic group of 4-HPR reduces its potency [179].

The fact that the alkyl chain can be as simple as an acetyl (Fig. 3.5), decanoyl (Fig. 3.8) or palmitoyl (Figs. 3.6 and 3.7) group suggests that other categories of hydrophobic phenols might inhibit DES and elevate DHSL. Support for this idea has been provided by a previously published study that found that resveratrol, a polyphenolic bioactive natural product (Fig. 3.10), increased DHCer in a human gastric cancer cell line and appeared to inhibit DES activity based on *in vitro* assay [109] (however, the latter activity measurements were made after 16 h of treatment with 50 μM resveratrol, so the effect might have been indirect, as was later presumed) [179]. To answer this question, we treated Hek293 cells with resveratrol to determine its effect on cellular (DH)SL (Fig. 3.10A & B) and its inhibition of DES activity *in vitro* using semi-permeabilized cells (Fig. 3.10C). Resveratrol significantly increased almost every DHCer subspecies shown in Fig. 3.10A, and DES inhibition *in vitro* was evident with sub-μM concentrations, and almost completely eliminated by 1 μM (Fig. 3.10C). Therefore, two distinct categories of phenolic compounds that have structures that differ substantially from 4-HPR also inhibit DES and elevate DHSL.

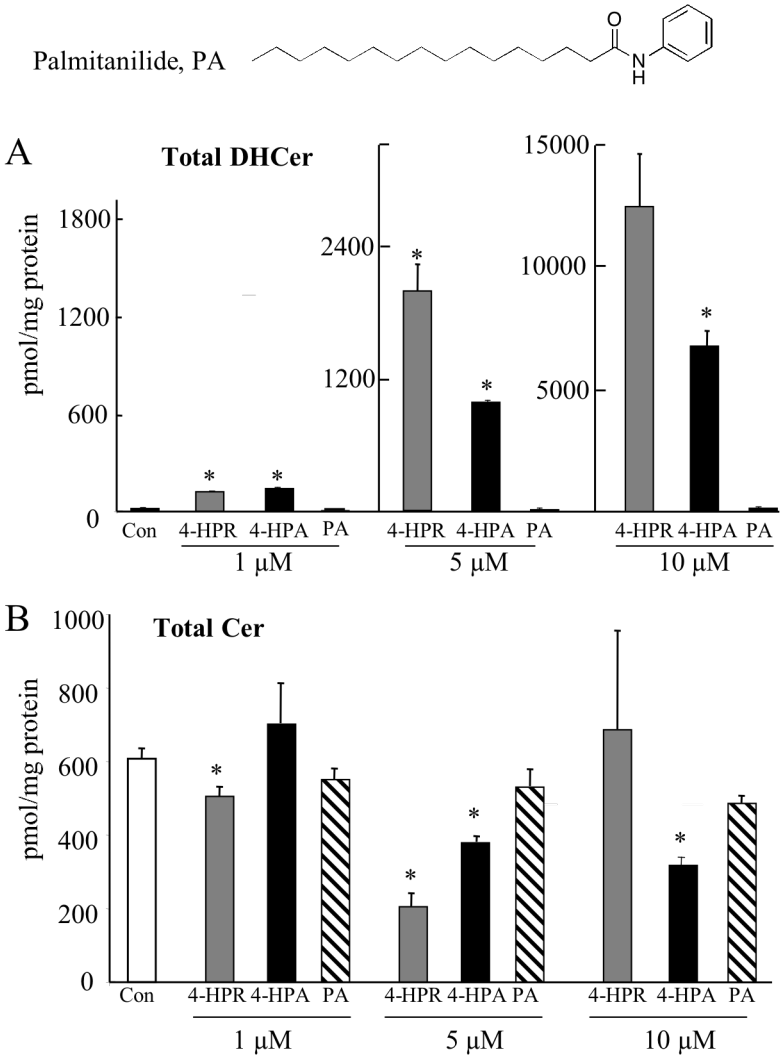

Figure 3.9 Comparison of Sphingolipid Composition in 4-HPR-, 4-HPA-, and PA-Treated Hek293 Cells Hek293 cells were incubated with vehicle control (EtOH), 4-HPR (1, 5, or 10 μM), 4-HPA (1, 5, or 10 μM), or PA (1, 5, or 10 μM) . Following treatment for 24 h, cells were harvested for lipid extraction and analysis by LC ESI-MS/MS. The structure of PA is shown. *A*, Amount of total DHCer (a summation of all chain lengths). Data represent the mean + SEM (n = 3); *p < 0.05. *B*, Amount of total Cer (a summation of all chain lengths). Data represent the mean + SEM (n = 3); *p < 0.05.

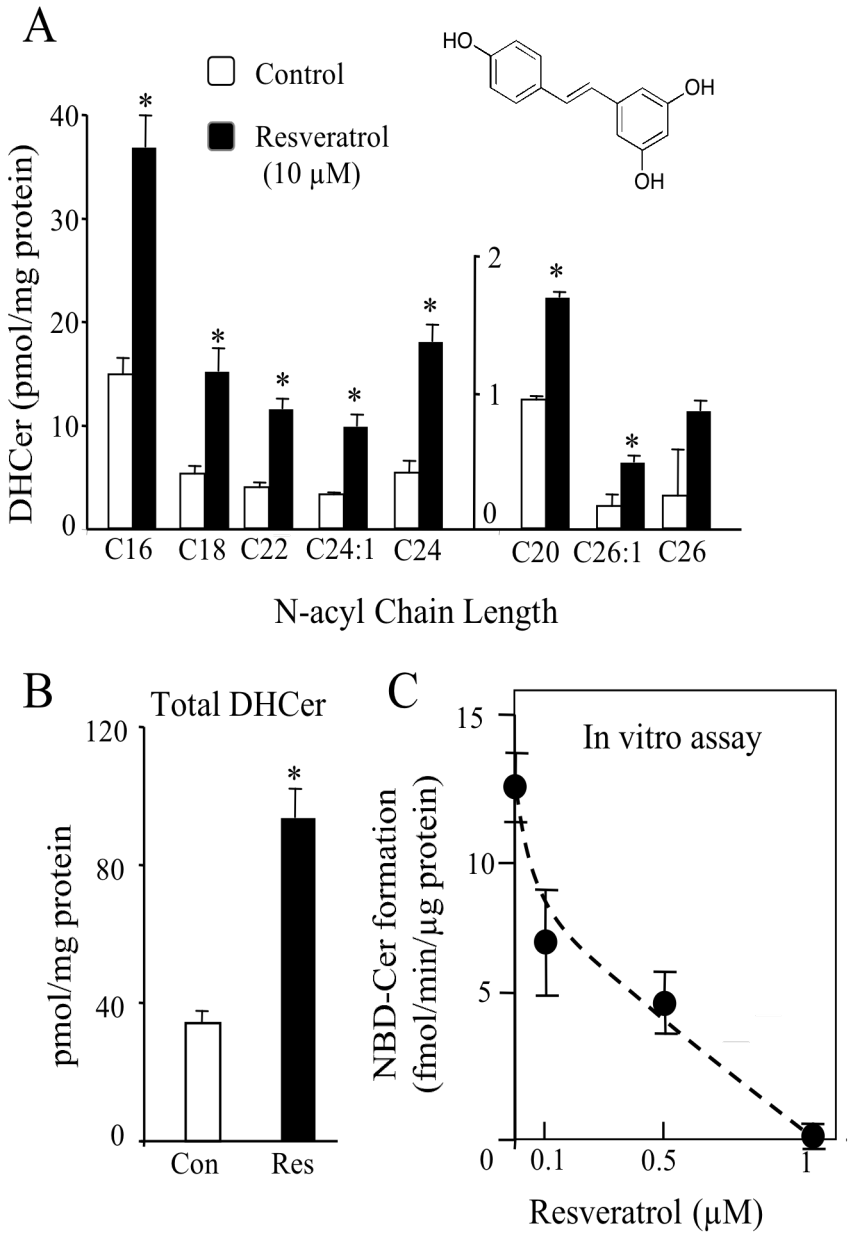

Figure 3.10 Resveratrol Increases Dihydroceramide Accumulation and Inhibits Dihydroceramide Desaturase in Hek293 Cells *A,* Hek293 cells were incubated with vehicle control (EtOH) or resveratrol (10 μM). Following treatment for 24 h, cells were harvested for lipid extraction and analysis by LC ESI-MS/MS. *A*, Amounts of the major chain length subspecies of DHCer Data represent the mean + SEM (n = 3); *p < 0.05. *B,* Total DHCer (a summation of all chain lengths) Data represent the mean + SEM (n = 3); *p < 0.05. *C,* Semi-intact Hek293 cells were prepared as described in the text and incubated with an NADPH regenerating system, 5 μM C_6-NBD-DHCer and the shown concentrations of resveratrol. After 60 min at 37°C, the assay was terminated through the addition of lipid extraction solvents and analyzed by reverse phase HPLC as described under *Materials and Methods*. Formation of NBD-Cer from NBD-DHCer was quantified by HPLC. Data represent average ± range for duplicate assays.

3.3.6 4-HPR and 4-HPA Differentially Affect *de novo* Sphingolipid Biosynthesis

There are noteworthy differences between 4-HPA and 4-HPR. While both elevate DHCer to a similar extent at 1 μM, at higher concentrations (5 and 10 μM), the elevation of DHCer (and other DHSL) was higher for 4-HPR (Fig. 3.9A) and, conversely, Cer (Fig. 3.9, lower panel), MH-Cer and SM (Fig. 3.11) are somewhat lower for cells treated with 5 μM 4-HPR than 4-HPA. Paradoxically, 10 μM 4-HPR elevates Cer (Fig. 3.9, lower panel), SM and MH-Cer (Fig. 3.11); however, these data are collected from fewer cells because significant cell death occurs at this concentration (perhaps accounting for the higher SEM for some metabolites). Since both 4-HPA and 4-HPR inhibit DES, one possible explanation for the greater increases in (DH)SL by 4-HPR might be its induction of *de novo* SL biosynthesis.

To consider this possibility, (DH)SL biosynthesis from [U-^{13}C]palmitate was compared for cells treated with 4-HPR or 4-HPA and these results (Fig. 3.12) recapitulated the differences in DHSL and SL mass noted above—i.e., 4-HPR caused greater incorporation of [U-^{13}C]palmitate into the DHSL and greater suppression of *de novo* biosynthesis of [^{13}C]Cer and [^{13}C]MH-Cer, but had higher labeling of [^{13}C]SM that, when totaled, reflected a higher level of *de novo* SL biosynthesis with 4-HPR than with 4-HPA (i.e., 478 $\pm$ 54 pmol/mg protein for 4-HPR-treated cells vs 352 $\pm$ 28 pmol/mg protein for 4-HPA-treated cells). Indeed, when the total incorporation for the control cells and the 4-HPA-treated cells are compared (400 $\pm$ 15 pmol/mg protein and 352 $\pm$ 28 pmol/mg protein, respectively), there was no evidence of a change in the rate of *de novo* (DH)SL biosynthesis by 4-HPA, only a redistribution of the subspecies toward higher DHSL.

This side-by-side comparison also confirmed that there is a large difference in the effect of 4-HPR and 4-HPA on cellular Sa (Fig. 3.12C). The increase in Sa in the 4-HPR treated cells was ~17-fold greater than the increase with 4-HPA, which would be consistent with the induction of *de novo* SL biosynthesis by 4-HPR.

Thus, the changes in (DH)SL in cells treated with 10 μM 4-HPR are more complicated than for 4-HPA treatment because 4-HPR not only inhibits DES but also causes a large increase in the rate of *de novo* SL biosynthesis, as has been previously noted [175, 178]. Another possible contributor to the more complicated SL metabolism in cells treated with 4-HPR (which we have not elected to address in these studies) is that 4-HPR has been reported to increase sphingomyelinase activity in neuroblastoma cell lines [189]. The interesting new finding of our studies is that 4-HPA inhibits DES with minimal effect on *de novo* biosynthesis, in contrast to the effect of 4-HPR on these cells.

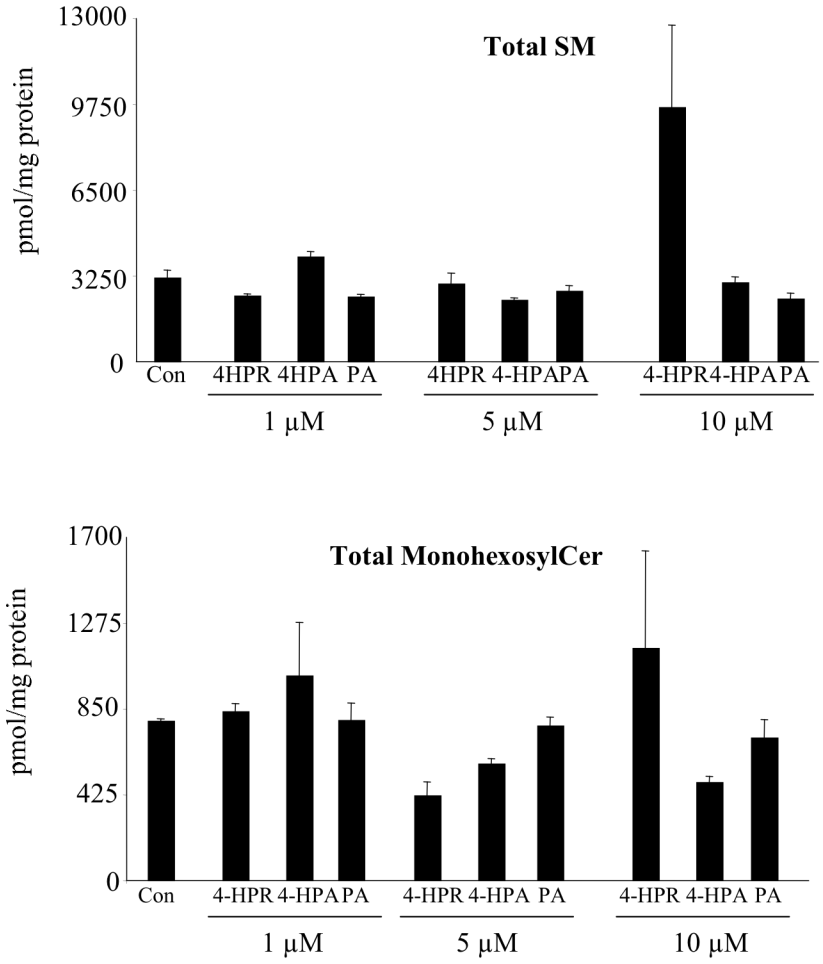

Figure 3.11 Comparison of Sphingomyelin and Monohexosylceramide Composition in 4-HPR-, 4-HPA-, and PA-Treated Hek293 Cells Hek293 cells were incubated with vehicle control (EtOH), 4-HPR (1, 5, or 10 μM), 4-HPA (1, 5, or 10 μM), or PA (1, 5, or 10 μM) . Following treatment for 24 h, cells were harvested for lipid extraction and analysis by LC ESI-MS/MS. Amounts of total SM and MH-Cer (a summation of all chain lengths). Data represent the mean + SEM (n = 3).

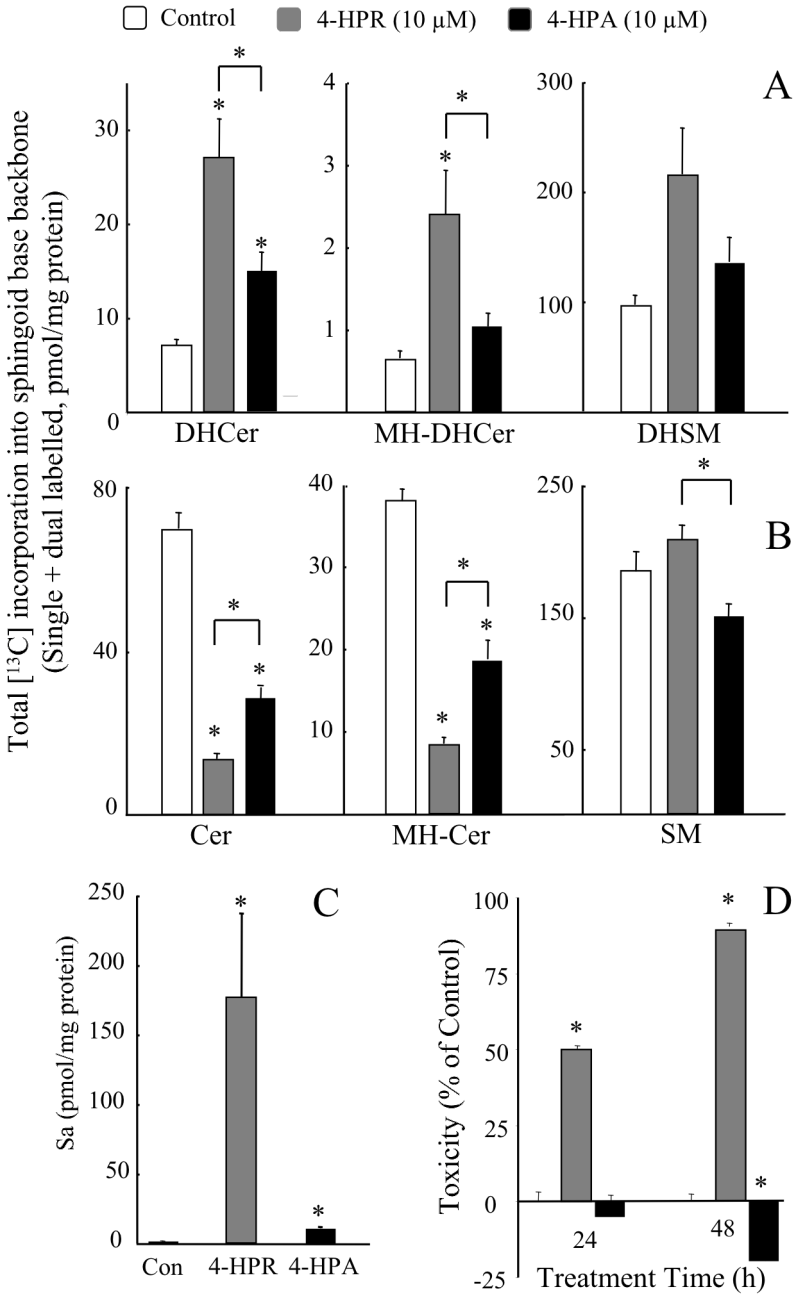

Figure 3.12 Analysis of *de novo* Sphingolipid Biosynthesis in Hek293 Cells by [^{13}C]Palmitate Labeling Hek293 cells were incubated with 0.1 mM [U-13C]-palmitic acid (as the BSA complex) with vehicle control (EtOH), 4-HPR (10 μM), or 4-HPA (10 μM). Following 6 h of treatment, the appearance of 13C in newly synthesized sphingolipids was quantified by mass spectrometry as described under *Experimental Procedures*. *A*, Summation of Base (Backbone) labeled and Dual (Backbone and Fatty Acid) labeled DHCer, MH-DHCer, and DHSM. Data represent the mean + SEM (n = 4); *p < 0.05. *B*, Summation of Base (Backbone) labeled and Dual (Backbone and Fatty Acid) labeled Cer, MH-Cer, and SM. Data represent the mean + SEM (n = 4); *p < 0.05. *C*, Hek293 cells were incubated with vehicle control (EtOH), 4-HPR (10 μM), or 4-HPA (10 μM). Following 24 h of treatment, cells were harvested for lipid extraction and analysis by LC ESI-MS/MS. Amounts of Sa are shown. Data represent the mean + SEM (n = 3). *D*, Viability was assessed using the WST-1 protocol following 24 and 48 h of treatment. Data represent the mean + SEM (n = 6); *p < 0.05.

3.3.7 4-HPA Uncouples Dihydroceramide Elevation and Induction of Autophagy from Cytotoxicity

4-HPR is cytotoxic for many types of cells in culture and this was also seen with Hek293 cells treated with 4-HPR but not 4-HPA, as shown in panel D of Fig. 3.12. When Hek293 cells were treated with 10 μM 4-HPR, the number of viable cells was reduced by about half versus the control after 24 h, and by 48 h there were few viable cells (Fig. 3.12D, grey bars). In contrast, the same concentration of 4-HPA caused no reduction in cell viability compared to the control, and appeared to have a slight stimulatory effect that was significant by 48 h (Fig.3.12D, black bars).

This lack of toxicity with 4-HPA was surprising because it has earlier been shown that *de novo* biosynthesis is necessary for 4-HPR toxicity (by experiments using myriocin to inhibit SPT) [190-192] therefore, the converse is often assumed—that perturbation of SL metabolism induces the toxicity. To explore this further, experiments were also conducted where the concentrations of 4-HPR and 4-HPA were adjusted to elevate DHCer to nearly equivalent amounts and determine the (DH)SL profiles and effects on cell viability. For these studies, the cells were incubated with 50 μM 4-HPA or 5 μM 4-HPR for 24 h, which increased the total amounts of DHCer of the 4-HPA and 4-HPR-treated cells to ~75% of each other (Fig. 3.13A) and Sa to ca 40% (Fig. 3.13C) versus ~6% in Fig. 3.12C; however, this caused no noticeable change in the effects of these agents on cell viability (Fig. 3.13D).

All together, these findings make it unlikely that the changes in "bulk" SL composition of Hek293 cells *per se* in response to DES inhibition are responsible for the toxicity of 4-HPR, although the combined effect of DES inhibition and induction of *de*

novo SL biosynthesis (with its potential implications for production of bioactive compounds in sensitive subcellular compartments) might play a role. In this context, it is noteworthy that the N-acyl-chain length of the DHCer that are elevated by 4-HPR span both the long (i.e., C16) and very-long- (C22 and C24) chain subspecies, whereas, the profile in 4-HPA treated cells favors the very-long-chain subspecies (C24 and C24:1) (Fig. 3.13). More definitively, the studies have uncoupled DES inhibition and elevations in (DH)SL by 4-HPA from cytotoxicity; therefore, this molecule is a useful tool to study the affects of perturbing the SL composition of cells (elevation of DHCer, etc.) without toxicity.

The first biological activity that was reported for DHCer was induction of autophagy in cells treated with 4-HPR or exogenous short-chain DHCer [1], which is interesting in general because SL have not only been shown to induce the formation of autophagosomes [1, 102, 104, 105, 193] but also to be required for formation of these intracellular vacuoles in response to a physiologically relevant agonist [45]. One of the tools that is used to assess autophagy is to analyze the state of the LC3 protein (microtubule-associated protein 1 light chain 3), which is present in cells mainly as a proteolytically cleaved form (LC3-I) that is conjugated to phosphatidylethanolamine to become LC3-II upon induction of autophagy [77-80]. The conversion of LC3-I to LC3-II can be followed via SDS-PAGE and Western blotting [77-80, 83]. As shown in Fig. 3.13D, treatment of Hek293 cells with both 4-HPA (50 μM) and 4-HPR (5 μM) for 24 h elevated the lipidated from of LC3 (LC3-II); therefore, although 4-HPA is not cytotoxic for these cells, it retains the ability to induce autophagy in Hek293 cells.

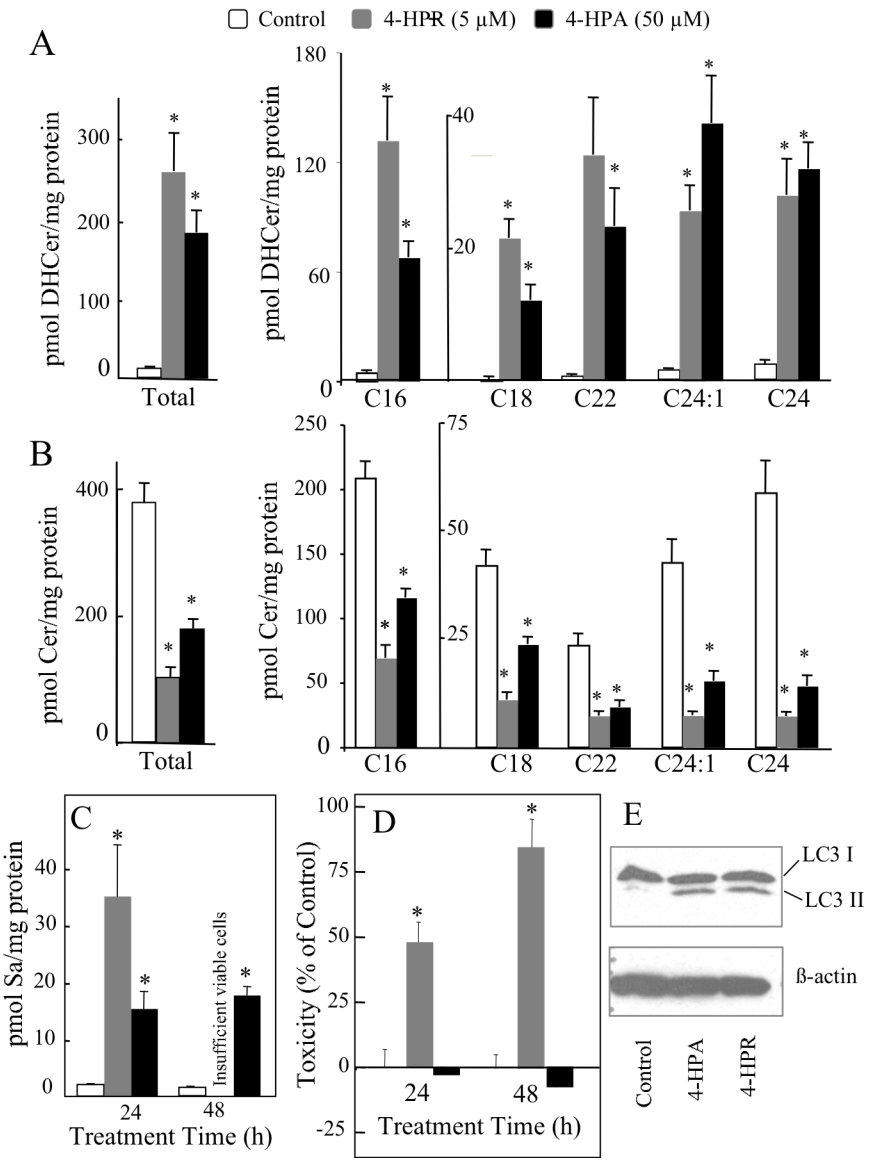

Figure 3.13 Dose Response Effects of 4-HPR and 4-HPA on Dihydroceramide, Ceramide, Sphinganine, Viability, and Autophagy Induction in Hek293 Cells Hek293 cells were incubated with vehicle control (EtOH) or 4-HPA (1 µM or 10 µM). Following treatment for 24 h, cells were harvested for lipid extraction and analysis by LC ESI-MS/MS. *A*, Amounts of the total and major chain length subspecies of DHCer. Data represent the mean ± (n=3); *p < 0.05. *B,* Amounts of the total and major chain length subspecies of Cer. Data represent the mean + SEM (n = 3); *p < 0.05. *C*, Amounts of Sa are shown. Data represent the mean + SEM (n = 3); *p < 0.05. *D,* Viability was assessed using the WST-1 protocol following 24, 48, and 72 h of treatment. Data represent the mean + SEM (n = 6); *p < 0.05. *E,* Immunoblot analysis of LC3B and ß-actin.

3.4 Discussion

These studies have determined that in addition to 4-HPR, structurally simpler N-acyl analogs (4-HPA and 4-hydroxyphenyldecanamide), and resveratrol inhibit DES activity and elevate DHCer and other DHSL in Hek293 cells. Nonetheless, comparison of 4-HPR and one of these alternative inhibitors, 4-HPA, reveal interesting differences in the SL subspecies that are affected and the cellular responses.

This study has not attempted to elucidate the mechanism of DES inhibition because the purified enzyme is not available for such studies, but it is noteworthy that a phenolic hydroxyl group is a common structural feature, and inhibition has been shown to be reduced when the phenolic hydroxyl is methylated for 4-HPR [179] or eliminated for PA (this study). It is likely that all of these compounds are able to access the active site of DES, which appears to accommodate compounds with fairly bulky substituents instead of the alkyl chains of the natural DHCer substrates as evidenced by its activity with C6-NBD-DHCer (Fig. 3.14); therefore, the phenol group of all of these compounds—and presumably others (Fig. 3.14)—would be predicted to be able to gain access to the active site. Based on analogies with other other lipid desaturases (such as Δ^9–stearoyl-CoA desaturase) [186, 194, 195], this might interfere with active site elements that participate in the redox chemistry (which might also account for inactivation of the enzyme by thiols and reactive oxygen species) [15, 196].

We think that one of the most important findings of these studies is the identification of 4-HPA as a novel DES inhibitor that was able to induce autophagy but not cytotoxic. This uncouples the elevation of a substantial number of compounds that might have been presumed to mediate the toxicity of 4-HPR (such as some subspecies of

DHSL) from cytotoxicity, and provides a tool to study these perturbations of (DH)SL content without the complication that the cells are dying. This also reconciles what had appeared to be a paradox: that inhibiton of DES by 4-HPR is cytotoxic but genetic ablation of one or both alleles of the DES enzyme produces homozygous null mice that live 8 to 10 weeks following birth and heterozygous mice with no obvious health abnormalities [197].

Several studies support the role of SL metabolism and particularly increases in DHCer in the induction of autophagy [1, 109]. Although, 4-HPA did not induce cell death under any of the tested conditions, it did trigger an accumulation of DHCer and increase in autophagy equivalent to that of treatment with 4-HPR as concluded from LC ESI-MS/MS and LC3-II immunoblot analysis. While autophagy, as a cellular process, is most often thought of as a cell survival mechanism in order to aid in the adaptation of cellular stress by enabling cells under adverse conditions to degrade cytosolic proteins/organelle and generate a supply of essential nutrients, activation of autophagy can also be induced as part of a cell death response, and the accumulation of autophagosomes is characteristic of "type II" or "autophagic" cell death [67, 86]. It is interesting that 4-HPR and 4-HPA seem to represent the dual nature of autophagy in cell survival, as shown following treatment with 4-HPA, and cell death, as shown following treatment with 4-HPR, suggesting that SL may play a role in many, if not all forms, of autophagy.

In conclusion, the studies described have mapped the concentration dependent changes in DHSL and SL metabolism in 4-HPR treated Hek293 cells as a result of both alterations in *de novo* biosynthesis and inhibition of DES, identified key structural

features which mediate DES inhibition, and distinguished 4-HPA as a novel non-toxic DES inhibitor, which may be a useful tool for future studies involving the cell-type specific effects of DES inhibition and the accumulation of DHCer and its metabolites, specifically studies of the dual role of DHCer in determining cell-fate decision following the induction of autophagy.

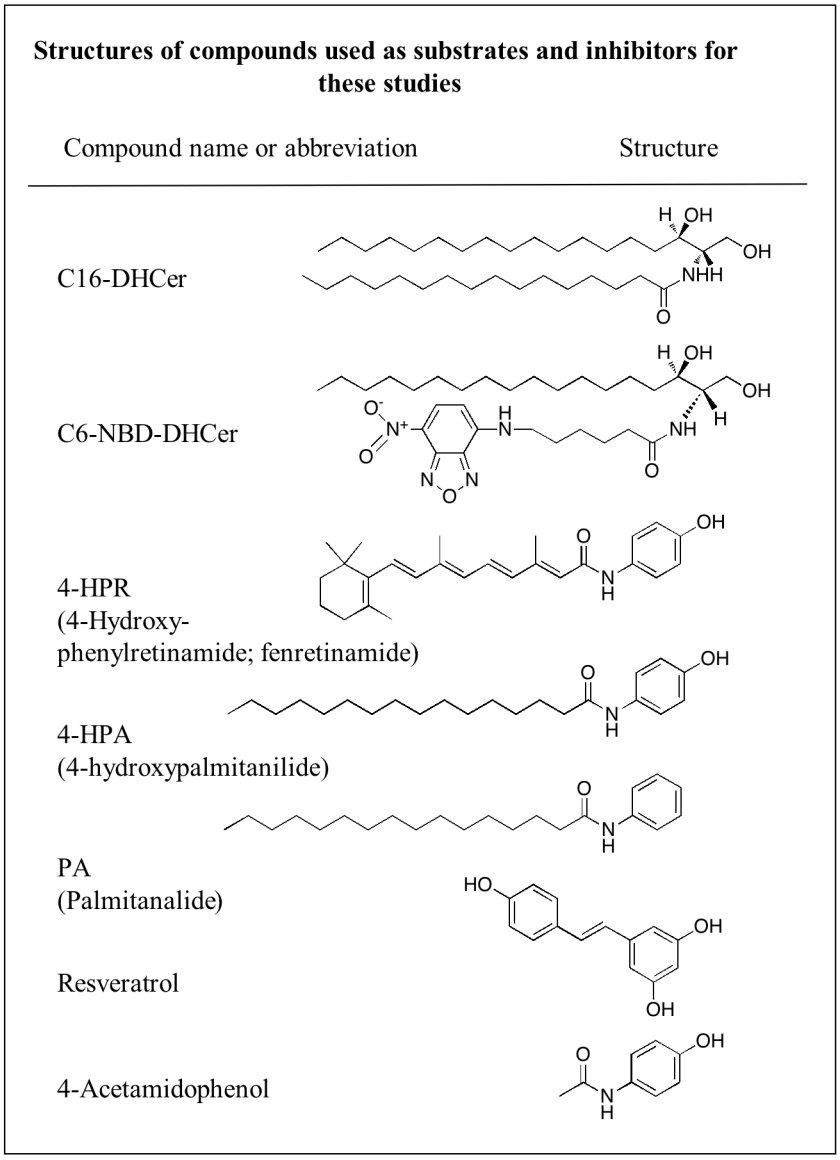

Figure 3.14 Structural Diversity of Compounds used to Monitor DES Inhibition

CHAPTER 4

PALMITATE ENHANCES FENRETINIDE INDUCED CELL DEATH IN MCF7 BREAST CANCER CELLS

4.1 Introduction

4-HPR, a synthetic derivative of retinoic acid, has been -- and continues to be -- evaluated in preclinical models and clinical trials for use in both the prevention and therapy of various cancers, with a special emphasis on breast cancer as a result of its ability to selectively accumulate in breast tissues [99, 172, 198]. A recent phase III clinical trial, with a 15-year follow-up study, indicates that 4-HPR treatment significantly reduces the incidence of second breast cancer recurrence in women diagnosed with Stage I breast cancer [99, 172]. This long-term analysis provides evidence for the persistent chemopreventive effects of 4-HPR even after therapeutic intervention is completed and makes it an attractive agent for continued evaluation in breast cancer therapy [172].

4-HPR appears to function by multiple mechanisms in tumor cell lines with the end result of caspase-dependent apoptotic [100, 172, 174, 199-201] and/or caspase-independent autophagic cell death [1, 99]. Interestingly, it has been demonstrated that many malignant cancers acquire genetic deletions or mutations [69, 96] that render them resistant to classical apoptotic cell death induced by many anti-cancer therapies including 4-HPR [99]. For example, a MCF7 breast cancer cell that does not express caspase-3, is resistant to caspase-dependent apoptotic cell death [97-99]. Therefore, the ability of 4-HPR to induce multiple forms of cell death suggests that this agent may be of therapeutic efficacy in cancer cells with deregulated apoptotic pathways [99]. One such component of 4-HPR-induced cytotoxicity, which might contribute to the regulation of caspase-independent autophagic cell death, is the alteration of SL metabolic pathways, as bioactive SL species, including Cer, S1P, and most recently DHCer, have been shown to mediate autophagic pathways [1, 102-104]. Furthermore, 4-HPR has been previously

reported to increase DHCer and its metabolites as much as 10-fold, as analyzed LC ESI-MS/MS [Chapter 3 and [1, 176-178]]. The accumulation of these DHSL is the result of both an increase in *de novo* biosynthesis [Chapter 3 and [175, 178]], as well as the inhibition of DES [Chapter 3 and [179]]. Thus, this study, described in Chapter 4, has confirmed the ability of 4-HPR to induce autophagic cell death in MCF7 cells, quantified the changes in the SL and DHSL species, and established the requirement of *de novo* SL biosynthesis in the induction of autophagy, suggesting that the production of SL mediators are essential for 4-HPR-induced autophagic cell death.

In addition, an emerging strategy in breast cancer therapy is to design multidrug combinations to enhance single-agent-induced cell death and increase the efficacy of chemotherapeutic intervention [172, 176, 198], and SL might be useful in this regard because a strong association has been found between *de novo* SL biosynthesis and 4-HPR-mediated cell death. Thus, we hypothesized that an agent, that would increase *de novo* biosynthesis, would enhance cell killing and improve chemotherapeutic efficacy. To this end, we investigated the effect of 4-HPR on MCF7 cells in the presence of palmitate (Pal), a precursor and known inducer of *de novo* SL biosynthesis [145, 202], as well as in the presence of oleate (OA), which appears to reduce SL biosynthesis [145, 202]. The addition of Pal was found to be effective at enhancing cell killing, while OA protected cells from 4-HPR-induced cytotoxicty. Surprisingly, analysis of the SL by LC-ESI MS/MS revealed that combined treatment with 4-HPR and Pal or OA had little effect on the total DHCer when compared with 4-HPR treatment alone; however, these combinations did affect the distribution of the subspecies of DHCer. This suggests that the interplay between various subspecies of DHCer may be an important mediator of the opposing roles of Pal and OA on 4-HPR-induced cytotoxicity. It was further shown that while the protective effects of OA on 4-HPR-induced cytotoxcity could be due to augmentation of autophagic cell death, the effects of Pal are more complex. None-the-less, these studies suggest that although the ability of Pal to enhance 4-HPR-induced cell

death is due to a surprisingly unsuspected level of complexity, the efficacy of 4-HPR may be improved by the addition of Pal to current treatment regimens.

4.2 Experimental Procedures

4.2.1 Materials

The suppliers for the reagents were: Fenretinide (4-HPR), Palmitate (Pal), and Oleate (OA), (Sigma Aldrich, St. Louis, MO); C2-Ceramide, C2-Dihydroceramide, and the internal standard cocktail for SL analysis by LC ESI-MS/MS (Ceramide/Sphingoid Internal Standard Mixture II, LM-6005) (Avanti Polar Lipids, Alabaster, AL); fatty acid-free BSA (Calbiochem, La Jolla, CA); myriocin/ISP1 (Biomol, Plymouth Meeting, PA); rabbit polyclonal LC3B antibody, rabbit monoclonal p62 antibogy, and mouse ß actin monoclonal antibody (Cell Signaling Technology, Boston, MA)

4.2.2 Cells and Cell Culture

MCF7 breast cancer cells were obtained from the American Type Culture Collection (ATCC) (Manassas, VA) and grown in MEM (MediaTech, Manassas VA) supplemented with 10% heat-inactivated fetal calf serum (HyClone Logan, UT), penicillin (100 U/mL) plus streptomycin (0.1mg/mL), nonessential amino acids, and sodium pyruvate (1mM). The cells were maintained in a 37°C, 90% relative humidity, 5% CO_2 environment. All cell culture conditions, unless otherwise noted, followed the standard protocol recommended by the ATCC.

4.2.3 Lipid Extraction and Analysis by LC-ESI MS/MS

The extraction and analysis method has been thoroughly described [127, 140]. The mass spectrometry data were collected using a PE Sciex API 3000 triple quadrupole and a 4000 quadrupole linear-ion trap mass spectrometer. For quantification, the samples were spiked with the internal standard cocktail (Avanti Polar Lipids, Alabaster, AL). Protein concentration was quantified using the BCA Assay Kit (Pierce, Rockford, IL). Statistical analysis was performed using a two-tailed Student's t-test.

4.2.4 Confocal Immunofluorescence Microscopy

MCF7 cells stably expressing GFP-LC3 were cultured on glass coverslips (VWR, Inc. West Chester, PA) in 24-well plates. Following treatment, cells were fixed with 4% formaldehyde for 15 minutes. Fixed cells were rinsed in PBS, and the nucleic acids were stained by incubating fixed cells with 1 μg/mL Hoechst 3342 for 7 min at room temperature. Stained cells were rinsed in PBS and mounted in Fluoromount G (Southern Biotechnology Associates, Inc., Birmingham, AL) prior to observation under a Zeiss LSM 510 inverted laser scanning confocal microscope (Heidelberg, Germany). Images were collected with the resident Zeiss confocal microscope software and analyzed using ImageJ version 1.41a (National Institute of Health). The ImageJ plug-in Analyze Particles was used to identify "autophagosomes" as defined by a threshold value of 159-255 [141] and a particle size of 0.07 to 7 μm^2 [142]. Statistical analysis was performed using a two-tailed Student's t-test.

4.2.5 Generation of MCF7 Cells Stably Expressing GFP-LC3

LC3A cDNA was obtained from Origene. To generate N-terminal GFP-tagged LC3, the LC3A gene was amplified using the following gene-specific primers: 5'-ATGCCCTCAGACCGGCCTTT-3' and 5'-GAAGCCGAAGGTTTCCTGGGAGG-3'. The PCR fragment corresponding to the coding sequence of LC3A was then cloned into pEGFP-C2/*SmaI* (Clonetech, Mountain View, CA) resulting pEGFP-C2-LC3A. Sequencing was used to confirm the fidelity of the construct.

MCF7 cells stably expressing GFP-LC3 were generated by transfection with pEFGP-C2-LC3A. Transfection was performed in 100-mm dishes (3.0×10^6 cells/dish) with 6 μg plasmid DNA/plate with GeneJuice® (Novagen; EMD Biosciences, San

Diego, CA) according to the manufacturer's protocol. Following overnight exposure, cells were washed with PBS and selected in media containing 600 μg/mL of G418 (Sigma-Aldrich; St. Louis, Mo) for 14 days. The media was changed every other day. After two weeks, pools of G418 resistant clones were sorted by FACS analysis, and the fluorescent cell population was cloned by limiting dilution in order to establish fluorescent colonies originating from a single cell. To confirm the presence of the GFP-LC3 protein, GFP-LC3 cells were analyzed by Western blotting using an anti-GFP antibody (Invitrogen; Carlsbad, Ca). In order to confirm localization of the LC3, GFP-LC3-transfected MCF7 cells were cultured on 12 mm cover slips (VWR; West Chester, PA). Following exposure to C2-ceramide (Avanti Polar Lipids; Alabaster, AL), a known inducer of autophagy in MCF7 cells [102] for 24 hrs, cells were fixed in 4% formaldehyde and analyzed by fluorescence confocal microscopy.

4.2.6 Viability Analysis

Viability was monitored by measuring the metabolic conversion of a water-soluble tetrazolium salt, WST-1 (Roche Applied Science, Indianapolis, IN), into formazan by mitochondrial dehydrogenases. The amount of formazan produced is proportional to the number of live cells and is expressed as cellular viability. For this procedure, cells were seeded in 96-well plates at 1 x 10^4 cells/well for 24 hours. Cells were then treated with the indicated reagents for 24, 48, or 72 h, and assays were performed by adding WST-1 directly to the culture wells and incubating them for 120 minutes at 37°C. Plates were then read by a scanning multiwell spectrophotometer by measuring the absorbance of the dye with a wavelength of 450 nm and 650 nm. The

reported values are equal to (absorbance$_{450nm}$- absorbance$_{650\ nm}$). Statistical analysis was performed using a two-tailed Student's t-test.

4.2.7 Western Blotting

MCF7 cells were treated with the indicated reagent for 24 h and harvested in RIPA buffer (PBS, 1% Nonidet P-40, 0.5% sodium deoxcholate, and 0.1% SDS). Cells were then lysed by sonication followed by 30 min incubation on ice. Lysates were centrifuged at 12,000 x g for 10 min at 4°C, and the protein concentration of the supernatant was determined using the BCA Assay Kit (Pierce, Rockford, IL). Aliquots of each sample (30 μg of protein) were separated on a 12% SDS-PAGE gel (Bio-Rad, Hercules, CA) and transferred to a PVDF membrane (Millipore, Billerica, MA). Membranes were blocked in 5% milk/Tris buffered saline containing 0.1% Tween 20 (TBS-T) for 1 hr at room temperature and incubated overnight at 4°C with rabbit anti-LC3B (1:300) (Cell Signaling Technology, Boston, MA), rabbit anti-p62 (1:400) (Cell Signaling Technology, Boston, MA), or mouse anti-ß actin (1:1000) (Cell Signaling Technology, Boston, MA) primary antibodies. The blot was washed with TBS-T and incubated with horseradish peroxidase conjugated anti-rabbit (Jackson ImmunoResearch Laboratories, West Grove, PA) or anti-mouse (Pierce, Rockford IL) secondary antibodies for 2 hrs at room temperature. Protein expression was determined using an enhanced chemiluminescent substrate (ECL) (Pierce, Rockford, IL).

4.3 Results

4.3.1 4-HPR Induces Autophagic Cell Death in MCF7 Breast Cancer Cells

MCF7 cells are well known to be caspase-3 deficient, which prevents them from undergoing classical apoptotic cell death and renders them resistant to many

pharmacological agents [97-99] that proceed through such mechanisms, such as 4-HPR. However MCF7 cells are sensitive to 4-HPR, in agreement with a previous study [99], with a significant loss in cell viability beginning 48 h after treatment when compared with control treated cells (Fig. 4.1A). This decrease in cell viability has been attributed to the induction of autophagic cell death as an alternative to caspase-dependent cell death [99].

In order to support this finding, autophagy was analyzed using MCF7 cells stably expressing a green-fluorescent-protein (GFP)-tagged LC3 protein (microtubule-associated protein 1 light chain 3), which like wild-type LC3, is recruited from the cytosol to become part of the autophagosome due to conjugation of the C-terminal glycine with phosphatidylethanolamine [77, 78]; therefore, the appearance and accumulation of GFP-LC3 puncta can be used to assess autophagy [77, 79, 80]. As shown in Fig. 4.1B, 4-HPR treatment of MCF7 cells stably expressing GFP-LC3 induced the characteristic redistribution of GFP-LC3 from diffuse fluorescence throughout the cytosol to numerous punctate fluorescent vesicles. A quantitative analysis of the confocal microscopic images revealed a statistically significant increase in both the number of cells expressing GFP-LC3 puncta, as well as the number of GFP-LC3 puncta/cell following 4-HPR treatment (Fig. 4.1C). For this analysis, C2-DHCer and C2-Cer were included as positive controls, as they are known inducers of autophagy [1, 102]. These results are in agreement with a previously published finding and confirm that 4-HPR is effective at inducing autophagic cell death in the apoptotic defective, MCF7 breast cancer cell line.

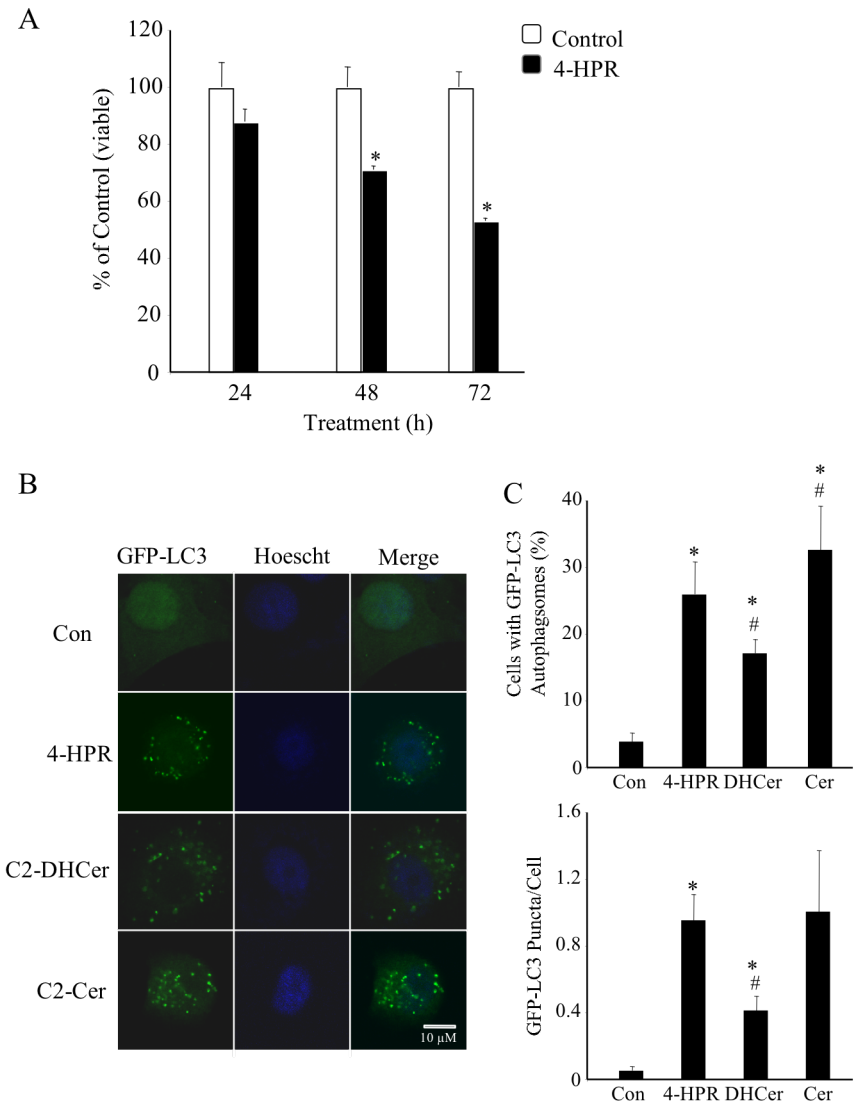

Figure 4.1 4-HPR Induces Autophagic Cell Death in MCF7 Cells *A,* MCF7 cells were incubated with vehicle control (EtOH) or 4-HPR (10 µM). Viability was assessed using the WST-1 protocol following 24, 48, and 72 h of treatment. Data represent the mean + SEM (n = 18); *p < 0.05. *B*. MCF7 cells stably expressing GFP-LC3 were incubated with vehicle control (EtOH), 4-HPR (10 µM), C2-DHCer (25 µM), or C2Cer (25 µM). Representative images are shown. *C,* The numbers of cells displaying GFP-LC3 puncta, as well as the number of GFP-LC3 puncta/cell were quantified using ImageJ. For each experimental condition, a minimum of 548 cells were counted. Data represent mean ± SEM (n = 4); # (n=3); *p < 0.05.

4.3.2 4-HPR Increases Dihydrosphingolipids in MCF7 Breast Cancer Cells

The induction of autophagic cell death is interesting from a SL perspective, as the exogenous addition, as well as the cellular accumulation of various SL species, including DHCer (Fig. 4.1B), has been shown to induce the formation of vacuolar autophagosomes and participate in autophagic cell death in various cell types including MCF7 cells [1, 102, 106, 110]. 4-HPR has been previously reported to elicit increases in DHSL in several human cancer cell lines, including prostate (DU145), ovarian (MCF7/AdrR and A2780), and neuroblastoma (SMS-KCRN) [1, 176-178], as well as non-transformed Hek293 cells [Chapter 3]. In Figure 4.2, these findings are extended to the MCF7 breast cancer cell line. Treatment of MCF7 cells with 4-HPR significantly increases all measured subspecies of DHCer and total DHCer when compared with control treated cells after 24 h (Fig. 4.2A). Additionally, 4-HPR significantly increases the subspecies of the metabolites of DHCer, DHSM and MH-DHCer (Fig. 4.2B-C). The accumulation of these DHSL has been found to be the result of both an increase in *de novo* biosynthesis, as 4-HPR has been shown to stimulate SPT and CerS activity [175, 178], and the inhibition of DES [Chapter 3 and [179]].

As would be expected following DES inhibition, treatment of MCF7 cells with 4-HPR decreases many of the subspecies of Cer including, C22, C24:1, C24, and C26 (Fig. 4.3A). Curiously, the C16-subspecies of Cer significantly increases (Fig. 4.3A). This increase could be the result of the turnover of the C16-subspecies of SM, as LC-ESI MS/MS analysis finds a significant decrease in this subspecies (and others) (Fig. 4.3B), and 4-HPR has previously reported to activate sphingomyelinase [189]. Likewise, the significant increase in the C24-subspecies of SM could be the result of the metabolism of

residual long-chain Cer species. These observations suggest that cells are attempting to maintain Cer and SM homeostasis by coordinating the formation and removal of these molecules, as has been described following the activation of RAW264.7 macrophage cells [Chapter 2 and [45]]. Further support for this idea is provided by the analysis of the total amounts of cellular Cer and SM, which change very little despite significant changes in specific chain lengths (Fig. 4.3A-B). Additionally, 4-HPR also alters the cellular amounts of another metabolite of Cer, MH-Cer (Fig. 4.3C). Significant decreases in the C22-, C24:1-, C24-, and C26:1-subspecies, as well as total MH-Cer, were found following treatment of MCF7 for 4-HPR for 24 h. In addition to these changes in DHCer and Cer and their metabolites, 4-HPR treatment of MCF7 cells was also marked by significant increases in Sa and Sa1P but not So and S1P (Fig. 4.4), as has been reported for other cell types [176]. Taken together, the above data establishes that 4-HPR treatment of MCF7 cells induces an accumulation of DHSL, while decreasing or changing Cer containing SL very little, and suggests that 4-HPR-induced autophagic cell death of MCF7 cells could be the result of alterations in SL metabolism.

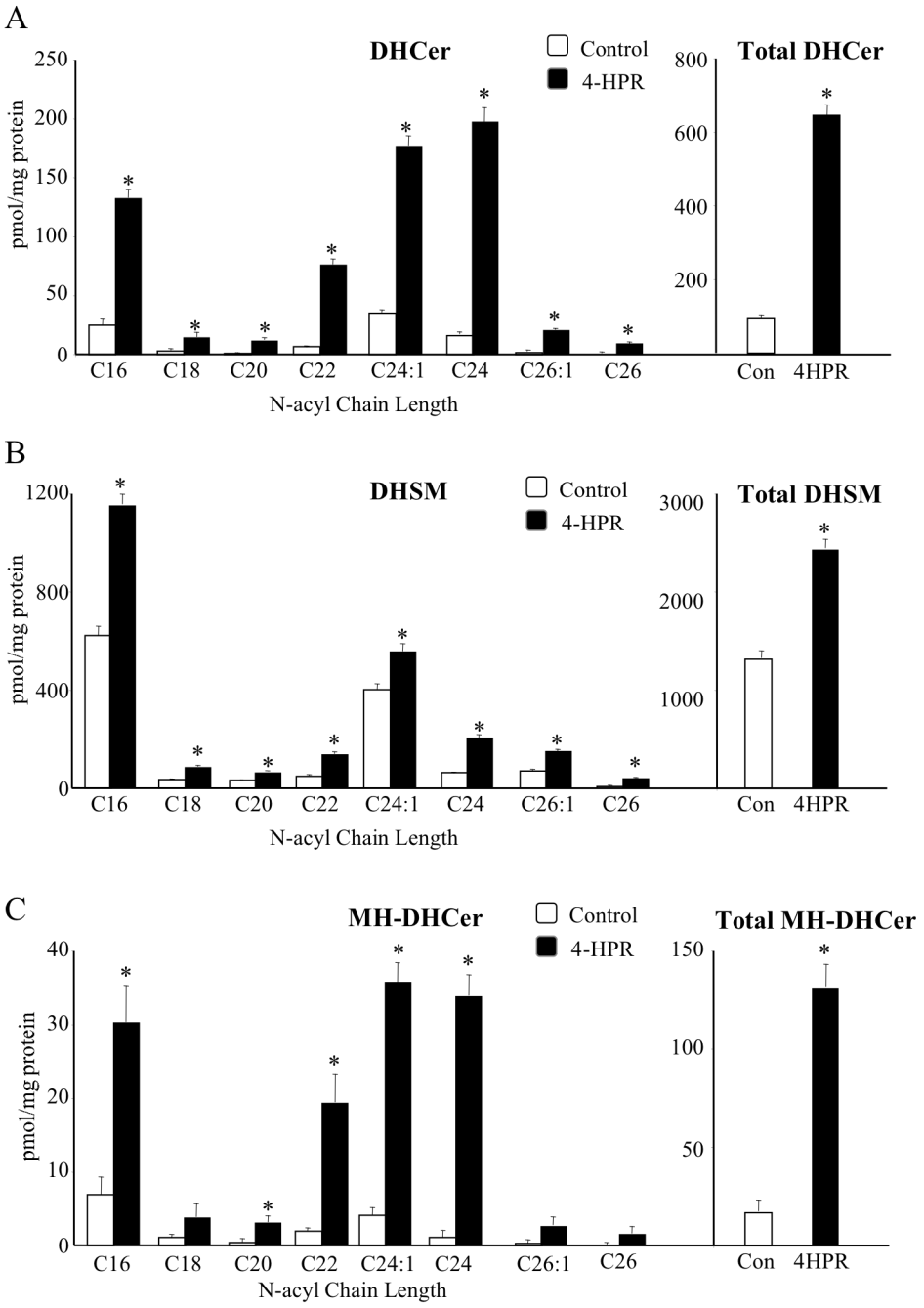

Figure 4.2 4-HPR Increases Dihydroceramide and its Metabolites in MCF7 Cells MCF7 cells were incubated with vehicle control (EtOH) or 4-HPR (10 μM). Following 24 h of treatment, cells were harvested for lipid extraction and analysis by LC ESI-MS/MS. *A*, Amounts of the major chain length subspecies of DHCer and total DHCer (a summation of all chain lengths). *B*, Amounts of the major chain length subspecies of DHSM and total DHSM (a summation of all chain lengths). *C*, Amounts of the major chain length subspecies of MH-DHCer and total MH-DHCer (a summation of all chain lengths). For all reported species, data represent the mean $\pm$ SEM (n=3); *$p < 0.05$.

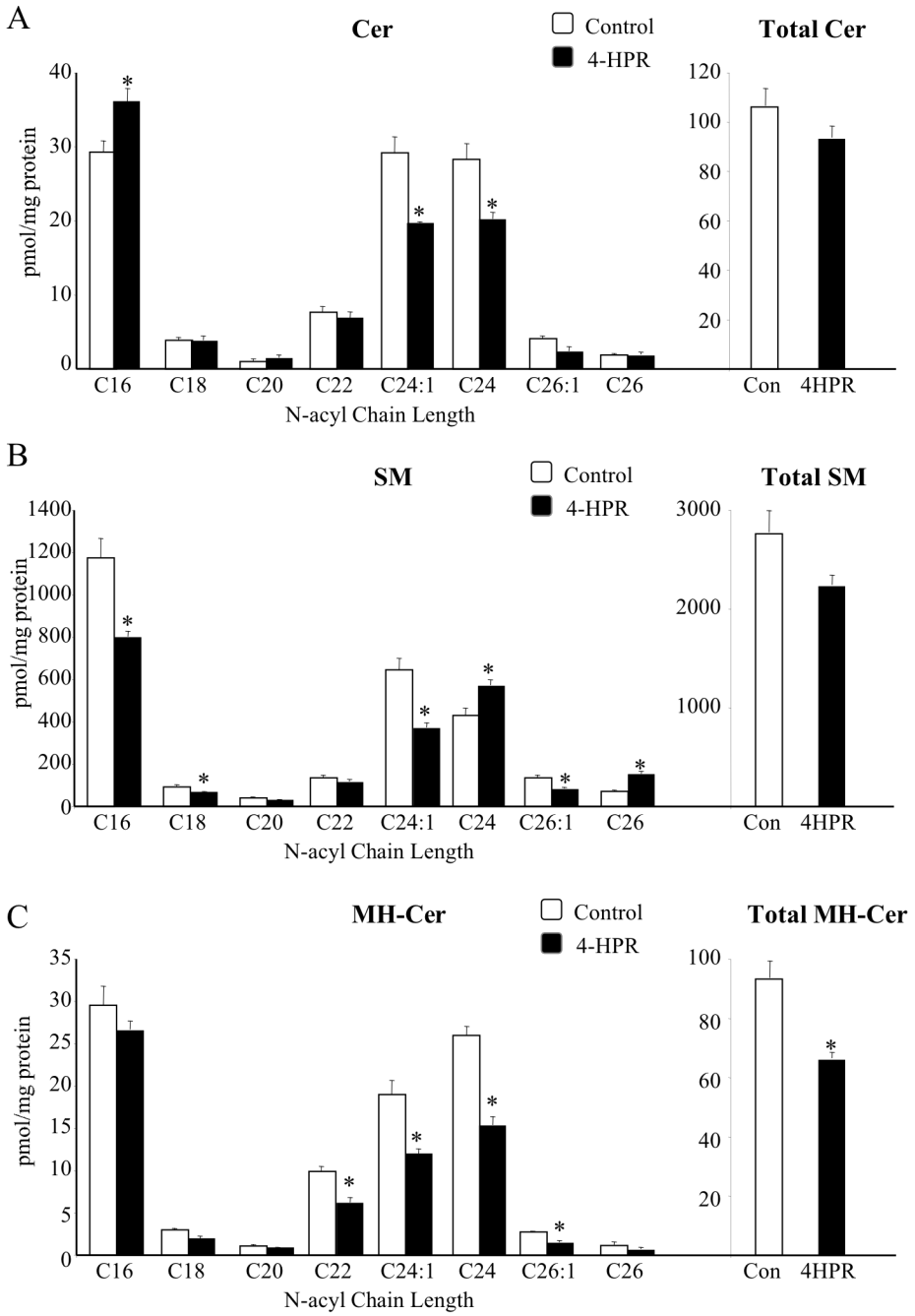

Figure 4.3 Ceramide and its Metabolites in 4-HPR-Treated MCF7 Cells MCF7 cells were incubated with vehicle control (EtOH) or 4-HPR (10 μM). Following 24 h of treatment, cells were harvested for lipid extraction and analysis by LC ESI-MS/MS. *A*, Amounts of the major chain length subspecies of Cer and total Cer (a summation of all chain lengths). *B*, Amounts of the major chain length subspecies of SM and total SM (a summation of all chain lengths). *C*, Amounts of the major chain length subspecies of MH-Cer and total MH-Cer (a summation of all chain lengths). For all reported species, data represent the mean ± SEM (n=3); *$p < 0.05$.

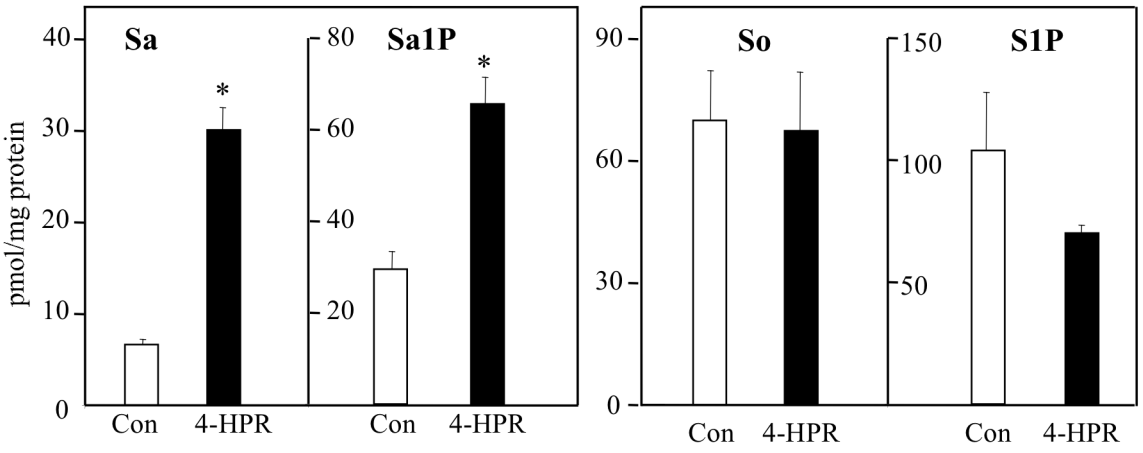

Figure 4.4 Sphingoid Bases and Sphingoid Base Phosphates in 4-HPR-Treated MCF7 Cells
MCF7 cells were incubated with vehicle control (EtOH) or 4-HPR (10 μM). Following treatment for 24 h, cells were harvested for lipid extraction and analysis by LC ESI-MS/MS. Amounts of sphingoid bases, Sa and So, as well as amounts of sphingoid base phosphates, Sa1P and S1P. Data represent the mean + SEM (n = 3); *$p < 0.05$.

4.3.3 4-HPR-Induced Autophagy Requires *de novo* Sphingolipid Biosynthesis

In order to determine if *de novo* SL biosynthesis is required for the induction of autophagy, and presumably autophagic cell death, following treatment with 4-HPR MCF7 cells stably expressing GFP-LC3 were treated with ISP1, an inhibitor of SPT which blocks *de novo* SL biosynthesis [150], for 1 h followed by the addition of 4-HPR and analysis of autophagosomal puncta. As shown in Figure 4.5, both the visual inspection (Fig. 4.5A) and quantitative analysis (Fig. 4.5B) of the confocal images reveals that the inhibition of *de novo* biosynthesis by ISP1 blocks the appearance of GFP-LC3-associated autophagosomes suggesting that SL biosynthesis is an important determinant of autophagic cell death following treatment of MCF7 cells with 4-HPR. Furthermore, this idea is consistent with the requirement of *de novo* SL biosynthesis in 4-HPR-induced apoptotic cell death in apoptotic competent cell lines [190-192].

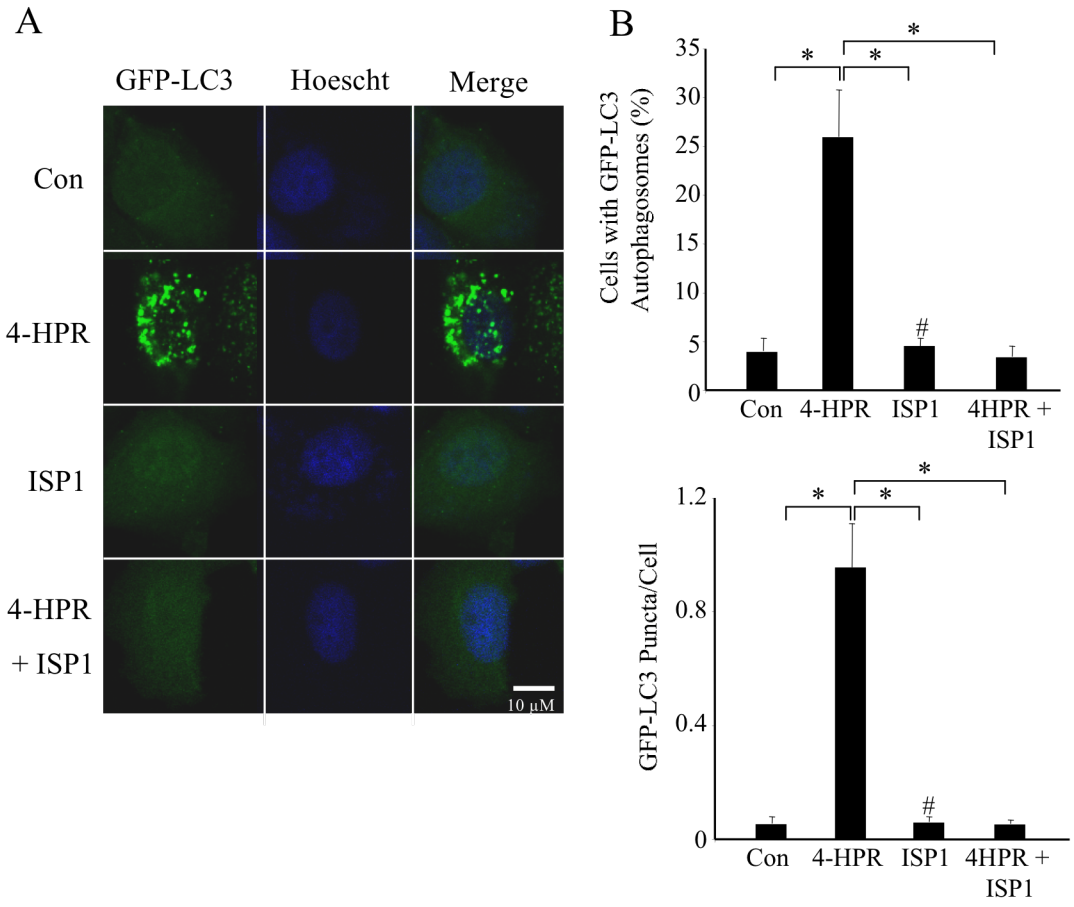

Figure 4.5 4-HPR-Induced Autophagy is Dependent on *de novo* Sphingolipid Biosynthesis. MCF7 cells stably expressing GFP-LC3 were incubated for 24 h with vehicle control (EtOH), 4-HPR (10 µM), ISP1 (1 µM), or 4-HPR + ISP1. For cells treated with 4-HPR + ISP1, ISP1 was added 1 h prior to the addition of 4-HPR. *A*, Representative images. *B*, The numbers of cells displaying GFP-LC3 puncta, as well as the number of GFP-LC3 puncta/cell were quantified using ImageJ. For each experimental condition, a minimum of 425 cells were counted. Data represent mean ± SEM (n = 4); # (n=3); *$p < 0.05$.

4.3.4 Palmitate, but not Oleate, Enhances 4-HPR-Induced Cell Death.

Treatment of cells with Pal, has been shown to increase the rate of *de novo* SL biosynthesis; whereas treatment with OA was inhibitory [145, 202]. Since *de novo* SL biosynthesis is required for 4-HPR induced autophagy, it is possible that concurrent treatment with Pal and 4-HPR could enhance cell killing by further increasing the production of bioactive SL mediators; while treatment with OA may protect cells from 4-HPR-induced cell death by decreasing these metabolites. The data in Fig. 4.6 reveals that 4-HPR's cytotoxicity was significantly enhanced by the inclusion of Pal when compared with both control treated and 4-HPR alone treated cells. Interestingly, a significant loss in viability was apparent after 24 h of concurrent treatment with 4-HPR and Pal; whereas 4-HPR alone did not result in significant cell death until at least 48 h post-treatment. Cellular viability was not significantly affected by the addition of Pal alone (Fig. 4.6), which is consistent with a previously reported finding that Pal induces lipotoxicity in ERBB2-positive (BT474 and MDA-MB-361) but not ERBB2-negative (MCF7) breast cancer cells [203]. Furthermore, the addition of OA alone was not toxic, and in contrast to Pal, the addition of OA significantly decreased the cytotoxicity of 4-HPR.

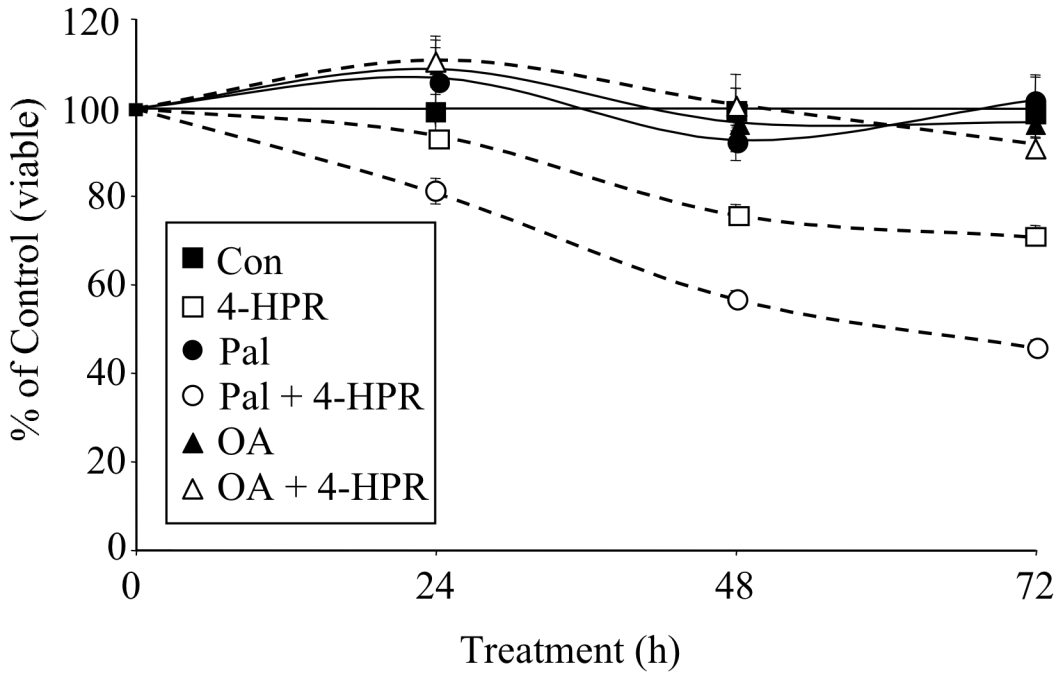

Figure 4.6 Palmitate, but not, Oleate Enhances 4-HPR-Induced Cell Death MCF7 cells were incubated with vehicle control (EtOH), 4-HPR (10 μM), Pal (0.1 mM), Pal + 4-HPR, OA (0.1mM), or OA + 4-HPR. Viability was assessed using the WST-1 protocol following 24, 48, or 72 h of treatment. Data represent the mean + SEM (n = 30).

4.3.5 Effects of Palmitate and Oleate on 4-HPR-Induced Alterations of Sphingolipid Metabolism

The cytotoxic effects of 4-HPR are thought to be due to increases in DHCer [1]. The ability of Pal to upregulate *de novo* biosynthesis [145, 202] suggests that the enhanced cytotoxicity of concurrent treatment with Pal and 4-HPR when compared with 4-HPR alone may be the result of further increases in DHCer. Surprisingly, as shown in Fig. 4.7A, the 4-HPR-induced accumulation of total DHCer was not significantly affected by the addition of Pal or OA when compared with 4-HPR treatment alone. However, these treatment combinations, Pal and 4-HPR, as well as OA and 4-HPR did drastically affect the chain length distribution of DHCer subspecies when compared with 4-HPR alone. As shown in Fig 4.7A, the addition of Pal significantly increases the 4-HPR-induced accumulation of the C16-, C18-, C20-, and C22-subspecies of DHCer; while significantly decreasing the C24:1 subspecies. In contrast, the addition of OA significantly decreases the 4-HPR-induced accumulation of the C16-, C18-, C20-, and C22-subspecies of DHCer; while significantly increasing the C24:1 subspecies (Fig. 4.7A). Interestingly, this sort of subspecies-specific regulation seems to be a common theme when deciding cell fate, as treatment of Hek293 cells with a non-toxic DES inhibitor, 4-HPA, also resulted in a preferential increase in C24:1 subspecies of DHCer; whereas the cytotoxic 4-HPR favored an accumulation of the C16- and C18-subspecies [Chapter 3]. In addition, Pal nor OA alone significantly altered total DHCer or total Cer when compared with control treated cells (data not shown).

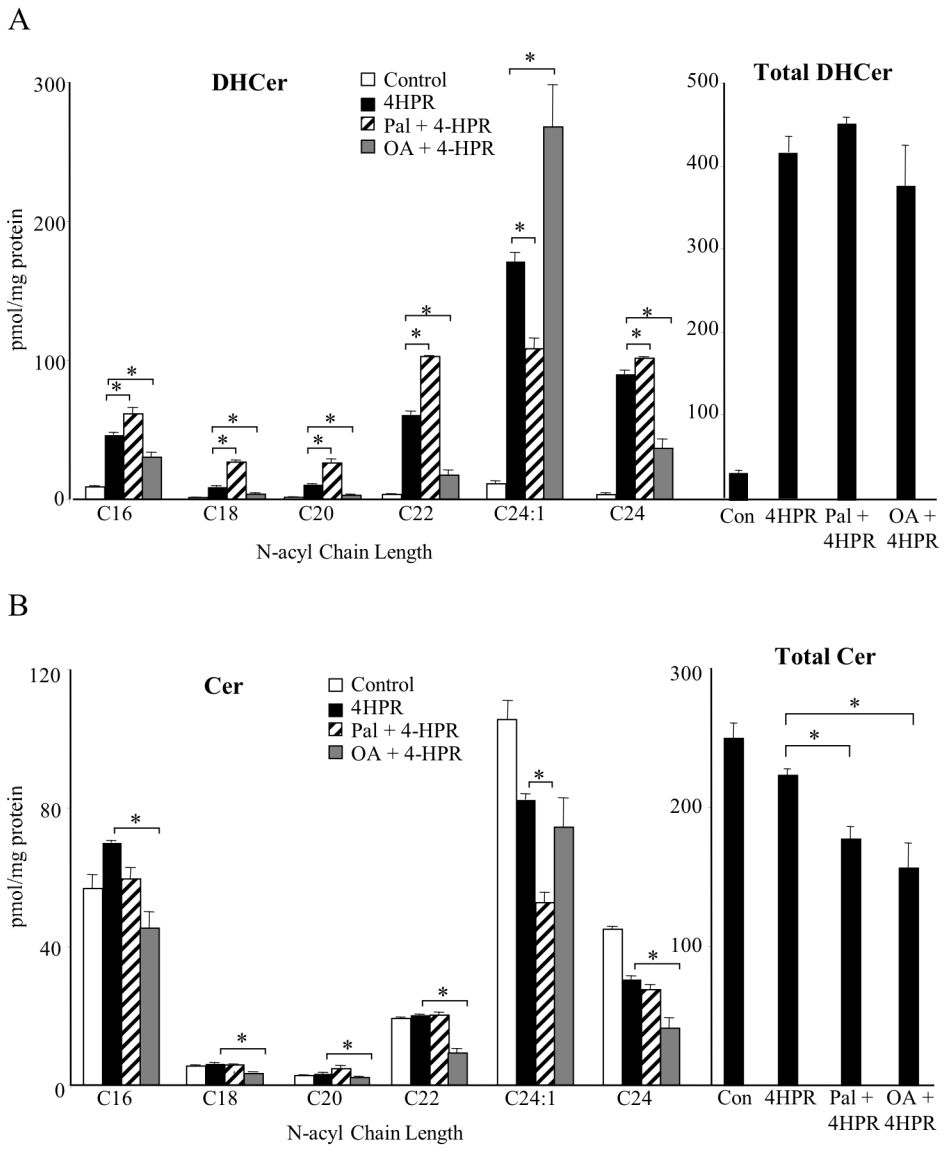

Figure 4.7 Effects of Palmitate and Oleate on 4-HPR-Induced Alterations of Sphingolipid Metabolism MCF7 cells were incubated with vehicle control (EtOH), 4-HPR (10 μM), Pal + 4-HPR, or OA + 4-HPR. Following treatment for 24 h, cells were harvested for lipid extraction and analysis by LC ESI-MS/MS. *A*, Amounts of the major chain length subspecies of Cer and total Cer (a summation of all chain lengths). *B*, Amounts of the major chain length subspecies of DHCer and total DHCer (a summation of all chain lengths). For all reported species, data represent the mean ± SEM (n=3); *$p < 0.05$.

4.3.6 Effect of Palmitate and Oleate on 4-HPR-Induced Autophagy and Autophagic Degradation

To further characterize the mechanism of the opposing effects of Pal and OA on 4-HPR-induced cell death in MCF7 cells, alterations in autophagy were monitored by following the conversion of LC3-I to LC3-II using SDS-PAGE and Western blotting [79, 80, 83]. Although molecular weight of LC3-II is greater than that of LC3-I, LC3-II experiences an increased mobility and migrates faster than LC3-I in SDS-PAGE due to the extreme hydrophobicity of LC3-II following its conjugation with phosphatidylethanolamine, which is necessary for autophagosome formation [79, 80, 83]. Therefore, the amount of LC3-II correlates with autophagosome formation, and thus, it can be used as an indicator of autophagy induction [79, 80, 83]. As shown in Fig. 4.8, the addition of Pal or OA alone did not enhance the conversion of LC3-I to LC3-II in MCF7 cells, but instead slightly decreased the level of LC3-II when compared with control treated cells. These results suggest that Pal and OA treatment alone are not effective at inducing autophagy in MCF7 cells. Furthermore, this decrease in basal autophagy levels may account for the slight increase in viability seen following treatment of MCF7 cells with Pal or OA alone for 24 h (Fig. 4.8). Although concurrent treatment of MCF7 breast cancer cells with Pal and 4-HPR did significantly enhance cellular toxicity when compared with 4-HPR alone (Fig. 4.6), the improved efficacy of this combination does not seem to be the result of increased autophagy induction, as the 4-HPR-induced increase in the conversion of LC3-I to LC3-II was not enhanced by the addition of Pal. In contrast, concurrent treatment with OA and 4-HPR decreases LC3-II levels when compared with 4-HPR-treatment alone (Fig. 4.8), suggesting a decrease in autophagy

induction and consistent with the ability of OA to protect cells from 4-HPR-induced cytotoxicity.

Moreover, these results were confirmed by monitoring the cellular level of p62. Because p62 is a selective substrate for the autophagic pathway, monitoring endogenous p62 levels is often used as a marker for enhanced [as noted by decreases in p62] or suppressed [as noted by increases in p62] autophagic degradation or in this case, autophagic cell death [204, 205]. As shown in Fig 4.8, treatment with Pal and OA alone slightly increased the accumulation of p62 when compared with control treated cells suggesting an abrogation of basal level autophagy induction and autophagic cell death consistent with the slight increase in cell viability noted above. Also consistent, the combined treatment of MCF7 cells with Pal and 4-HPR did not enhance 4-HPR-induced p62 degradation; whereas, the addition of OA to 4-HPR treatment prevented p62 degradation. Taken together, these results suggest that while the protective effects of OA on 4-HPR-induced cell death may be due to a decrease in the induction autophagy and autophagic cell death, the addition of Pal does not enhance toxicity through modulation of the autophagic pathway.

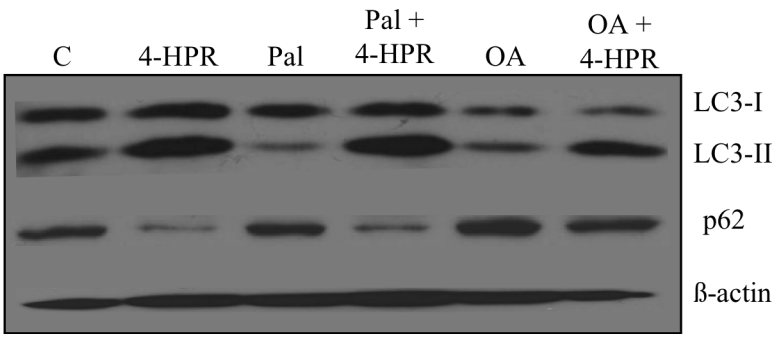

Figure 4.8 Effect of Palmitate and Oleate on 4-HPR-Induced Autophagy and Autophagic Degradation MCF7 cells were incubated with vehicle control (EtOH), 4-HPR (10 µM), Pal (0.1 mM), Pal + 4-HPR, OA (0.1mM), or OA + 4-HPR. Following treatment for 24 h, cells were harvested for western blot analysis of LC3 and p62. Two bands were obtained for LC3, the cytosolic LC3-I and the autophagosomal LC3-II. ß-actin was used as a loading control.

4.4 Discussion

4-HPR has been encouraging as a breast cancer chemopreventive and therapeutic agent in clinical trials [99, 172]. Furthermore, the promise of 4-HPR as a therapeutic agent is enhanced by its unique ability to activate the autophagic cell death pathway when the apoptotic pathway is deregulated, a characteristic not shared by other chemotherapeutic agents such as cisplatin and etoposide [99]. Interestingly, this idea proves to be particularly important when considering therapy for breast cancer, as a recent study of malignant breast tissue samples revealed that 75% of the analyzed tissues were apoptotic defective [101]. With this in mind, this study first confirmed the ability of 4-HPR to activate the autophagic pathway in the caspase-3-defective MCF7 breast cancer cell line (Fig. 4.1B-C). One mechanism whereby 4-HPR has been reported to induce autophagy in other cancer cell lines is via increases in DHCer [1], and LC ESI-MS/MS analyses has revealed that treatment of MCF7 cells with 4-HPR results in significant increases in DHCer and other DHSL within this cell line (Fig. 4.2), which is likely due to the concurrent stimulation of *de novo* biosynthesis [Chapter 3 and [175]] and inhibition of DES [Chapter 3 and [179]]. Furthermore, *de novo* SL biosynthesis was shown to be necessary for autophagosome formation (Fig. 4.5), as has also been recently reported for the induction of autophagy in other cellular systems [Chapter 2 and [45]].

Because combination chemotherapy is emerging as a viable strategy to improve single-agent efficacy and SL biosynthesis was found in this and other studies to be important in 4-HPR-mediated cell death [172, 176, 190, 198], this study sought to determine if the administration of 4-HPR in combination with a precursor of *de novo* SL biosynthesis, Pal, would increase toxicity in breast cancer cells. The results demonstrated

that Pal enhanced 4-HPR-induced cytotoxicity in breast cancer cells, while the addition of OA protected MCF7 cells from 4-HPR-induced cyotoxiciy (Fig. 4.6). Interestingly, the addition of serine, a second precursor of *de novo* SL biosynthesis, had no effect on 4-HPR-induced cytotoxicity (data not shown). This lack of response might be linked the metabolism of extracellular serine to alpha-ketoglutarate [206], which contributes to glutaminolysis, an important pathway responsible for energy production and proliferation in breast cancer cells [207, 208].

To explore the biological basis for the opposing effects of Pal and OA on 4-HPR-induced cytotoxicity, the effects of these fatty acids on SL metabolism were investigated. Surprisingly, combination treatment with Pal and 4-HPR, as well as OA and 4-HPR, minimally affected total DHCer and DHCer subspecies when compared to 4-HPR alone (Fig. 4.7). Moreover, treatment of cells with either Pal or OA alone also decreased total (DH)Cer, as well as most (DH)Cer subspecies when compared with control treated cells (data not shown). These results were unexpected for Pal, as it is a known inducer of SL biosynthesis [145, 202]. Three hypotheses can be considered to explain these observations: (1) Pal decreases *de novo* SL biosynthesis in MCF7 cells; (2) Pal increases the turnover of (DH)Cer to more complex (DH)SL in MCF7 cells; and (3) Pal enhances the extracellular export of SL. The first hypothesis is unlikely because Pal is a well-documented inducer of *de novo* biosynthesis in numerous cell lines [145, 202, 209]; the second hypothesis is also not likely because all measured categories of SL decreased following the addition of Pal (data not shown). Interestingly, there is strong rationale for the third hypothesis because it is well established that tumor cells, secrete small membrane vesicles termed exosomes, both *in vivo* and *in vitro* [210-214]. Furthermore, a

previous study has found exosomes to be enriched in Cer and other SL including SM [215], while a more recent study has reported that Pal is able to trigger the release of exosomes [216, 217]. Therefore, it is possible that while the cellular decreases in (DH)Cer following treatment with OA could be due to its ability to inhibit SL biosynthesis, the changes seen following Pal treatment may be the result of the Pal-induced release of (DH)Cer-containing exosomes into the extracelluar environment.

Although total DHCer levels were not significantly affected, the addition of Pal and OA to 4-HPR did alter the chain length distribution of the subspecies of DHCer when compared with 4-HPR alone (Fig. 4.7). This effect could be due to a shift in the fatty acyl-CoA distribution and thereby substrate availability for the CerS family of enzymes. The consequences of this regulation are intriguing, as they suggest that preferential increases in C16 and C18 DHCer, following treatment with Pal and 4-HPR, as well as the preferential increase in C24:1 DHCer, following the addition of OA to 4-HPR treatment, may be important in determining the opposing effects of these fatty acids on 4-HPR-induced cell death.

In continuing to explore the basis for the opposing effects of Pal and OA on 4-HPR-induced cytotoxicity, the ability of these fatty acids to differentially regulate autophagy induction and autophagic degradation was analyzed. The protective effects of OA on 4-HPR-induced cytoxicity can be explained by its ability to decrease both the induction of autophagy, as shown by a decrease in the conversion of LC3-I to LC3-II, as well autophagic degradation, as shown by an accumulation of a specific substrate for autophagic degradation (p62), when compared with 4-HPR-treatment alone. In contrast, the regulation of enhanced cell death following the addition of Pal to 4-HPR treatment is

much more complex. Interestingly, combination treatment with Pal and 4-HPR did not enhance 4-HPR-induced autophagy or autophagic degradation suggesting that this combination may activate a second cell death pathway, which is responsible for the increased cell killing. Furthermore, this concept of combining agents, which activate cell death via multiple mechanisms, is an active area of study for breast cancer researchers as a way to improve therapeutic efficacy and minimize therapeutic resistance [172].

In conclusion, this study has demonstrated that Pal induces particular alterations in SL metabolism and enhances 4-HPR-induced cell death in MCF7 cells. These changes are likely to be the result of multiple mechanisms, and warrant further study because the combination of Pal and 4-HPR could be clinically useful.

CHAPTER 5

CONCLUSIONS AND FUTURE DIRECTIONS

SL are a complex family of molecules [2] that participate in many facets of cell structure and function [35, 60]. Therefore, the use of "-omic" approaches – i.e., to analyze as many as possible of the molecular species, mRNAs for pathway genes, etc. – is likely to uncover interesting, and sometimes unexpected, links between their metabolism, cell behavior, and disease [1, 31, 218]. Using the multi-faceted approach of lipidomic and genomic analyses combined with cell biology techniques, these studies integrate various aspects of SL biology in order to obtain a more clearly defined 'big picture' of the cellular effects of different agents, KLA and 4-HPR, on SL metabolism and the associated functional consequences (Fig. 5.1A-B). In addition, these studies have bridged two major paradigms of the biological consequences of altered SL metabolism (i.e, the role of SL in lipotoxicity and the role of SL in cancer therapy) in order to develop a new strategy for the enhancement of current cancer therapies (Fig. 5.1C).

Activation of the macrophage cell with LPS has been reported to elevate Cer by either the induction of turnover of pre-existing SL [115, 131, 219-221] in some studies or by stimulation of *de novo* biosynthesis [222] in others. Through the use of KLA, a homogenous preparation of the component of LPS specific for TLR4 receptor activation [128], as well as LC ESI-MS/MS [127] and microarray analysis (www.lipidmaps.org), the study described in Chapter 2 and [45] has reconciled these seemingly contradictory findings in order to provide a more complete picture of what is going within the macrophage cell with regard to SL biosynthesis and metabolism following activation. Incubation of RAW264.7 cells, a macrophage-like cell line, with KLA induces significant

increases in cellular SL [Chapter 2; Figs. 2.1-2.6 and [45]]. The additional SL arise primarily from *de novo* SL biosynthesis based on labeling with [U-^{13}C]palmitate and inhibition by ISP1; however, increases in Cer are also due to elevated turnover [Chapter 2; Figs. 2.9 and 2.11 and [45]]. Consistent with these metabolite changes, microarray analysis provided additional support for this idea of dual regulation of Cer production revealing that KLA elevated the mRNAs for not only enzymes of the biosynthetic pathway such as SPT, CerS, and DES but also enzymes of the turnover pathway such as acid sphingomyelinase (SMPD1) [Chapter 2; Figs 2.7-2.8 and [45]]. Therefore, the use of this multi-faceted lipidomic approach has changed how we must view SL metabolism in activated macrophage cells from inducing *de novo* SL biosynthesis OR activating of the turnover pathway to inducing *de novo* SL biosynthesis AND activating the turnover pathway (Fig. 5.1A). Furthermore, it is not surprising that the cells would have mechanism(s) to coordinate the formation and removal of this bioactive species in order to maintain some level of homeostasis.

In LPS-activated macrophages, the functional implications of increases in Cer resulting from the turnover pathway have been extensively explored as depicted in Fig. 5.1A; whereas the consequences of the upregulation of *de novo* biosynthesis is less understood. Cer resulting from the turnover of pre-existing SL species, namely SM, has been found to be essential for the assembly and activation of the TLR4 complex [219], responsible for increases in protein kinase C zeta (PKCζ) [220], extracellular signal-regulated kinase 1 and 2 (ERK1/2) [220], and cyclooxygenase 2 (COX-2) [221] enzyme activities, and necessary for the activation of inducible nitric oxide synthase (iNOS) and the production of nitric oxide [115]. Interestingly, nothing was known about the

biological purpose of Cer generated from *de novo* biosynthesis with the exception that it is involved in the release of arachidonic acid [222], a substrate for the generation of prostaglandins and leukotrienes. Therefore, increasing knowledge of signaling pathways regulated by *de novo* biosynthesis became an essential goal of these studies in order to continue to build a more complete picture of macrophage activation. Chapter 2 and [45] established that autophagosome formation is induced following KLA activation of macrophage cells (Fig. 2.13-2.14), which might be related to the increase in Cer, and perhaps other SL, because exogenous addition, or endogenous accumulation, of Cer is sufficient to induce autophagy [102, 104, 105]. Indeed, inhibition of *de novo* SL biosythesis prevented the accumulation of autophagic vacuoles in KLA-treated RAW264.7 cells [Chapter 2; Fig. 2.15 and [45]]. Furthermore, immunohistochemical analysis of the KLA-treated cells found Cer co-localized with autophagosomes, which was inhibited by ISP1 [Chapter 2; Fig. 2.17 and [45]]. These findings are strongly suggestive that elevation of Cer by KLA treatment of RAW264.7 cells is essential for induction of autophagy, and that the Cer must be derived from *de novo* biosynthesis because autophagosomes were not seen in ISP1-treated cells.

In addition to uncovering a novel role for *de novo* biosynthesized SL in macrophage activation, this study also found that KLA, as has been reported for LPS [151], inhibits cell growth [Chapter 2; Fig. 2.12 and [45]]. Although the role of Cer and other SL in KLA-induced growth inhibition is unclear, it is easy to envision that regulation of this cellular process represents the importance of the dual mechanism of Cer production from both turnover and *de novo* biosynthesis. As discussed above, Cer resulting from the turnover of SM has been found to increase the activity of ERK1/2

[220], highly conserved serine/threonine kinase isoforms whose activation has been found to inhibit cell-cycle progression leading to growth arrest [223, 224]. One can hypothesize that activation of macrophage cells with LPS or KLA could induce sphingomyelinase at the cell surface in order to promote the formation of Cer and activation of ERK1/2. In turn ERK1/2 translocates from the cytoplasm to the nucleus where it mediates cell cycle arrest in the G2/M phase, as has been reported for macrophages exposed to cadmium [225]. This inhibition of proliferation concurrent with continued SL biosynthesis due to upregulation of the *de novo* pathway results in an expansion of membrane area (and cell size) as the newly biosynthesized lipids remain with the original cells rather than being divided into daughter cells [as discussed in Chapter 2 and [45]]. In turn, Cer (and other metabolites) resulting from increased *de novo* biosynthesis in ER then provide the driving force for formation of the autophagosomal membrane [as discussed in Chapter 2 and [45]]. Because the ER is thought to be a key organelle in autophagic membrane biogenesis [155, 156] Cer's localization within the autophagosome suggests that it may be important in the formation of the limiting membrane by participating in ER-targeted signaling events. Furthermore, this may explain why elevation of Cer by SL turnover alone did not appear to be adequate for induction of autophagy following growth arrest by KLA in RAW264.7 cells [Chapter 2 and [45]]. Additionally, the idea is intriguing because several recent studies have found that autophagosome formation is associated with cell cycle arrest in the G2/M phase [226-229]. Thus, the interconnectivity of Cer production from both turnover and *de novo* biosynthesis could help to regulate multiple cellular processes in order to promote the innate immune response and clearance of pathogens in macrophage cells.

This study [Chapter 2 and [45]] provided the most comprehensive 'sphingolipidomic' analysis of activated macrophages to date and demonstrated a direct link between KLA induced *de novo* SL biosynthesis and autophagy, which not only deepens our understanding of macrophage biology but also reveals a new facet of SL biology and innate immunity. This opens the door to future studies to define the contribution of specific Cer subspecies in the induction of autophagy. It will be additionally interesting to determine the interrelationship between KLA-induced autophagy and inhibition of proliferation. These may be linked through mTOR because Cer has been shown to inhibit the activation of the mTOR cascade resulting in the induction of autophagy [102], and microarray data generated by the LIPID MAPS Consortium (www.lipidmaps.org) revealed a decrease in the mRNA levels of mTOR in KLA treated RAW264.7 cells. Thus, there are correlates with both the induction of autophagy and changes in SL metabolism, suggesting a possible mechanism of KLA induced autophagy through Cer mediated repression of the mTOR signaling pathway. More recently, addition of exogenous Cer1P has been found to stimulate macrophage proliferation via activation of mTOR [230]. As noted in Chapter 2 and [45], Cer1P was one of the few SL species not elevated versus time zero control following treatment with KLA. Therefore, it would be interesting to determine if Cer1P and Cer serve as a 'one-two punch' to repress cytosolic mTOR activation and ER-localized mTOR activation following KLA stimulation resulting in growth arrest and autophagy.

The studies described herein have not only expanded our knowledge of alterations in SL metabolism and the associated consequences following macrophage activation but have also improved our understanding of the mechanisms of action of the

chemotherapeutic agent, 4-HPR (Fig. 5.1B). In Chapter 2 and [45], the chemotherapeutic agent and known inducer of autophagy, 4-HPR, was a useful tool in confirming the requirement of *de novo* SL biosythesis in the induction of autophagy. Furthermore, 4-HPR has been reported to increase DHCer and other DHSL by increasing *de novo* biosynthesis as a result of the coordinate activation of SPT and CerS [175], by activating the turnover of pre-existing SL through activation of sphingomyelinase [189], and by inhibiting the DES enzyme [179]. In Chapter 3, a 'sphingolipidomic' analysis reconciled these seemingly contradictory obsevations by providing a more accurate assessment of the alterations in SL metabolism, using Hek293 cells as a model system. As has been reported for other cell lines, 4-HPR significantly increases the DHSL content of Hek293 cells (Chapter 3; Fig 3.1), and this effect is primarily due to the inhibition of DES (Chapter 3; Figs. 3.2 and 3.3).

Because of the prominent role of DES inhibition in the elevation of DHSL, this study additionally examined which structural features of 4-HPR (Fig. 5.1B) contribute to its inhibition of DES by comparing 4-HPR, its individual constituents (ATRA and 4-aminophenol), and analogs where ATRA was replaced by a simple fatty amide (including 4-HPA). These comparisons, which included analysis of the DHSL by mass spectrometry with complementary *in situ* and *in vitro* DES assays where appropriate, revealed that the retinoid moiety is not essential for DES inhibition (Chapter 3; Fig. 3.5) and (Fig. 5.1B), and the elevation of DHSL could be recapitulated with 4-HPA (Chapter 3; Fig. 3.6). Furthermore, many other phenols, including resveratrol, were also inhibitors (Chapter 3; Fig. 3.10). When 4-HPR and 4-HPA were added at concentrations that elevated DHSL to comparable levels, both were equivalent in induction of autophagy

(Chapter 3; Fig. 3.13), but 4-HPA was not cytotoxic, in stark contrast to 4-HPR (Chapter 3; Fig. 3.13).

It is noteworthy that in addition to their opposing effects on toxicity, these DES inhibitors also differently affect the N-acyl-chain-length distribution of the DHCer subspecies (Chapter 3; Fig. 3.13), with 4-HPR increasing both the long (i.e., C16) and very-long- (C22 and C24) chain subspecies, whereas, 4-HPA increases mainly the very-long-chain subspecies (C24:1). This differential regulation provides an interesting avenue for future study to determine if the opposing effects of 4-HPR and 4-HPA on cellular toxicity are the result of altered regulation of CerS family members, that define which fatty acyl-CoAs are used to form distinct DHCer subspecies [1, 3, 11-13]. Studies by others have, indeed, found that increases in CerS1 activity [231-233], which regulate the synthesis of C18-SL, and CerS5 and CerS6 activity [231, 233, 234], which regulate the synthesis of C16-SL, are responsible for the cellular toxicity of chemotherapeutic agents and combination therapies. In contrast, increases in CerS2 activity [233, 234], which produces C24- and C24:1-SL, was found to offer protection from ionizing radiation therapy. Thus, these studies provide further evidence that activation of specific CerSs generate pro-death (CerS1, CerS5, and CerS6) versus pro-survival (CerS2) signals, and suggests that the ability of 4-HPR to preferentially promote larger increases in C16- and C18-DHCer might play a role in its cytotoxicity; whereas 4-HPA preferentially increases C24- and C24:1-DHCer, and thus, is not toxic. Using siRNA technology and other recently developed inhibitors [235], it will be interesting to continue to investigate this phenomena, particularly in the regulation of autophagy and autophagic cell death, which

suggests the possibility of species-specific functions for DHCer, that until this point has only been considered for the subspecies of Cer [233].

In addition to the potential role of subspecies-specific functions in contributing to the opposing effects of 4-HPR and 4-HPA on cell viability, a second mechanism could also be considered. A recent study by Zhang, *et al.* reported the ability of arsenic trioxide to alter SL metabolism through increases in both *de novo* biosynthesis, as well as the hydrolysis of SM [236]. This dual regulation was associated with the downreglation of matrix metalloproteinase-9 (MMP-9), an endoproteinase known to be important in metastasis, which prevented carcinoma cell invasion resulting in subsequent cell death [236]. It would be interesting to compare the effects of 4-HPR and 4-HPA on MMP-9 expression in order to determine if the ability of 4-HPR to activate *de novo* biosynthesis, in addition to inhibiting DES and in contrast to 4-HPA (Chapter 3; Fig. 12), is critical in its ability to mediate a cell-death response.

Additionally, while this study has not attempted to elucidate the mechanism of DES inhibition, it is interesting to speculate about the importance of phenolic group. The phenol group is hypothesized to interfere with electron transport. DES, like the Δ^9–stearoyl-CoA desaturase [194] and the Δ^1–alkyl desaturase [195], is part of a multi-enzyme complex, which consists of coupled reactions that transport electrons from NAD(P)H to the terminal desaturase leading to the reduction of oxygen [186]. Oxidation of phenols can form phenoxyl radicals that are either further oxidized to yield quinones or reduced back to the phenol by cellular reductants [237]. Interestingly, cell lines responsive to 4HPR treatment were found to have a lower cellular antioxidant thiol levels [238]. Therefore, DES inhibition by 4-HPR and other phenolic compounds may be

dependent on the dual mechanism of the quinoid derivative (which increase when cellular reductants decrease) to behave directly as an electron acceptor shunting electrons away from the desaturase electron transport chain and indirectly through the generation of reactive oxygen species (ROS) leading to changes in cellular redox status, which has been recently shown to potently inhibit desaturase activity [196]. Furthermore, it can be envisioned that the presence of the fatty acyl-chain in 4-HPR and 4-HPA has enough structural similarity with DHCer for these molecules to fit into the binding pocket of the enzyme, perhaps positioning the phenol near the redox center. This would also explain why 4-aminophenol and 4-acetamidophenol caused little or no DES inhibition (Chapter 3; Fig. 3.5).

The requirement appears to be for a hydrophobic group rather than an alkyl chain since resveratrol was also found to be an effective inhibitor of DES activity *in vitro* (Chapter 3; Fig. 3.10). Indeed, the multiple phenolic groups of resveratrol may compensate for the presence of the acyl chain by adding enough bulkiness for the molecule to fit into the DES binding pocket. Furthermore, once in the pocket, the multiple phenol groups of resveratrol may increase inhibition efficiency through the formation of multiple quinoid derivatives resulting in the increased ability of resveratrol to shunt electrons away from the DES electron transport chain. Additional support for this idea is provided by our identification of numerous other polyphenolic compounds which inhibit DES activity with an IC_{50} of ≤ 25 μM including genistein, with three phenolic hydroxyl groups, curcumin, with two phenolic hydroxyl groups, and quercetin, with four phenolic hydroxyl groups (unpublished observations).

The studies described herein have not only expanded our previous view of the effects of macrophage activation and chemotherapeutic intervention on SL metabolism and the associated functional consequences, but have also bridged two major themes of SL research: the role of SL in lipotoxicity and the role of SL in cancer therapy (Fig. 5.1C).

Epidemiological studies have found a positive correlation between diets high in saturated fats and the development of insulin resistance and complications associated with metabolic disease [209, 239]. The dependence of *de novo* SL biosynthesis on one of the most abundant dietary saturated fatty acids [240], Pal, made this pathway an attractive target for the investigation of the mechanisms associated with lipotoxicity [239], a collective term often used to describe the adverse effects associated with fatty acid accumulation including cell death and dysfunction [241]. Indeed, numerous studies, as reviewed by Dr. Scott Summers, have linked the production of the bioactive SL metabolite Cer to saturated fatty acid-induced lipotoxic processes [239]. While Cer is likely only one of several nutrient metabolites responsible for this phenomenon, inhibition of the *de novo* SL biosynthetic pathway negated the effects of fatty acid induced-toxicity suggesting that Pal and aberrant *de novo* SL biosynthesis are key players in lipotoxic processes [239]. Additionally, alterations in SL metabolism, particularly decreases in Cer production, have been found to be important in the protective role of diets high in unsaturated fatty acids, such as OA [209, 239].

In contrast to the desire to decrease or limit the production of bioactive SL mediators, like Cer, in order to combat/prevent lipotoxicity, many cancer therapies seek to increase the cellular levels of SL mediators, including Cer and DHCer, as a mechanism

to induce cell death, and these molecules have been implicated in mediating the effects of many chemopreventive agents [112, 242, 243]. For example, increases in endogenous Cer have been found to contribute to the cell death response induced by radiation therapy, etoposide, doxorubicin, and daunorubicin, *inter alia* [112, 242, 243]. Furthermore, the accumulation of DHCer following treatment with 4-HPR was found to induce cell cycle arrest in neuroblastoma cells [177, 243], as well as stimulate autophagic cell death in MCF7 breast cancer cells [Chapter 4; Fig. 4.1 and [99]]. With this in mind, an attractive strategy to increase the efficacy of cancer therapy became to combine the concept of Pal-induced aberrant SL biosynthesis with chemotherapeutic agents, such as 4-HPR, whose mechanisms of action has been found to depend on the production of bioactive SL mediators (Fig. 5.1C). To this end, the study described in Chapter 4 of this work examined if the single agent efficacy of 4-HPR could be enhanced by the addition Pal. Indeed, it was found that the addition of Pal was effective at increasing 4-HPR induced cell death in MCF7 breast cancer cells (Chapter 4; Fig. 4.6) suggesting that the combination of Pal and 4-HPR may be clinically useful in enhancing the efficacy of 4-HPR.

In addition to its ability to enhance the single agent efficacy of 4-HPR, a second interesting reason why this combination warrants continued evaluation as a potential candidate combination therapy is that clinical studies indicate that the concentrations evaluated *in vitro* are physiologically achievable *in vivo* [176, 244, 245]. In a Phase II clinical trial, steady state plasma levels from 0.61 μM to 14.6 μM were achieved in patients using twice-daily dosing of oral 4-HPR capsules (900 mg/m^2) [244]. Furthermore, this dosage was well tolerated by all patients enrolled in the trial [244], and

additional Phase I trials are currently being conducted on improved oral formulations which increase 4-HPR-bioavailablity in order to extend the clinical benefit to a significantly greater number of patients [245, 246]. One additional factor to consider is that the steady-state levels of 4-HPR in breast tissue have been reported to be greater than those in plasma for a variety of doses [247] providing further evidence that the concentrations tested *in vitro* are likely to be clinically achievable. Additionally, the relatively low dose of Pal, which is non-toxic alone and well within the physiological range [248], was effective in enhancing 4-HPR-induced toxicity suggesting that this combination is likely to be well-tolerated by patients.

An investigation into the biological basis of the ability of Pal to enhance 4-HPR-mediated cell death suggests that the mechanism of action is much more complex than originally imagined. Surprisingly, Pal treatment alone, as well as the combination of Pal and 4-HPR, minimally affected or decreased the total cellular accumulation of (DH)Cer in MCF7 cells (Chapter 4; Fig. 4.7). This was unexpected, particularly for Pal treatment alone, due to the known ability of Pal to increase flux through the biosynthetic pathway [145, 202]. However, it is possible that the exogenously added Pal is rapidly taken up and used for *de novo* biosynthesis within the first six hours of administration, as has been previously reported by Haynes, *et al* [249]. Following the initial "burst" of SL production, the newly synthesized lipids, including (DH)Cer and possibly (DH)SM, become components of membrane vesicles, such as exosomes, where they are released into the extracellular milieu for signaling purposes (as discussed in Chapter 4). This recommends future experiments to analyze the time-dependent effects of Pal alone and Pal in combination with 4-HPR on the intracellular SL composition, as well as the SL

composition of the exosomes released from MCF7 cells. Furthermore, it will be interesting to determine if the combination of Pal and 4-HPR exploits exosome release for delivering pro-death signals to neighboring cells as a mechanism to increase cellular toxicity. This idea is intriguing as it could be effective in explaining not only the enhanced cytotoxicty seen following treatment with Pal and 4-HPR, but also the lack of cytotoxicty following treatment with Pal alone. The Pal-induced release of exosomes did not result in significant cellular toxicity in a rat adipocyte cell model used for study [216], which is in agreement with the findings in Chapter 4 of the inability of Pal alone to induce toxicity in MCF7 cells (Chapter 4; Fig. 4.6). Furthermore, it was found that the addition of exosomes derived from untreated BT-474 breast cancer cells bound to the cell surface and actually stimulated the proliferation of parental BT-474 cells [212]. This idea agrees with the ability of Pal alone to slightly increase viability of MCF7 cells after 24 h of stimulation (Chapter 4; Fig. 4.6). Additionally, this concept may provide a novel part of the mechanism for the enhanced cell death observed following combination treatment with Pal and 4-HPR. It has been suggested that exosomes may bear different combinations of ligands dependent on cellular conditions [211]. Therefore, it is possible that the while Pal alone stimulates the release of (DH)Cer-enriched exosomes, the addition of 4-HPR alters the contents of these vesicles resulting in the transfer death inducing molecules, such as FasL, to neighboring cancer cells ultimately stimulating a second cell death response, likely necrosis [211]. Further support for this idea is provided by three independent studies reporting: (1) the ability of 4-HPR to upregulate the cell surface expression of Fas [250], which is expected to prime cells for activation of cell death by FasL, (2) the ability colorectal cancer cells to release exosomes containing FasL

that induce cell death in neighboring cells [211, 251], and (3) the ability of FasL to stimulate caspase independent cell death (CICD) with necrotic features when caspases are inhibited [252], such as the case in caspase-3 defective MCF7 cells used for this study. Further support for this idea is provided by the inability of Pal addition to enhance 4-HPR-mediated autophagy and presumably autophagic cell death (Chapter 4; Fig. 4.8).

A second possible contributor to cell death that has been found to be activated by both Pal [253-255] and 4-HPR [191, 256] is the production of ROS. Pal is known to stimulate a small accumulation of ROS in MCF7 cells [203]. Although, Pal-induced ROS accumulation is not sufficient to induce cell death in MCF7 cells [203], it is likely that the addition of 4-HPR, which also has been shown to generate ROS [100, 172], could enhance this accumulation to a level sufficient to create mitochondrial dysfunction resulting in necrosis. Distinguishing between these two possible mechanisms of activation of necrosis by comparing the effect of concurrent treatment with Pal and 4-HPR with the effect of purified exosomes derived from concurrent treatment with Pal and 4-HPR on MCF7 cells is an interesting area for continued investigation.

Although these ideas seem intriguing, it is possible that the mechanism of enhanced 4-HPR-cytotoxcity following the addition of Pal is not due to the formation of Cer-containing exosomes or related to the production of ROS, but instead due to the species-specific functions of DHCer (as discussed above). One of the most interesting findings from the study in Chapter 4 was the differential regulation of Pal and OA on the distribution of the subspecies of DHCer (Chapter 4; Fig. 4.7), which correlated with opposing functions on 4-HPR-induced cell death (Chapter 4; Fig. 4.6). Therefore, it would be interesting to determine the effects of upregulating or inhibiting various CerS

family members on 4-HPR-induced toxicity in the presence of Pal or OA. Furthermore, the ability of different subspecies of DHCer to regulate intracellular signaling associated with cell death in combination with the ability of SL-enriched exosomes to participate in intercellular signaling processes is an exciting idea that may provide a synergistic mechanism for the enhanced cell death seen following the addition of Pal to 4-HPR-treatment. Additionally, with regard to the potential regulation of cell death activation via SL signaling, the possible contribution of changes in Sa should not be omitted. In MCF7 cells, 4-HPR increases Sa levels (Fig. 4.4). Furthermore, the elevation of Sa has been hypothesized to participate in 4-HPR-induced cytotoxicity in some cell systems [176]. Therefore, it is possible that Pal enhances 4HPR-induced cytotoxicity due to futher increases in Sa. This is currently an active area of investigation within the lab. Although the mechanism is no doubt the result of a surprisingly unexpected level of complexity, the ability of Pal to enhance 4-HPR-induced cell death provides evidence that the strategy of combining Pal-induced SL biosynthesis during lipotoxicity with chemotherapeutic agents may be clinically effective in increasing the single agent efficacy of 4-HPR (Fig. 5.1C).

In conclusion, the studies described in this thesis have provided a more comprehensive picture of the cellular effects of KLA and 4-HPR on SL metabolism and regulation of the autophagic pathway, as well as investigated a novel strategy for the enhancement of current cancer therapies (Fig. 5.1). Through the use lipidomic technologies, genomic analysis, and cellular biology techniques, these studies have uncovered potentially interesting links between SL metabolism, autophagy, and other cellular behaviors, and it is hoped that these findings will prove informative in leading

future researchers to design new strategies for the treatment of infection, cancer, and other diseases.

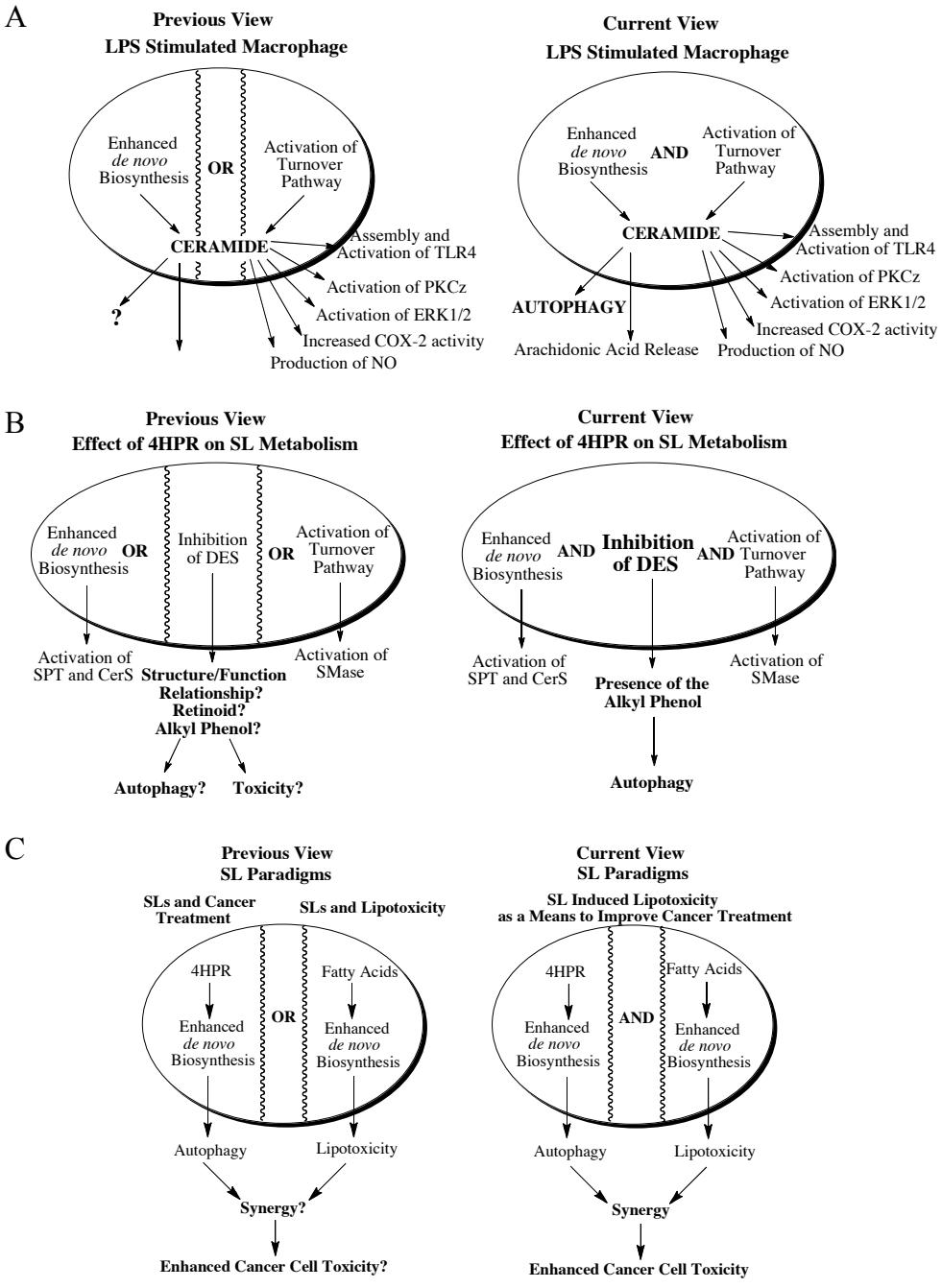

Figure 5.1 Summary
A, Changing view of macrophage activation *B*, Changing view of the ability of 4-HPR to regulate SL metabolism *C*, New strategy for the enhancement of current cancer therapies based on SL paradigms

REFERENCES

1. Zheng, W., et al., *Ceramides and other bioactive sphingolipid backbones in health and disease: lipidomic analysis, metabolism and roles in membrane structure, dynamics, signaling and autophagy.* Biochim Biophys Acta, 2006. **1758**(12): p. 1864-84.

2. Merrill, A.H., Jr., et al., *(Glyco)sphingolipidology: an amazing challenge and opportunity for systems biology.* Trends Biochem Sci, 2007. **32**(10): p. 457-68.

3. Merrill, A.H., Jr., *Sphingolipid and glycosphingolipid metabolic pathways in the era of sphingolipidomics.* Chem Rev, 2011. **In press**.

4. Pinto, W.J., et al., *Sphingolipid long-chain-base auxotrophs of Saccharomyces cerevisiae: genetics, physiology, and a method for their selection.* J Bacteriol, 1992. **174**(8): p. 2565-74.

5. Hanada, K., M. Nishijima, and Y. Akamatsu, *A temperature-sensitive mammalian cell mutant with thermolabile serine palmitoyltransferase for the sphingolipid biosynthesis.* J Biol Chem, 1990. **265**(36): p. 22137-42.

6. Hojjati, M.R., Z. Li, and X.C. Jiang, *Serine palmitoyl-CoA transferase (SPT) deficiency and sphingolipid levels in mice.* Biochim Biophys Acta, 2005. **1737**(1): p. 44-51.

7. Adachi-Yamada, T., et al., *De novo synthesis of sphingolipids is required for cell survival by down-regulating c-Jun N-terminal kinase in Drosophila imaginal discs.* Mol Cell Biol, 1999. **19**(10): p. 7276-86.

8. Hanada, K., et al., *Molecular machinery for non-vesicular trafficking of ceramide.* Nature, 2003. **426**(6968): p. 803-9.

9. Mandon, E.C., et al., *Subcellular localization and membrane topology of serine palmitoyltransferase, 3-dehydrosphinganine reductase, and sphinganine N-acyltransferase in mouse liver.* J Biol Chem, 1992. **267**(16): p. 11144-8.

10. Berdyshev, E.V., et al., *De novo biosynthesis of dihydrosphingosine-1-phosphate by sphingosine kinase 1 in mammalian cells.* Cell Signal, 2006. **18**(10): p. 1779-92.

11. Pewzner-Jung, Y., S. Ben-Dor, and A.H. Futerman, *When do Lasses (longevity assurance genes) become CerS (ceramide synthases)?: Insights into the regulation of ceramide synthesis.* J Biol Chem, 2006. **281**(35): p. 25001-5.

12. Mizutani, Y., A. Kihara, and Y. Igarashi, *Mammalian Lass6 and its related family members regulate synthesis of specific ceramides.* Biochem J, 2005. **390**(Pt 1): p. 263-71.

13. Stiban, J., R. Tidhar, and A.H. Futerman, *Ceramide synthases: roles in cell physiology and signaling.* Adv Exp Med Biol. **688**: p. 60-71.

14. Merrill, A.H., Jr. and E. Wang, *Biosynthesis of long-chain (sphingoid) bases from serine by LM cells. Evidence for introduction of the 4-trans-double bond after de novo biosynthesis of N-acylsphinganine(s).* J Biol Chem, 1986. **261**(8): p. 3764-9.

15. Michel, C., et al., *Characterization of ceramide synthesis. A dihydroceramide desaturase introduces the 4,5-trans-double bond of sphingosine at the level of dihydroceramide.* J Biol Chem, 1997. **272**(36): p. 22432-7.

16. Voelker, D.R. and E.P. Kennedy, *Cellular and enzymic synthesis of sphingomyelin.* Biochemistry, 1982. **21**(11): p. 2753-9.

17. Ullman, M.D. and N.S. Radin, *The enzymatic formation of sphingomyelin from ceramide and lecithin in mouse liver.* J Biol Chem, 1974. **249**(5): p. 1506-12.

18. Kumagai, K., et al., *CERT mediates intermembrane transfer of various molecular species of ceramides.* J Biol Chem, 2005. **280**(8): p. 6488-95.

19. Sugiura, M., et al., *Ceramide kinase, a novel lipid kinase. Molecular cloning and functional characterization.* J Biol Chem, 2002. **277**(26): p. 23294-300.

20. Wijesinghe, D.S., et al., *Substrate specificity of human ceramide kinase.* J Lipid Res, 2005. **46**(12): p. 2706-16.

21. Futerman, A.H. and R.E. Pagano, *Determination of the intracellular sites and topology of glucosylceramide synthesis in rat liver.* Biochem J, 1991. **280 (Pt 2)**: p. 295-302.

22. Sprong, H., et al., *Association of the Golgi UDP-galactose transporter with UDP-galactose:ceramide galactosyltransferase allows UDP-galactose import in the endoplasmic reticulum.* Mol Biol Cell, 2003. **14**(8): p. 3482-93.

23. Paul, P., et al., *Purification and characterization of UDP-glucose:ceramide glucosyltransferase from rat liver Golgi membranes.* J Biol Chem, 1996. **271**(4): p. 2287-93.

24. Berger, E.G.a.R., Jurgen, *The Golgi apparatus*, ed. E.G. Berger. 1997: Birkauser. 306.

25. Koch, J., et al., *Molecular cloning and characterization of a full-length complementary DNA encoding human acid ceramidase. Identification Of the first molecular lesion causing Farber disease.* J Biol Chem, 1996. **271**(51): p. 33110-5.

26. Mao, C., et al., *Cloning and characterization of a novel human alkaline ceramidase. A mammalian enzyme that hydrolyzes phytoceramide.* J Biol Chem, 2001. **276**(28): p. 26577-88.

27. El Bawab, S., et al., *Molecular cloning and characterization of a human mitochondrial ceramidase.* J Biol Chem, 2000. **275**(28): p. 21508-13.

28. Mao, Z., et al., *Alkaline ceramidase 2 (ACER2) and its product dihydrosphingosine mediate the cytotoxicity of N-(4-hydroxyphenyl)retinamide in tumor cells.* J Biol Chem. **285**(38): p. 29078-90.

29. Hu, W., et al., *Alkaline ceramidase 3 (ACER3) hydrolyzes unsaturated long-chain ceramides, and its down-regulation inhibits both cell proliferation and apoptosis.* J Biol Chem. **285**(11): p. 7964-76.

30. Tettamanti, G., *Ganglioside/glycosphingolipid turnover: new concepts.* Glycoconj J, 2004. **20**(5): p. 301-17.

31. Hait, N.C., et al., *Sphingosine kinases, sphingosine 1-phosphate, apoptosis and diseases.* Biochim Biophys Acta, 2006. **1758**(12): p. 2016-26.

32. Mandala, S.M., *Sphingosine-1-Phosphate Phosphatases.* Prostaglandins, 2001. **64**(1-4): p. 143-156.

33. Reiss, U., et al., *Sphingosine-phosphate lyase enhances stress-induced ceramide generation and apoptosis.* J Biol Chem, 2004. **279**(2): p. 1281-90.

34. Ikeda, M., et al., *Sphingolipid-to-glycerophospholipid conversion in SPL-null cells implies the existence of an alternative isozyme.* Biochem Biophys Res Commun, 2005. **329**(2): p. 474-9.

35. Hannun, Y.A. and L.M. Obeid, *Principles of bioactive lipid signalling: lessons from sphingolipids.* Nat Rev Mol Cell Biol, 2008. **9**(2): p. 139-50.

36. Bartke, N. and Y.A. Hannun, *Bioactive sphingolipids: metabolism and function.* J Lipid Res, 2009. **50 Suppl**: p. S91-6.

37. Hanada, K., et al., *CERT-mediated trafficking of ceramide.* Biochim Biophys Acta, 2009. **1791**(7): p. 684-91.

38. Lamour, N.F., et al., *Ceramide kinase uses ceramide provided by ceramide transport protein: localization to organelles of eicosanoid synthesis.* J Lipid Res, 2007. **48**(6): p. 1293-304.

39. Jeckel, D., et al., *Glucosylceramide is synthesized at the cytosolic surface of various Golgi subfractions.* J Cell Biol, 1992. **117**(2): p. 259-67.

40. D'Angelo, G., et al., *Glycosphingolipid synthesis requires FAPP2 transfer of glucosylceramide.* Nature, 2007. **449**(7158): p. 62-7.

41. Arana, L., et al., *Ceramide and ceramide 1-phosphate in health and disease.* Lipids Health Dis, 2010. **9**: p. 15.

42. Boath, A., et al., *Regulation and traffic of ceramide 1-phosphate produced by ceramide kinase: comparative analysis to glucosylceramide and sphingomyelin.* J Biol Chem, 2008. **283**(13): p. 8517-26.

43. Wennekes, T., et al., *Glycosphingolipids--nature, function, and pharmacological modulation.* Angew Chem Int Ed Engl, 2009. **48**(47): p. 8848-69.

44. Ding, Z., H. Kawashima, and M. Miyasaka, *Sulfatide binding and activation of leukocytes through an L-selectin-independent pathway.* J Leukoc Biol, 2000. **68**(1): p. 65-72.

45. Sims, K., et al., *Kdo2-lipid A, a TLR4-specific agonist, induces de novo sphingolipid biosynthesis in RAW264.7 macrophages, which is essential for induction of autophagy.* J Biol Chem. **285**(49): p. 38568-79.

46. Ohta, H., et al., *Induction of apoptosis by sphingosine in human leukemic HL-60 cells: a possible endogenous modulator of apoptotic DNA fragmentation occurring during phorbol ester-induced differentiation.* Cancer Res, 1995. **55**(3): p. 691-7.

47. Merrill, A.H., Jr., et al., *Inhibition of phorbol ester-dependent differentiation of human promyelocytic leukemic (HL-60) cells by sphinganine and other long-chain bases.* J Biol Chem, 1986. **261**(27): p. 12610-5.

48. Dbaibo, G.S., et al., *Activation of a retinoblastoma-protein-dependent pathway by sphingosine.* Biochem J, 1995. **310 (Pt 2)**: p. 453-9.

49. Hannun, Y.A., et al., *Sphingosine inhibition of protein kinase C activity and of phorbol dibutyrate binding in vitro and in human platelets.* J Biol Chem, 1986. **261**(27): p. 12604-9.

50. Xin, M. and X. Deng, *Protein phosphatase 2A enhances the proapoptotic function of Bax through dephosphorylation.* J Biol Chem, 2006. **281**(27): p. 18859-67.

51. Chalfant, C.E., et al., *De novo ceramide regulates the alternative splicing of caspase 9 and Bcl-x in A549 lung adenocarcinoma cells. Dependence on protein phosphatase-1.* J Biol Chem, 2002. **277**(15): p. 12587-95.

52. Ruvolo, P.P., et al., *Ceramide induces Bcl2 dephosphorylation via a mechanism involving mitochondrial PP2A.* J Biol Chem, 1999. **274**(29): p. 20296-300.

53. Chiang, C.W., et al., *Protein phosphatase 2A dephosphorylation of phosphoserine 112 plays the gatekeeper role for BAD-mediated apoptosis.* Mol Cell Biol, 2003. **23**(18): p. 6350-62.

54. Chen, C.L., et al., *Lithium inhibits ceramide- and etoposide-induced protein phosphatase 2A methylation, Bcl-2 dephosphorylation, caspase-2 activation, and apoptosis.* Mol Pharmacol, 2006. **70**(2): p. 510-7.

55. Kajimoto, T., et al., *Ceramide-induced apoptosis by translocation, phosphorylation, and activation of protein kinase Cdelta in the Golgi complex.* J Biol Chem, 2004. **279**(13): p. 12668-76.

56. Laouar, A., D. Glesne, and E. Huberman, *Involvement of protein kinase C-beta and ceramide in tumor necrosis factor-alpha-induced but not Fas-induced apoptosis of human myeloid leukemia cells.* J Biol Chem, 1999. **274**(33): p. 23526-34.

57. Sawai, H., et al., *Ceramide-induced translocation of protein kinase C-delta and -epsilon to the cytosol. Implications in apoptosis.* J Biol Chem, 1997. **272**(4): p. 2452-8.

58. Heinrich, M., et al., *Cathepsin D targeted by acid sphingomyelinase-derived ceramide.* EMBO J, 1999. **18**(19): p. 5252-63.

59. Heinrich, M., et al., *Cathepsin D links TNF-induced acid sphingomyelinase to Bid-mediated caspase-9 and -3 activation.* Cell Death Differ, 2004. **11**(5): p. 550-63.

60. Maceyka, M., S. Milstien, and S. Spiegel, *Sphingosine-1-phosphate: the Swiss army knife of sphingolipid signaling.* J Lipid Res, 2009. **50 Suppl**: p. S272-6.

61. Gomez-Munoz, A., et al., *Stimulation of DNA synthesis by natural ceramide 1-phosphate.* Biochem J, 1997. **325 (Pt 2)**: p. 435-40.

62. Miranda, G.E., et al., *Ceramide-1-phosphate, a new mediator of development and survival in retina photoreceptors.* Invest Ophthalmol Vis Sci, 2011. **52**(9): p. 6580-6588.

63. Lamour, N.F., et al., *Ceramide 1-phosphate is required for the translocation of group IVA cytosolic phospholipase A2 and prostaglandin synthesis.* J Biol Chem, 2009. **284**(39): p. 26897-907.

64. Mizushima, N., *Autophagy: process and function.* Genes Dev, 2007. **21**(22): p. 2861-73.

65. Barth, S., D. Glick, and K.F. Macleod, *Autophagy: assays and artifacts.* J Pathol, 2010. **221**(2): p. 117-124.

66. Mehrpour, M., et al., *Overview of macroautophagy regulation in mammalian cells.* Cell Res. **20**(7): p. 748-62.

67. Kundu, M. and C.B. Thompson, *Autophagy: basic principles and relevance to disease.* Annu Rev Pathol, 2008. **3**: p. 427-55.

68. Maiuri, M.C., et al., *Functional and physical interaction between Bcl-X(L) and a BH3-like domain in Beclin-1.* EMBO J, 2007. **26**(10): p. 2527-39.

69. Eisenberg-Lerner, A. and A. Kimchi, *The paradox of autophagy and its implication in cancer etiology and therapy.* Apoptosis, 2009. **14**(4): p. 376-91.

70. Chen, N. and J. Debnath, *Autophagy and tumorigenesis.* FEBS Lett. **584**(7): p. 1427-35.

71. Jung, C.H., et al., *mTOR regulation of autophagy.* FEBS Lett. **584**(7): p. 1287-95.

72. Glick, D., S. Barth, and K.F. Macleod, *Autophagy: cellular and molecular mechanisms.* J Pathol. **221**(1): p. 3-12.

73. Geng, J. and D.J. Klionsky, *The Golgi as a potential membrane source for autophagy.* Autophagy. **6**(7): p. 950-1.

74. Maiuri, M.C., et al., *Self-eating and self-killing: crosstalk between autophagy and apoptosis.* Nat Rev Mol Cell Biol, 2007. **8**(9): p. 741-52.

75. Liang, C., et al., *UVRAG: a new player in autophagy and tumor cell growth.* Autophagy, 2007. **3**(1): p. 69-71.

76. Pattingre, S., et al., *Bcl-2 antiapoptotic proteins inhibit Beclin 1-dependent autophagy.* Cell, 2005. **122**(6): p. 927-39.

77. Kabeya, Y., et al., *LC3, a mammalian homologue of yeast Apg8p, is localized in autophagosome membranes after processing.* EMBO J, 2000. **19**(21): p. 5720-8.

78. Sou, Y.S., et al., *Phosphatidylserine in addition to phosphatidylethanolamine is an in vitro target of the mammalian Atg8 modifiers, LC3, GABARAP, and GATE-16.* J Biol Chem, 2006. **281**(6): p. 3017-24.

79. Klionsky, D.J., et al., *Guidelines for the use and interpretation of assays for monitoring autophagy in higher eukaryotes.* Autophagy, 2008. **4**(2): p. 151-75.

80. Mizushima, N., T. Yoshimori, and B. Levine, *Methods in mammalian autophagy research.* Cell. **140**(3): p. 313-26.

81. Kuma, A., M. Matsui, and N. Mizushima, *LC3, an autophagosome marker, can be incorporated into protein aggregates independent of autophagy: caution in the interpretation of LC3 localization.* Autophagy, 2007. **3**(4): p. 323-8.

82. Man, N., et al., *Induction of genuine autophagy by cationic lipids in mammalian cells.* Autophagy. **6**(4).

83. Mizushima, N. and T. Yoshimori, *How to interpret LC3 immunoblotting.* Autophagy, 2007. **3**(6): p. 542-5.

84. Nara, A., et al., *SKD1 AAA ATPase-dependent endosomal transport is involved in autolysosome formation.* Cell Struct Funct, 2002. **27**(1): p. 29-37.

85. Kouroku, Y., et al., *ER stress (PERK/eIF2alpha phosphorylation) mediates the polyglutamine-induced LC3 conversion, an essential step for autophagy formation.* Cell Death Differ, 2007. **14**(2): p. 230-9.

86. Todde, V., M. Veenhuis, and I.J. van der Klei, *Autophagy: principles and significance in health and disease.* Biochim Biophys Acta, 2009. **1792**(1): p. 3-13.

87. Xu, Y., et al., *Toll-like receptor 4 is a sensor for autophagy associated with innate immunity.* Immunity, 2007. **27**(1): p. 135-44.

88. Deretic, V. and B. Levine, *Autophagy, immunity, and microbial adaptations.* Cell Host Microbe, 2009. **5**(6): p. 527-49.

89. Sanjuan, M.A. and D.R. Green, *Eating for good health: linking autophagy and phagocytosis in host defense.* Autophagy, 2008. **4**(5): p. 607-11.

90. Rich, K.A., C. Burkett, and P. Webster, *Cytoplasmic bacteria can be targets for autophagy.* Cell Microbiol, 2003. **5**(7): p. 455-68.

91. Prigione, A. and G. Cortopassi, *Mitochondrial DNA deletions and chloramphenicol treatment stimulate the autophagic transcript ATG12.* Autophagy, 2007. **3**(4): p. 377-80.

92. Deretic, V., et al., *Mycobacterium tuberculosis inhibition of phagolysosome biogenesis and autophagy as a host defence mechanism.* Cell Microbiol, 2006. **8**(5): p. 719-27.

93. Saiga, H., Y. Shimada, and K. Takeda, *Innate immune effectors in mycobacterial infection.* Clin Dev Immunol. **2011**: p. 347594.

94. Brech, A., et al., *Autophagy in tumour suppression and promotion.* Mol Oncol, 2009. **3**(4): p. 366-75.

95. Bellodi, C., et al., *Targeting autophagy potentiates tyrosine kinase inhibitor-induced cell death in Philadelphia chromosome-positive cells, including primary CML stem cells.* J Clin Invest, 2009. **119**(5): p. 1109-23.

96. Schleicher, S.M., et al., *Progress in the unraveling of the endoplasmic reticulum stress/autophagy pathway and cancer: implications for future therapeutic approaches.* Drug Resist Updat. **13**(3): p. 79-86.

97. Janicke, R.U., et al., *Caspase-3 is required for DNA fragmentation and morphological changes associated with apoptosis.* J Biol Chem, 1998. **273**(16): p. 9357-60.

98. Wesierska-Gadek, J., et al., *Reconstitution of human MCF-7 breast cancer cells with caspase-3 does not sensitize them to action of CDK inhibitors.* J Cell Biochem. **112**(1): p. 273-88.

99. Fazi, B., et al., *Fenretinide induces autophagic cell death in caspase-defective breast cancer cells.* Autophagy, 2008. **4**(4): p. 435-41.

100. Wu, J.M., A.M. DiPietrantonio, and T.C. Hsieh, *Mechanism of fenretinide (4-HPR)-induced cell death.* Apoptosis, 2001. **6**(5): p. 377-88.

101. Devarajan, E., et al., *Down-regulation of caspase 3 in breast cancer: a possible mechanism for chemoresistance.* Oncogene, 2002. **21**(57): p. 8843-51.

102. Scarlatti, F., et al., *Ceramide-mediated macroautophagy involves inhibition of protein kinase B and up-regulation of beclin 1.* J Biol Chem, 2004. **279**(18): p. 18384-91.

103. Lavieu, G., et al., *Regulation of autophagy by sphingosine kinase 1 and its role in cell survival during nutrient starvation.* J Biol Chem, 2006. **281**(13): p. 8518-27.

104. Pattingre, S., et al., *Role of JNK1-dependent Bcl-2 phosphorylation in ceramide-induced macroautophagy.* J Biol Chem, 2009. **284**(5): p. 2719-28.

105. Daido, S., et al., *Pivotal role of the cell death factor BNIP3 in ceramide-induced autophagic cell death in malignant glioma cells.* Cancer Res, 2004. **64**(12): p. 4286-93.

106. Salazar, M., et al., *Cannabinoid action induces autophagy-mediated cell death through stimulation of ER stress in human glioma cells.* J Clin Invest, 2009. **119**(5): p. 1359-72.

107. Lepine, S., et al., *Sphingosine-1-phosphate phosphohydrolase-1 regulates ER stress-induced autophagy.* Cell Death Differ. **18**(2): p. 350-61.

108. Beljanski, V., C. Knaak, and C.D. Smith, *A novel sphingosine kinase inhibitor induces autophagy in tumor cells.* J Pharmacol Exp Ther. **333**(2): p. 454-64.

109. Signorelli, P., et al., *Dihydroceramide intracellular increase in response to resveratrol treatment mediates autophagy in gastric cancer cells.* Cancer Lett, 2009. **282**(2): p. 238-43.

110. Jiang, Q., et al., *Gamma-tocotrienol induces apoptosis and autophagy in prostate cancer cells by increasing intracellular dihydrosphingosine and dihydroceramide.* Int J Cancer, 2011.

111. Lavieu, G., et al., *Is autophagy the key mechanism by which the sphingolipid rheostat controls the cell fate decision?* Autophagy, 2007. **3**(1): p. 45-7.

112. Oskouian, B. and J.D. Saba, *Cancer treatment strategies targeting sphingolipid metabolism.* Adv Exp Med Biol. **688**: p. 185-205.

113. Monick, M.M., et al., *Cooperative prosurvival activity by ERK and Akt in human alveolar macrophages is dependent on high levels of acid ceramidase activity.* J Immunol, 2004. **173**(1): p. 123-35.

114. Weigert, A., N. Weis, and B. Brune, *Regulation of macrophage function by sphingosine-1-phosphate.* Immunobiology, 2009. **214**(9-10): p. 748-60.

115. Knapp, K.M. and B.K. English, *Ceramide-mediated stimulation of inducible nitric oxide synthase (iNOS) and tumor necrosis factor (TNF) accumulation in murine macrophages requires tyrosine kinase activity.* J Leukoc Biol, 2000. **67**(5): p. 735-41.

116. Gangoiti, P., et al., *Ceramide 1-phosphate stimulates macrophage proliferation through activation of the PI3-kinase/PKB, JNK and ERK1/2 pathways.* Cell Signal, 2008. **20**(4): p. 726-36.

117. Gutierrez, M.G., et al., *Role of lipids in killing mycobacteria by macrophages: evidence for NF-kappaB-dependent and -independent killing induced by different lipids.* Cell Microbiol, 2009. **11**(3): p. 406-20.

118. Grabowski, G.A., *Delivery of lysosomal enzymes for therapeutic use: glucocerebrosidase as an example.* Expert Opin Drug Deliv, 2006. **3**(6): p. 771-82.

119. Schaade, L., et al., *Characterization of cytostatically active glycosphingolipids isolated from thioglycollate-elicited murine macrophages.* IUBMB Life, 1999. **48**(3): p. 353-8.

120. Berenson, C.S., et al., *The role of ceramide of human macrophage gangliosides in activation of human macrophages.* J Leukoc Biol, 2002. **72**(3): p. 492-502.

121. Stamatos, N.M., et al., *Differential expression of endogenous sialidases of human monocytes during cellular differentiation into macrophages.* FEBS J, 2005. **272**(10): p. 2545-56.

122. Cho, J.Y., *Effect of L-cycloserine on cellular responses mediated by macrophages and T cells.* Biol Pharm Bull, 2007. **30**(11): p. 2105-12.

123. Park, T.S., et al., *Modulation of lipoprotein metabolism by inhibition of sphingomyelin synthesis in ApoE knockout mice.* Atherosclerosis, 2006. **189**(2): p. 264-72.

124. Blom, T., et al., *FTY720 stimulates 27-hydroxycholesterol production and confers atheroprotective effects in human primary macrophages.* Circ Res. **106**(4): p. 720-9.

125. Goldsmith, M., et al., *Synergistic IL-10 induction by LPS and the ceramide-1-phosphate analog PCERA-1 is mediated by the cAMP and p38 MAP kinase pathways.* Mol Immunol, 2009. **46**(10): p. 1979-87.

126. Emoto, M., et al., *Alpha-galactosylceramide promotes killing of Listeria monocytogenes within the macrophage phagosome through invariant NKT-cell activation.* Infect Immun. **78**(6): p. 2667-76.

127. Shaner, R.L., et al., *Quantitative analysis of sphingolipids for lipidomics using triple quadrupole and quadrupole linear ion trap mass spectrometers.* J Lipid Res, 2009. **50**(8): p. 1692-1707.

128. Raetz, C.R., et al., *Kdo2-Lipid A of Escherichia coli, a defined endotoxin that activates macrophages via TLR-4.* J Lipid Res, 2006. **47**(5): p. 1097-111.

129. Memon, R.A., et al., *Regulation of glycosphingolipid metabolism in liver during the acute phase response.* J Biol Chem, 1999. **274**(28): p. 19707-13.

130. Memon, R.A., et al., *Regulation of sphingolipid and glycosphingolipid metabolism in extrahepatic tissues by endotoxin.* J Lipid Res, 2001. **42**(3): p. 452-9.

131. MacKichan, M.L. and A.L. DeFranco, *Role of ceramide in lipopolysaccharide (LPS)-induced signaling. LPS increases ceramide rather than acting as a structural homolog.* J Biol Chem, 1999. **274**(3): p. 1767-75.

132. Delgado, M.A. and V. Deretic, *Toll-like receptors in control of immunological autophagy.* Cell Death Differ, 2009. **16**(7): p. 976-83.

133. Delgado, M.A., et al., *Toll-like receptors control autophagy.* EMBO J, 2008. **27**(7): p. 1110-21.

134. Krishnamurthy, K., S. Dasgupta, and E. Bieberich, *Development and characterization of a novel anti-ceramide antibody.* J Lipid Res, 2007. **48**(4): p. 968-75.

135. Grassme, H., et al., *Host defense against Pseudomonas aeruginosa requires ceramide-rich membrane rafts.* Nat Med, 2003. **9**(3): p. 322-30.

136. Rotolo, J.A., et al., *Caspase-dependent and -independent activation of acid sphingomyelinase signaling.* J Biol Chem, 2005. **280**(28): p. 26425-34.

137. Grassme, H., et al., *Rhinoviruses infect human epithelial cells via ceramide-enriched membrane platforms.* J Biol Chem, 2005. **280**(28): p. 26256-62.

138. Yin, X., et al., *A ceramide-binding C1 domain mediates kinase suppressor of ras membrane translocation.* Cell Physiol Biochem, 2009. **24**(3-4): p. 219-30.

139. Wang, G., et al., *Direct binding to ceramide activates protein kinase Czeta before the formation of a pro-apoptotic complex with PAR-4 in differentiating stem cells.* J Biol Chem, 2005. **280**(28): p. 26415-24.

140. Sullards, M.C., et al., *Structure-specific, quantitative methods for analysis of sphingolipids by liquid chromatography-tandem mass spectrometry: "inside-out" sphingolipidomics.* Methods Enzymol, 2007. **432**: p. 83-115.

141. Iwata, A., et al., *HDAC6 and microtubules are required for autophagic degradation of aggregated huntingtin.* J Biol Chem, 2005. **280**(48): p. 40282-92.

142. Eskelinen, E.L., *Fine structure of the autophagosome.* Methods Mol Biol, 2008. **445**: p. 11-28.

143. Momin, A.A., et al., *Characterization of mutant serine palmitoyltransferase 1 in LY-B cells.* Lipids, 2009. **44**(8): p. 725-32.

144. Tiwari, M., et al., *Inhibition of N-(4-hydroxyphenyl)retinamide-induced autophagy at a lower dose enhances cell death in malignant glioma cells.* Carcinogenesis, 2008. **29**(3): p. 600-9.

145. Merrill, A.H., Jr., E. Wang, and R.E. Mullins, *Kinetics of long-chain (sphingoid) base biosynthesis in intact LM cells: effects of varying the extracellular concentrations of serine and fatty acid precursors of this pathway.* Biochemistry, 1988. **27**(1): p. 340-5.

146. Gal, D., et al., *Effect of cell density and confluency on cholesterol metabolism in cancer cells in monolayer culture.* Cancer Res, 1981. **41**(2): p. 473-7.

147. Dahlquist, K.D., et al., *GenMAPP, a new tool for viewing and analyzing microarray data on biological pathways.* Nat Genet, 2002. **31**(1): p. 19-20.

148. Sakata, A., et al., *Acid sphingomyelinase inhibition suppresses lipopolysaccharide-mediated release of inflammatory cytokines from macrophages and protects against disease pathology in dextran sulphate sodium-induced colitis in mice.* Immunology, 2007. **122**(1): p. 54-64.

149. Rozenova, K.A., et al., *Studies on the role of acid sphingomyelinase and ceramide in the regulation of tumor necrosis factor alpha (TNFalpha)-converting enzyme activity and TNFalpha secretion in macrophages.* J Biol Chem. **285**(27): p. 21103-13.

150. Hanada, K., et al., *Specificity of inhibitors of serine palmitoyltransferase (SPT), a key enzyme in sphingolipid biosynthesis, in intact cells. A novel evaluation system using an SPT-defective mammalian cell mutant.* Biochem Pharmacol, 2000. **59**(10): p. 1211-6.

151. Raschke, W.C., et al., *Functional macrophage cell lines transformed by Abelson leukemia virus.* Cell, 1978. **15**(1): p. 261-7.

152. Saxena, R.K., V. Vallyathan, and D.M. Lewis, *Evidence for lipopolysaccharide-induced differentiation of RAW264.7 murine macrophage cell line into dendritic like cells.* J Biosci, 2003. **28**(1): p. 129-34.

153. Funk, J.L., et al., *Lipopolysaccharide stimulation of RAW 264.7 macrophages induces lipid accumulation and foam cell formation.* Atherosclerosis, 1993. **98**(1): p. 67-82.

154. Yamaji, T., et al., *Two sphingolipid transfer proteins, CERT and FAPP2: their roles in sphingolipid metabolism.* IUBMB Life, 2008. **60**(8): p. 511-8.

155. Yoshimori, T. and T. Noda, *Toward unraveling membrane biogenesis in mammalian autophagy.* Curr Opin Cell Biol, 2008. **20**(4): p. 401-7.

156. Mijaljica, D., M. Prescott, and R.J. Devenish, *Endoplasmic reticulum and Golgi complex: Contributions to, and turnover by, autophagy.* Traffic, 2006. **7**(12): p. 1590-5.

157. Axe, E.L., et al., *Autophagosome formation from membrane compartments enriched in phosphatidylinositol 3-phosphate and dynamically connected to the endoplasmic reticulum.* J Cell Biol, 2008. **182**(4): p. 685-701.

158. Hamasaki, M. and T. Yoshimori, *Where do they come from? Insights into autophagosome formation.* FEBS Lett. **584**(7): p. 1296-301.

159. Rosenwald, A.G. and R.E. Pagano, *Intracellular transport of ceramide and its metabolites at the Golgi complex: insights from short-chain analogs.* Adv Lipid Res, 1993. **26**: p. 101-18.

160. Hoffmann, P.M. and R.E. Pagano, *Retrograde movement of membrane lipids from the Golgi apparatus to the endoplasmic reticulum of perforated cells: evidence for lipid recycling.* Eur J Cell Biol, 1993. **60**(2): p. 371-5.

161. Hu, W., et al., *Golgi fragmentation is associated with ceramide-induced cellular effects.* Mol Biol Cell, 2005. **16**(3): p. 1555-67.

162. Yamashita, S., et al., *PI4P-signaling pathway for the synthesis of a nascent membrane structure in selective autophagy.* J Cell Biol, 2006. **173**(5): p. 709-17.

163. Nakayama, Y., et al., *Molecular mechanisms of the LPS-induced non-apoptotic ER stress-CHOP pathway.* J Biochem. **147**(4): p. 471-83.

164. He, C. and D.J. Klionsky, *Regulation mechanisms and signaling pathways of autophagy.* Annu Rev Genet, 2009. **43**: p. 67-93.

165. Senkal, C.E., et al., *Antiapoptotic roles of ceramide-synthase-6-generated C16-ceramide via selective regulation of the ATF6/CHOP arm of ER-stress-response pathways.* FASEB J. **24**(1): p. 296-308.

166. Xu, K., et al., *Autophagy plays a protective role in free cholesterol overloading induced smooth muscle cells death.* J Lipid Res.

167. Veronesi, U., et al., *Randomized trial of fenretinide to prevent second breast malignancy in women with early breast cancer.* J Natl Cancer Inst, 1999. **91**(21): p. 1847-56.

168. Veronesi, U., et al., *Fifteen-year results of a randomized phase III trial of fenretinide to prevent second breast cancer.* Ann Oncol, 2006. **17**(7): p. 1065-71.

169. De Palo, G., et al., *Effect of fenretinide on ovarian carcinoma occurrence.* Gynecol Oncol, 2002. **86**(1): p. 24-7.

170. Garaventa, A., et al., *Phase I trial and pharmacokinetics of fenretinide in children with neuroblastoma.* Clin Cancer Res, 2003. **9**(6): p. 2032-9.

171. Schneider, B.J., et al., *Phase II trial of fenretinide (NSC 374551) in patients with recurrent small cell lung cancer.* Invest New Drugs, 2009.

172. Sogno, I., et al., *Angioprevention with fenretinide: targeting angiogenesis in prevention and therapeutic strategies.* Crit Rev Oncol Hematol. **75**(1): p. 2-14.

173. Tiberio, P., et al., *4-oxo-N-(4-hydroxyphenyl)retinamide: two independent ways to kill cancer cells.* PLoS One. **5**(10): p. e13362.

174. Dmitrovsky, E., *Fenretinide activates a distinct apoptotic pathway.* J Natl Cancer Inst, 2004. **96**(17): p. 1264-5.

175. Wang, H., et al., *N-(4-hydroxyphenyl)retinamide elevates ceramide in neuroblastoma cell lines by coordinate activation of serine palmitoyltransferase and ceramide synthase.* Cancer Res, 2001. **61**(13): p. 5102-5.

176. Wang, H., et al., *N-(4-Hydroxyphenyl)retinamide increases dihydroceramide and synergizes with dimethylsphingosine to enhance cancer cell killing.* Mol Cancer Ther, 2008. **7**(9): p. 2967-76.

177. Kraveka, J.M., et al., *Involvement of dihydroceramide desaturase in cell cycle progression in human neuroblastoma cells.* J Biol Chem, 2007. **282**(23): p. 16718-28.

178. Valsecchi, M., et al., *Sphingolipidomics of A2780 human ovarian carcinoma cells treated with synthetic retinoids.* J Lipid Res. **51**(7): p. 1832-40.

179. Rahmaniyan, M., et al., *Identification of Dihydroceramide Desaturase as a Direct in vitro target for Fenretinide.* J Biol Chem, 2011. **286**(28): p. 24754-24764.

180. Villani, M.G., et al., *Identification of the fenretinide metabolite 4-oxo-fenretinide present in human plasma and formed in human ovarian carcinoma cells through induction of cytochrome P450 26A1.* Clin Cancer Res, 2004. **10**(18 Pt 1): p. 6265-75.

181. Messner, M.C. and M.C. Cabot, *Cytotoxic responses to N-(4-hydroxyphenyl)retinamide in human pancreatic cancer cells.* Cancer Chemother Pharmacol, 2011. **68**(2): p. 477-487.

182. Lee, L., A. Abe, and J.A. Shayman, *Improved inhibitors of glucosylceramide synthase.* J Biol Chem, 1999. **274**(21): p. 14662-9.

183. Wei, J., et al., *Serine palmitoyltransferase subunit 1 is present in the endoplasmic reticulum, nucleus and focal adhesions, and functions in cell morphology.* Biochim Biophys Acta, 2009. **1791**(8): p. 746-56.

184. Kok, J.W., et al., *Dihydroceramide biology. Structure-specific metabolism and intracellular localization.* J Biol Chem, 1997. **272**(34): p. 21128-36.

185. Funakoshi, T., et al., *Reconstitution of ATP- and cytosol-dependent transport of de novo synthesized ceramide to the site of sphingomyelin synthesis in semi-intact cells.* J Biol Chem, 2000. **275**(39): p. 29938-45.

186. Geeraert, L., G.P. Mannaerts, and P.P. van Veldhoven, *Conversion of dihydroceramide into ceramide: involvement of a desaturase.* Biochem J, 1997. **327 (Pt 1)**: p. 125-32.

187. Martin, O.C. and R.E. Pagano, *Normal- and reverse-phase HPLC separations of fluorescent (NBD) lipids.* Anal Biochem, 1986. **159**(1): p. 101-8.

188. Pagano, R.E. and O.C. Martin, *A series of fluorescent N-acylsphingosines: synthesis, physical properties, and studies in cultured cells.* Biochemistry, 1988. **27**(12): p. 4439-45.

189. Lovat, P.E., et al., *Gangliosides link the acidic sphingomyelinase-mediated induction of ceramide to 12-lipoxygenase-dependent apoptosis of neuroblastoma in response to fenretinide.* J Natl Cancer Inst, 2004. **96**(17): p. 1288-99.

190. Maurer, B.J., et al., *Synergistic cytotoxicity in solid tumor cell lines between N-(4-hydroxyphenyl)retinamide and modulators of ceramide metabolism.* J Natl Cancer Inst, 2000. **92**(23): p. 1897-909.

191. Maurer, B.J., et al., *Increase of ceramide and induction of mixed apoptosis/necrosis by N-(4-hydroxyphenyl)- retinamide in neuroblastoma cell lines.* J Natl Cancer Inst, 1999. **91**(13): p. 1138-46.

192. Erdreich-Epstein, A., et al., *Ceramide signaling in fenretinide-induced endothelial cell apoptosis.* J Biol Chem, 2002. **277**(51): p. 49531-7.

193. Park, M.A., et al., *Vorinostat and sorafenib increase ER stress, autophagy and apoptosis via ceramide-dependent CD95 and PERK activation.* Cancer Biol Ther, 2008. **7**(10): p. 1648-62.

194. Morton, R.E., et al., *The acyl-CoA desaturases of microsomes from rat liver and the Morris 7777 hepatoma.* Biochim Biophys Acta, 1979. **573**(2): p. 321-31.

195. Oshino, N., Y. Imai, and R. Sato, *Electron-transfer mechanism associated with fatty acid desaturation catalyzed by liver microsomes.* Biochim Biophys Acta, 1966. **128**(1): p. 13-27.

196. Idkowiak-Baldys, J., et al., *Dihydroceramide desaturase activity is modulated by oxidative stress.* Biochem J. **427**(2): p. 265-74.

197. Holland, W.L., et al., *Inhibition of ceramide synthesis ameliorates glucocorticoid-, saturated-fat-, and obesity-induced insulin resistance.* Cell Metab, 2007. **5**(3): p. 167-79.

198. Gouaze-Andersson, V., et al., *Inhibition of acid ceramidase by a 2-substituted aminoethanol amide synergistically sensitizes prostate cancer cells to N-(4-hydroxyphenyl) retinamide.* Prostate. **71**(10): p. 1064-73.

199. Zou, C.P., et al., *Higher potency of N-(4-hydroxyphenyl)retinamide than all-trans-retinoic acid in induction of apoptosis in non-small cell lung cancer cell lines.* Clin Cancer Res, 1998. **4**(5): p. 1345-55.

200. Puduvalli, V.K., et al., *Induction of apoptosis in primary meningioma cultures by fenretinide.* Cancer Res, 2005. **65**(4): p. 1547-53.

201. Montaldo, P.G., et al., *N-(4-hydroxyphenyl) retinamide is cytotoxic to melanoma cells in vitro through induction of programmed cell death.* Int J Cancer, 1999. **81**(2): p. 262-7.

202. Messmer, T.O., et al., *Sphingolipid biosynthesis by rat liver cells: effects of serine, fatty acids and lipoproteins.* J Nutr, 1989. **119**(4): p. 534-8.

203. Kourtidis, A., et al., *Peroxisome proliferator-activated receptor-gamma protects ERBB2-positive breast cancer cells from palmitate toxicity.* Breast Cancer Res, 2009. **11**(2): p. R16.

204. Bjorkoy, G., et al., *Monitoring autophagic degradation of p62/SQSTM1.* Methods Enzymol, 2009. **452**: p. 181-97.

205. Ichimura, Y. and M. Komatsu, *Selective degradation of p62 by autophagy.* Semin Immunopathol. **32**(4): p. 431-6.

206. Possemato, R., et al., *Functional genomics reveal that the serine synthesis pathway is essential in breast cancer.* Nature. **476**(7360): p. 346-50.

207. Deberardinis, R.J., et al., *Brick by brick: metabolism and tumor cell growth.* Curr Opin Genet Dev, 2008. **18**(1): p. 54-61.

208. Friday, E., et al., *Glutaminolysis and glycolysis regulation by troglitazone in breast cancer cells: Relationship to mitochondrial membrane potential.* J Cell Physiol. **226**(2): p. 511-9.

209. Hu, W., et al., *Differential regulation of dihydroceramide desaturase by palmitate versus monounsaturated fatty acids: implications for insulin resistance.* J Biol Chem. **286**(19): p. 16596-605.

210. Liu, C., et al., *Murine mammary carcinoma exosomes promote tumor growth by suppression of NK cell function.* J Immunol, 2006. **176**(3): p. 1375-85.

211. Lee, T.H., et al., *Microvesicles as mediators of intercellular communication in cancer-the emerging science of cellular 'debris'.* Semin Immunopathol. **33**(5): p. 455-67.

212. Koga, K., et al., *Purification, characterization and biological significance of tumor-derived exosomes.* Anticancer Res, 2005. **25**(6A): p. 3703-7.

213. Iero, M., et al., *Tumour-released exosomes and their implications in cancer immunity.* Cell Death Differ, 2008. **15**(1): p. 80-8.

214. Zhang, H.G., et al., *Curcumin reverses breast tumor exosomes mediated immune suppression of NK cell tumor cytotoxicity.* Biochim Biophys Acta, 2007. **1773**(7): p. 1116-23.

215. Trajkovic, K., et al., *Ceramide triggers budding of exosome vesicles into multivesicular endosomes.* Science, 2008. **319**(5867): p. 1244-7.

216. Muller, G., et al., *Induced release of membrane vesicles from rat adipocytes containing glycosylphosphatidylinositol-anchored microdomain and lipid droplet signalling proteins.* Cell Signal, 2009. **21**(2): p. 324-38.

217. Muller, G., et al., *Transfer of the glycosylphosphatidylinositol-anchored 5'-nucleotidase CD73 from adiposomes into rat adipocytes stimulates lipid synthesis.* Br J Pharmacol. **160**(4): p. 878-91.

218. Hannun, Y.A., C. Luberto, and K.M. Argraves, *Enzymes of sphingolipid metabolism: from modular to integrative signaling.* Biochemistry, 2001. **40**(16): p. 4893-903.

219. Cuschieri, J., J. Billgren, and R.V. Maier, *Phosphatidylcholine-specific phospholipase C (PC-PLC) is required for LPS-mediated macrophage activation through CD14.* J Leukoc Biol, 2006. **80**(2): p. 407-14.

220. Monick, M.M., et al., *A phosphatidylcholine-specific phospholipase C regulates activation of p42/44 mitogen-activated protein kinases in lipopolysaccharide-stimulated human alveolar macrophages.* J Immunol, 1999. **162**(5): p. 3005-12.

221. Claycombe, K.J., et al., *Ceramide mediates age-associated increase in macrophage cyclooxygenase-2 expression.* J Biol Chem, 2002. **277**(34): p. 30784-91.

222. Balsinde, J., M.A. Balboa, and E.A. Dennis, *Inflammatory activation of arachidonic acid signaling in murine P388D1 macrophages via sphingomyelin synthesis.* J Biol Chem, 1997. **272**(33): p. 20373-7.

223. Chambard, J.C., et al., *ERK implication in cell cycle regulation.* Biochim Biophys Acta, 2007. **1773**(8): p. 1299-310.

224. Cagnol, S. and J.C. Chambard, *ERK and cell death: mechanisms of ERK-induced cell death--apoptosis, autophagy and senescence.* FEBS J. **277**(1): p. 2-21.

225. Kim, J., et al., *Extracellular signal-regulated kinase-signaling-dependent G2/M arrest and cell death in murine macrophages by cadmium.* Environ Toxicol Chem, 2005. **24**(12): p. 3069-77.

226. Filippi-Chiela, E.C., et al., *Autophagy interplay with apoptosis and cell cycle regulation in the growth inhibiting effect of resveratrol in glioma cells.* PLoS One. **6**(6): p. e20849.

227. Shin, S.Y., et al., *5-Methoxyflavanone induces cell cycle arrest at the G2/M phase, apoptosis and autophagy in HCT116 human colon cancer cells.* Toxicol Appl Pharmacol. **254**(3): p. 288-98.

228. Chen, M.Y., et al., *Decitabine and suberoylanilide hydroxamic acid (SAHA) inhibit growth of ovarian cancer cell lines and xenografts while inducing expression of imprinted tumor suppressor genes, apoptosis, G2/M arrest, and autophagy.* Cancer, 2011. **117**(19): p. 4424-4438.

229. Shingu, T., et al., *The polynuclear platinum BBR3610 induces G2/M arrest and autophagy early and apoptosis late in glioma cells.* Neuro Oncol, 2010. **12**(12): p. 1269-77.

230. Gangoiti, P., et al., *Activation of mTOR and RhoA is a major mechanism by which Ceramide 1-phosphate stimulates macrophage proliferation.* Cell Signal, 2011. **23**(1): p. 27-34.

231. Min, J., et al., *(Dihydro)ceramide synthase 1 regulated sensitivity to cisplatin is associated with the activation of p38 mitogen-activated protein kinase and is abrogated by sphingosine kinase 1.* Mol Cancer Res, 2007. **5**(8): p. 801-12.

232. Senkal, C.E., et al., *Role of human longevity assurance gene 1 and C18-ceramide in chemotherapy-induced cell death in human head and neck squamous cell carcinomas.* Mol Cancer Ther, 2007. **6**(2): p. 712-22.

233. Hannun, Y.A. and L.M. Obeid, *Many ceramides.* J Biol Chem, 2011. **286**(32): p. 27855-62.

234. Mesicek, J., et al., *Ceramide synthases 2, 5, and 6 confer distinct roles in radiation-induced apoptosis in HeLa cells.* Cell Signal, 2010. **22**(9): p. 1300-7.

235. Schiffmann, S., et al., *Inhibitors of specific ceramide synthases.* Biochimie, 2011.

236. Zhang, S., et al., *Arsenic trioxide inhibits HCCLM3 cells invasion through de novo ceramide synthesis and sphingomyelinase-induced ceramide production.* Med Oncol, 2011.

237. Kagan, V.E., et al., *Ascorbate is the primary reductant of the phenoxyl radical of etoposide in the presence of thiols both in cell homogenates and in model systems.* Biochemistry, 1994. **33**(32): p. 9651-60.

238. Sun, S.Y., et al., *Mediation of N-(4-hydoxyphenyl)retinamide-induced apoptosis in human cancer cells by different mechanisms.* Cancer Res, 1999. **59**(10): p. 2493-8.

239. Summers, S.A., *Ceramides in insulin resistance and lipotoxicity.* Prog Lipid Res, 2006. **45**(1): p. 42-72.

240. Beare-Rogers, J., A. Dieffenbacher, and J.V. Holm, *Lexicon of Lipid Nutrition.* Pure Appl. Chem. , 2001. **73**(4): p. 685-744.

241. Schaffer, J.E., *Lipotoxicity: when tissues overeat.* Curr Opin Lipidol, 2003. **14**(3): p. 281-7.

242. Henry, B., et al., *Targeting the ceramide system in cancer.* Cancer Lett, 2011.

243. Ryland, L.K., et al., *Dysregulation of sphingolipid metabolism in cancer.* Cancer Biol Ther. **11**(2): p. 138-49.

244. Garcia, A.A., et al., *Phase II trial of fenretinide (4-HPR) in recurrent ovarian and primary peritoneal carcinoma: A California Cancer Consortium trial.* Journal of Clinical Oncology, 2004. **22**(14S).

245. Cooper, J.P., et al., *Fenretinide metabolism in humans and mice: utilizing pharmacological modulation of its metabolic pathway to increase systemic exposure.* Br J Pharmacol. **163**(6): p. 1263-75.

246. Marachelian, A., et al., *Phase I study of fenretinide (4-HPR) oral powder in patients with recurrent or resistant neuroblastoma: New Approaches to Neuroblastoma Therapy (NANT) Consortium trial.* J Clin Oncol, 2009. **27**(15S).

247. Sabichi, A.L., et al., *Breast tissue accumulation of retinamides in a randomized short-term study of fenretinide.* Clin Cancer Res, 2003. **9**(7): p. 2400-5.

248. Merrill, G.F., et al., *Influence of malonyl-CoA and palmitate concentration on rate of palmitate oxidation in rat muscle.* J Appl Physiol, 1998. **85**(5): p. 1909-14.

249. Haynes, C.A., et al., *Factors to consider in using [U-C]palmitate for analysis of sphingolipid biosynthesis by tandem mass spectrometry.* J Lipid Res. **52**(8): p. 1583-94.

250. White, D.E. and S.A. Burchill, *Fenretinide-dependent upregulation of death receptors through ASK1 and p38alpha enhances death receptor ligand-induced cell death in Ewing's sarcoma family of tumours.* Br J Cancer, 2010. **103**(9): p. 1380-90.

251. Huber, V., et al., *Human colorectal cancer cells induce T-cell death through release of proapoptotic microvesicles: role in immune escape.* Gastroenterology, 2005. **128**(7): p. 1796-804.

252. Chen, T.Y., et al., *Reactive oxygen species are involved in FasL-induced caspase-independent cell death and inflammatory responses.* Free Radic Biol Med, 2009. **46**(5): p. 643-55.

253. Kong, J.Y. and S.W. Rabkin, *Palmitate-induced apoptosis in cardiomyocytes is mediated through alterations in mitochondria: prevention by cyclosporin A.* Biochim Biophys Acta, 2000. **1485**(1): p. 45-55.

254. Cnop, M., J.C. Hannaert, and D.G. Pipeleers, *Troglitazone does not protect rat pancreatic beta cells against free fatty acid-induced cytotoxicity.* Biochem Pharmacol, 2002. **63**(7): p. 1281-5.

255. Cnop, M., et al., *Inverse relationship between cytotoxicity of free fatty acids in pancreatic islet cells and cellular triglyceride accumulation.* Diabetes, 2001. **50**(8): p. 1771-7.

256. Barna, G., et al., *Different ways to induce apoptosis by fenretinide and all-trans-retinoic acid in human B lymphoma cells.* Anticancer Res, 2005. **25**(6B): p. 4179-85.

VITA

Kacee Hall Sims was born in Dothan, Alabama in 1983. She graduated from Dothan High School in 2001 and went on to earn a B.S. in Chemistry, with Highest Honors, from Jacksonville State University in April of 2005 before coming to the Georgia Institute of Technology to pursue a doctorate in Biochemistry under the direction of Dr. Al Merrill. Kacee is married to Jeremy Sims and enjoys exercising, reading, and traveling in her spare time.